Polymeric phosphorus chalcogenides and boracite-type inclusion compounds containing Pn_4Q_3 cage molecules in metal halide frameworks

Dissertation

zur Erlangung des Doktorgrades
der Naturwissenschaften (Dr. rer. nat.)
der Fakultät für Chemie und Pharmazie
der Universität Regensburg

vorgelegt von

M. Sc. Ria Mandal

aus Chinsurah / Indien

Regensburg, May 2020

Dedicated to my parents

This thesis was supervised by Prof. Dr. Arno Pfitzner

Submission of the doctoral application: 21.02.2020

Date of the oral examination: 27.05.2020

Examination committee

Chairman: Prof. Dr. Alkwin Slenczka

1st reviewer: Prof. Dr. Arno Pfitzner

2nd reviewer: Prof. Dr. Richard Weihrich (University of Augsburg)

Further examiner: Prof. Dr. Frank-Michael Matysik

Acknowledgement

The research work of this thesis was conducted from July 2016 to August 2019 under the supervision of Prof. Dr. Arno Pfitzner at the Chair of Inorganic Chemistry in University of Regensburg.

I would like to thank those without whom this work would not be possible:

- Prof. Dr. Arno Pfitzner for giving me the opportunity to explore this interesting and challenging research topic and guiding me through this journey. I also thank him for financial support.
- Prof. Dr. Jürgen Senker for performing and evaluating the solid state NMR spectra of the compound P_2S_6Te.
- Prof. Dr. Jörn Schmedt auf der Günne of the University of Siegen for performing and evaluating the solid state NMR spectra of the compound $(P_4S_3)@Zn_7SI_{12}$
- Prof. Dr. Alkwin Slenzcka for Raman measurement.
- Dr. Michael Bodensteiner and the X-Ray structure analysis Department for solving the difficulties during X-Ray measurements.
- Dr. Marc Schlosser for teaching me how to perform PXRD measurements and helping me with the practical courses.
- Dr. Florian Pielnhofer for theoretical calculations and fruitful scientific discussions.
- Mrs. Ulrike Schießl for carrying out the thermal analyses and SEM-EDS measurements, and Florian Truksa for providing the starting material P_4Se_3.
- Ms. Bianca Frömel and Mrs. Katharina Trögl for helping me with the paper work and translating numerous documents into English.
- Dr. Christoph Vitzthumecker, Dr. Max Vilsmeier, Dr. Thomas Buchecker, Dr. Daniel Fiedler, M. Sc. Thomas Rothenaigner, M. Sc. Christian Klimas, and M. Sc. Igor Plokhikh for sharing their scientific knowledge with me and helping me with the laboratory instruments.
- All the present and past members of the Pfitzner group for their help and the pleasant working atmosphere: Dr. Martina Andratschke, Dr. Claudia De Giorgi, Dr. Victoria Telser, M. Sc. Severin Bauer, M. Sc. Dominik Gigl, Dr. Sebastian Haumann, M. Sc. Sebastian Fäth, M. Sc. Michael Földi, M. Sc. Christoph Meier, M. Sc. Maximilian Sehr, M. Sc. Florian Wegner and M. Sc. Salil Bal.
- Finally, my family and my husband Indra for their constant support, encouragement, and understanding.

Declaration

I, Ria Mandal, declare that this thesis titled, ‘Polymeric phosphorus chalcogenides and boracite-type inclusion compounds containing Pn_4Q_3 cage molecules in metal halide framework’, and the work presented in it are my own under the supervision of Prof. Dr. Arno Pfitzner and I did not use any unnamed sources or aid. This work has not been submitted at any other University, and I am aware of § 25 Abs. 5 and its legal consequences.

Regensburg, February

Abstract

This thesis introduces ternary and quaternary polymeric phosphorus chalcogenide compounds. Five such compounds, α-P_2S_6Se, β-P_2S_6Se, P_2S_6Te, $P_2S_{6.35}Se_{0.64}$, and P_2S_5SeTe were synthesised by using hexa-hydrated ferric chloride as mineraliser and characterised. P_2S_6Te is the first inorganic compound containing phosphorus and tellurium starting from elemental precursors. These phosphorus mixed-chalcogenide compounds, in which four-membered P-S rings are connected via quite rare, chalcogen (Q_1)-chalcogen (Q_2) bonds. The repeated formation of two types of binary chemical bonds, i.e., (P-S)–(Q)–(S-P), allows formation of parallel-stacked polymeric chains in which the four-membered P-S units are connected via Q_1-Q_2-Q_1 bridges. The reported structures, therefore, also allows some insight into chalcogen bonds by Raman spectroscopy. $P_3S_8Te_3$, another polymeric compound, was synthesised starting from P_2S_6Te. This compound has a unique sheet like structure containing unusual Te-Te bond. Hexa-hydrated ferric chloride as mineraliser is also needed for this synthesis.

We have also clarified the crystal structure of $(P_4S_3)@Zn_7SI_{12}$ identifying guest cage molecule as P_4S_3 and synthesised a series of new compounds, $(Pn_4Q_3)@Cu_7M_3I_{13}$. Even though all the compounds are isostructural with same space group but the host–guest interaction is different. $(P_4S_3)@Zn_7SI_{12}$, containing only Zn (II), shows non-bonding host–guest interaction between the cage molecule and metal halide framework whereas $(Pn_4Q_3)@Cu_7M_3I_{13}$, containing Cu (I) and another transition metal M (II) has van der Waal interaction between the cage molecule and mix metal halide framework.

New phase of tetraphosphorus nonasulphide P_4S_9 and phosphorus sulphide iodide $P_4S_3I_2$ was synthesised, characterised, and compared with the reported phases. A new triclinic phase of P_4S_9 was found by using excess iodine with the precursors. The structural analysis on a non-merohedral twinned single crystal shows that triclinic P_4S_9, like all phosphorus sulphides, is composed of neutral molecules. The new $P_4S_3I_2$ has tetragonal symmetry like α'-$P_4S_3I_2$ but with different space group *P43* and designated as α''-$P_4S_3I_2$.

Table of Content

1. Introduction……..1

2. Experimental…….……..…10

2.1 Chemicals……..……10

2.1.1 Preparation of P_4S_3…….10

2.1.2 Purification of CuI……11

2.2 Preparation techniques……...12

2.2.1 Preparation in ampoules…….13

2.3 Instrumental techniques……..13

2.3.1 Single crystal X-ray diffraction measurement ……...13

2.3.2 Powder diffraction……...14

2.3.3 Vibration spectroscopy……...14

2.3.4 UV-vis Spectroscopy……..…….15

2.3.5 Thermal analysis…….16

2.3.6 SEM-EDS measurement ……16

2.3.7 Solid State NMR Spectroscopy……...16

2.4 Reference……17

3. Phosphorus polychalcogenides……..19

3.1 Phosphorus selenium sulphides, P_2S_6Se…….19

3.1.1 Synthesis…….20

3.1.2 Single crystal measurement……21

3.1.3 Powder XRD……...26

3.1.4 Thermal analysis……....27

3.1.5 SEM-EDS measurement…….27

3.1.6 Raman Spectroscopy……...29

3.1.7 UV-vis spectroscopy……...30

3.2 Phosphorus selenium sulphides, $P_2S_{6.36}Se_{0.64}$……31

3.2.1 Synthesis…….31

3.2.2 Single crystal measurement……31

3.2.3 SEM-EDS measurement…….33

3.3 Phosphorus tellurium sulphides, P_2S_6Te……34
3.3.1 Synthesis……34
3.3.2 Single crystal measurement……35
3.3.3 Powder XRD……39
3.3.4 Thermal analysis……40
3.3.5 SEM-EDS measurement……40
3.3.6 Raman Spectroscopy……41
3.3.7 UV-vis spectroscopy……43
3.3.8 NMR spectroscopy……43
3.4 Phosphorus tellurium selenium sulphides, P_2S_5SeTe……45
3.4.1 Synthesis……45
3.4.2 Single crystal measurement……45
3.4.3 Powder XRD……48
3.4.4 SEM-EDS measurement……48
3.4.5 Raman Spectroscopy……49
3.5 Comparison between the compounds……51
3.5.1 Structural comparison……51
3.5.2 Comparison between the Raman spectra……54
3.6 Another new phosphorus tellurium sulphide, $P_2S_8Te_3$……56
3.6.1 Synthesis……55
3.6.2 Single crystal measurement……56
3.6.3 SEM-EDS measurement……60
3.6.4 Raman Spectroscopy……61
3.7 Reference……63
4. Boracite-type host-guest and adduct compounds……66
4.1 $(P_4S_3)@Zn_7SI_{12}$……67
4.1.1 Synthesis……67
4.1.2 Single crystal measurement……67
4.1.3 Powder-XRD……72
4.1.4 Raman spectroscopy……73
4.1.5 NMR spectroscopy……75

4.2 $(Pn_4Q_3)@Cu_7M_3I_{13}$ [M= Zn, Cd; Pn = P, As; Q= S, Se]……..…..……78
4.2.1 Synthesis…….78
4.2.2 Single crystal measurement……...….79
4.2.3 Powder-XRD…….….85
4.2.4 SEM-EDS measurement…….86
4.2.5 Raman Spectroscopy……..87
4.3 Reference……....90
5. New phase of phosphorus sulphide and phosphorus sulphide iodide……..….93
5.1 Tetraphosphorus nonasulphide, P_4S_9…….….93
5.1.1 Synthesis……..…94
5.1.2 Single crystal measurement……94
5.1.3 Raman spectroscopy…….…...97
5.1.4 SEM-EDS measurement……..…98
5.1.5 Comparison between 3 modifications……..……98
5.2 Phosphorus sulphide iodide $P_4S_3I_2$……...……100
5.2.1 Synthesis……..……..…101
5.2.2 Single crystal measurement……..……101
5.2.3 SEM-EDS measurement……...…105
5.3 Reference……...……...105
6. Conclusion…….……107
7. Supporting Information…….……...i

1. Introduction

One of the most commonly used elements phosphorus was prepared accidentally by alchemist Henning Brandt in 1669 while he was researching for 'philosopher's stone' from urine [1]. As phosphorus is highly reactive, it has never been found as a free element on the earth surface. Therefore even though Brandt was unable to make 'philosopher's stone' (probably) he opened a new window in Chemistry by discovering this irreplaceable element with incomparable properties. Brandt and his fellow alchemists drew fame by using the element only as a glowing agent for entertainment of the aristocrats because of its chemi-luminescence property. It took century to finally recognise it as phosphorus (by Antoine Lavoisier). Use of phosphorus started intensively to prepare light anywhere matches with mass production from bones. For centuries, Phosphorus has made our life easier and better in the form of fertilizer, detergent, food additives, etc..

On the other hand even though sulphur was mentioned several times in the bible but was recognised for the first time by Antoine Lavoisier in 1777. Since then it was used for black gun powder preparation to vulcanisation of rubber to fungicides. Tellurium was discovered before selenium, in 1782 in a gold mine but identified in 1798 by Martin Heinrich Klaproth. It is important to note that gold telluride minerals are one of the most significant sources of gold. In 1817, Jöns Jacob Berzelius discovered selenium by noting similarity with previously known element tellurium. These three elements of group 16 are called as chalcogens along with oxygen and radioactive polonium.

Now phosphorus and chalcogens have a range of binary and very few ternary compounds of distinct and useful properties. Other than phosphorus oxides, phosphorus sulphides always fascinated chemists with its simple yet interesting structures and useful properties for multiple applications. With the exception of $P_{14}S$[2] and P_2S_7[3] , they consist of cage-like molecules having the general formula P_4S_n (n = 2-10) which can be derived from P_4 tetrahedra by inserting S into the P–P bond or exocyclic addition or both. More than 275 years ago, Marggraf[4], in 1740 first reported the synthesis of phosphorus sulphide at elevated temperature under vigorous reaction between phosphorus and sulphur. And, this chemistry has led to the foundation for the synthesis of various phosphorus sulphides. In the 19th century, Berzelius reacted white phosphorus with sulphur and synthesised P_2S_5 and published his results in 1843 as *'Ueber die Verbindungen des Phosphors mit dem Schwefel* in the journal *Annalen der Physik'*. Even though more than twenty-five compounds have been

synthesised in last two centuries, it has always been difficult to rationalise the synthesis. Additionally proper crystal data or clear investigation are lacking for several of them.

In the beginning of 20th century, Stock and co-workers first elucidated this as 'komödie der Irrungen' (comedy of errors) by synthesising three phosphorus sulphides, P_4S_3, P_4S_7 and P_4S_{10}[5–8] by thermal reaction of corresponding elements and evaluating those by molecular weight determination and careful analysis of X-ray diffraction results. The compounds those are found in literature till date, some are characterised by single-crystal X-ray diffraction like α-P_4S_3[9–11], β-P_4S_3[10], γ-P_4S_3[12], α-P_4S_4[13–15], α-P_4S_5[16,17], β-P_4S_5[18], β-P_4S_6[19], γ-P_4S_6[20], α-P_4S_7[16,21], β-P_4S_7[22], P_4S_{10}[16–18,23], α-P_2S_7[3] and β-P_2S_7[3] when others are determined only by spectroscopic methods for example β-P_4S_4[13], γ-P_4S_5[24], α-P_4S_6[24], δ-P_4S_6[25], ε-P_4S_6[25], δ-P_4S_7[26], α-P_4S_8[27], β-P_4S_8[19] and γ-P_4S_8[28]. There are compounds like P_4S_2, γ-P_4S_4 and γ-P_4S_7 which are only mentioned in the literature but neither spectroscopic nor crystallographic evidence were found[27]. Phosphorus sulphide compounds with reasonable data are shown in Figure 1.1. However as it can be seen, among the above-mentioned compounds most of them have similar compositions because one composition can have more than one modification depending on their connectivity (i.e., constitutional isomers) or cell parameters or space group basically different crystal structure. The nomenclature problem arises from here as they are jumbled by Greek letter prefix and Roman number suffix. Here Greek letters as prefix were used principally for identification of different isomers. Roman number suffixes were only used if same constitutional isomer has different space group (i.e., α-P_4S_n-I and α-P_4S_n-II). The latest discovered neutral and thermodynamically stable phosphorus sulphide P_2S_7, which was synthesised by Pfitzner and co-workers[3], has a polymeric structure. The compound has unique S-S-S bridging unit which is not known in phosphorus sulphide compounds. Recently a metastable compound PS_2[29] was synthesised which is only stable above 8 GPa.

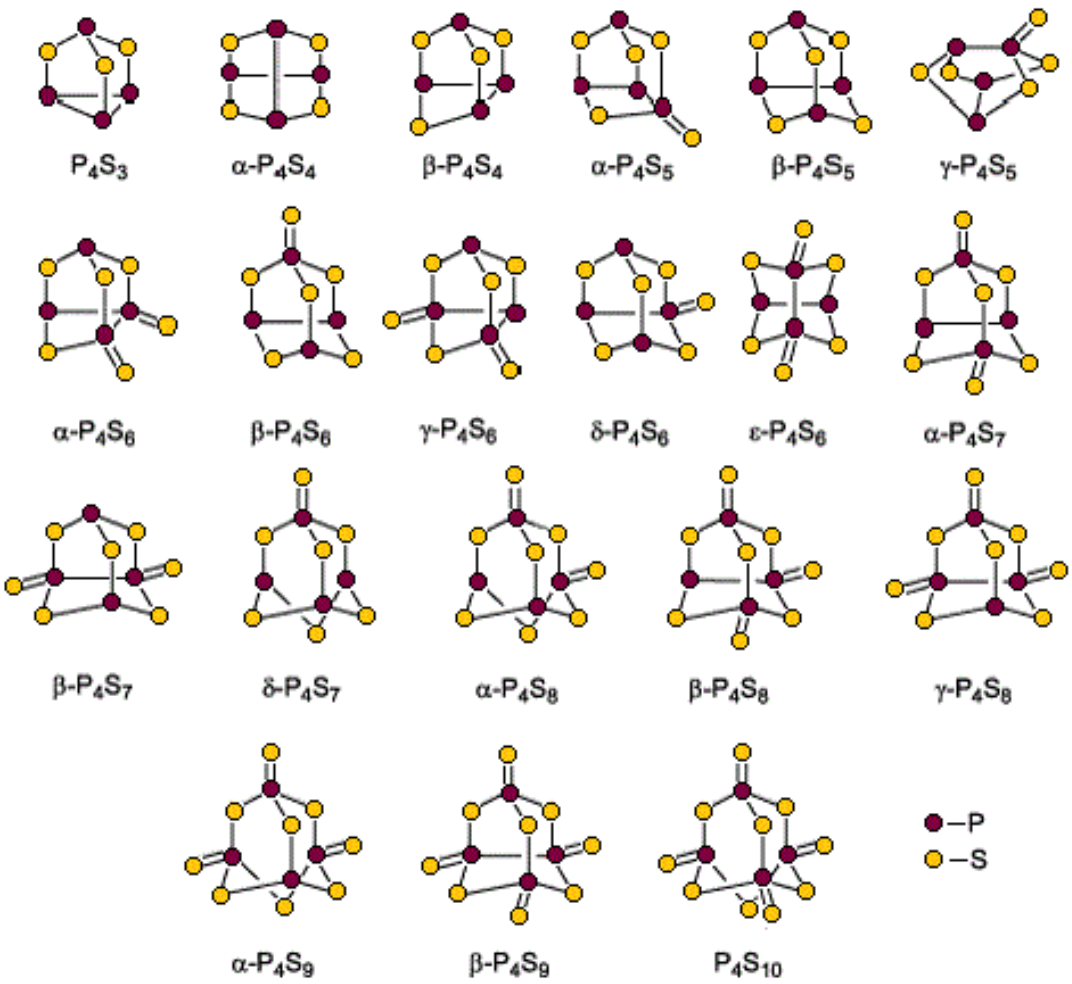

Figure 1.1: Overview of phosphorus sulphide cages examined by X-ray diffraction and NMR study to date, ordered by increasing sulphur content[51].

In literature there are few examples of phosphorus mix-chalcogenides, for example, Blachnik and co-workers[30] claimed to synthesise the phosphorus sulphide tellurides from the melt of the corresponding elements, but any crystallographic structure or solid evidence to these compounds are missing. And there is no crystallographic data available for phosphorus sulphide selenide. Now a day, these types of compounds are getting more interest among the scientists because of their use in materials for energy applications. Phosphorus sulphides are very useful inorganic non-flammable reliable electrolyte materials[31–33] in solid state Li-S batteries. However, in these types of batteries, often the problem is the insulating nature of sulphur or formation of soluble poly-sulphides. Recently, scientists tried to solve this problem by selenium or tellurium doping especially as the cathode material[5,34,35] where introduction of elements of larger ionic size or significantly

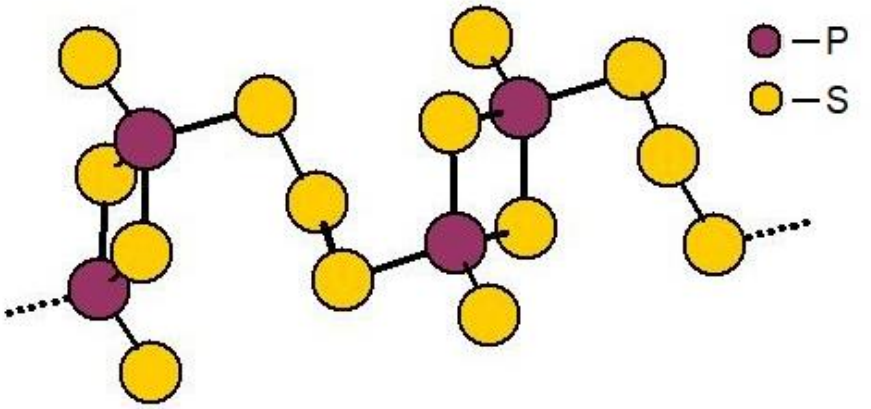

Figure 1.2: Unique repetitive unit of polymeric P_2S_7 synthesised by Pfitzner[3]

higher polarizability increases lattice parameter of the crystal, and thus, decreases electrostatic binding energy of the lithium ion in its anion site resulting into better Li^+ transport pathway. Recently Te_xS_{1-x} was used with carbon nanotube in a composite form as cathode material in carbonate-based electrolytes for lithium chalcogen batteries[34]. The latter one is getting the interest of the scientists because of opposite but complementary properties between sulphur and tellurium in heteroatomic chalcogen moiety. Also tellurium has higher utilization rate and better and faster electrochemical interaction with lithium than sulphur. Therefore, it can be predicted that phosphorus chalcogenide compounds containing Te-S bond can show higher polarizability for battery applications than P_2S_5 or P_2Se_5. On the other hand, the lack in research of phosphorus chalcogenides containing tellurium was partly because of the low abundance of tellurium on earth and also due to the instable Te-P bond. Phosphorus telluride or miscellaneous compound like phosphorus sulphide telluride were always tried to be synthesised analogous to cage molecules like P_4S_3 but no way the weak P-Te bond formation can be avoided in such cage structure though binary phosphorus telluride anions are stabilised by alkali metal ion e.g. BaP_4Te_2[36].

The aim of this thesis is to synthesize ternary or quadratic phosphorus chalcogenide compounds. For the synthesis of pnictogen chalcogenides often solid-state synthesis or diffusion techniques were used. In solid-state synthesis, the precursors are heated to a certain temperature expecting the components (precursors or intermediate) to react. However, diffusion is always a problem in such reactions and thus obtaining good quality crystals or even sometimes the desired products. To solve this problem often mineralisers are used in solid-state synthesis, especially in transport reactions[37]. These mineralisers facilitate the reaction equilibrium at lower temperature, and thus permitting the reaction at much lower

temperature (described in details in Section 2.1). In this thesis it was shown that by choosing the right mineraliser, different interesting compounds can be synthesised that are otherwise not possible by simple solid state or diffusion reactions.

However, some pnictogen chalcogenides or pnictogen polymers, i.e., group 15 and group 16 compounds, are still not accessible or stabilised thermodynamically or kinetically by 'conventional' synthetic routes. In order to achieve the stability of such theoretical or metastable compounds chemists started using 'solid solvents' like copper(I) halide which can exist in different structural motifs like zig-zag chains, split-stair chains or columns[38] owing of their high structural flexibility. These 'solid solvents' stabilise these group 15-group 16 or only group 15 reactants by co-ordination or via simply host-guest interaction, and therefore thermodynamically un-stable structures or wide range of structural verities with different co-ordination motifs can be achieved[39–45]. The later component can be neutral cage molecules like P_4S_3 exhibiting different coordination motifs in the host-guest compounds which eventually help to understand the difference between geometry and co-ordination nature of the apical and basal phosphorus or free rotation in the host-guest compound[44,46]. The other compounds like P_8Se_3 or β-P_4Se_4 which can not be otherwise synthesised directly, are also accessible via adduct compounds like $(CuX)_2(P_8Se_3)$ (X=Br, I)[41] and $(CuI)_3(P_4Se_4)$[42] or unknown $^1_\infty[P_{12}]$ or $^1_\infty[P_{14}]$ polymeric moieties in adducts compounds, $(CuI)_3P_{12}$[39] and $(CuI)_2P_{14}$[40] respectively. In all of these adduct compounds, CuI acts as a 'solid solvent' and stabilised the cage or the polymeric component by co-ordinating with it as a solvent. For example, it is always difficult to synthesis phosphorus selenide compounds. Till date only 4 compounds are known in the literature with proper crystallographic Data. They tend to form polymers or oligomers depending on temperature. Pfitzner and co-workers showed that P_8Se_3, an previously unknown phosphorus selenide compound, can be synthesised by co-ordination of CuI which in turn control the polymerisation and kind of embedded phosphorus selenide structure[41].

Even though in the last paragraph mainly adduct compounds of CuI are discussed, halides of Ag^+[9,43], Au^+[45], Hg^{2+}[47] also show such activities towards group 15- group 16 compounds or group 15 polymers. In these adduct compounds the interaction between metal halides and cage or polymeric compounds is Lewis acid-Lewis base interaction following Pearson concept[48]. The bond distances in such compounds and physical properties (Raman data) also support such interaction. In 2004, Jung synthesised $[(ZnI_2)_6(ZnQ)][Pn_4Q_x]$ (Pn = P, As ; Q =

S, Se)[44] which are host guest type inclusion compounds which have [S@Zn_4@I_{12}] icosahedron which are connected by ZnI_4 octahedrons making a 3D host network where Pn_4Q_x guest-cage molecules are trapped. Isostructural compound [$(CdI_2)_6$(CdS)][As_4S_x][45] was synthesised by Bräu. In all of the above mentioned compounds the distance between pnictogen chalcogenide cages and metal halide framework are higher than corresponding van-der-Waal distances establishing non-bonding host-guest interactions. And the cage molecules show a very unusual rotation in the metal halide cavities which makes its structural solution very difficult. Later Vitzthumecker prepared another family of isostructural compounds $(CuI)_7(MI_2)_3(Pn_4Q_x)$ (M= Zn, Cd, Hg; *Pn* = P, As; Q= S, Se)[49] which have [I@Cu_4@I_{12}] unit instead of a[S@Zn_4@I_{12}]. Furthermore when [S@M_4@I_{12}] (M= Zn^{2+}, Cd^{2+}) moiety was replaced by [I@Cu_4@I_{12}] containing 'Cu^+' ion the host-guest interaction changed to Lewis acid-Lewis base interaction which was supported by bond distances and Raman spectra, retaining similar transitional unit in three dimension. However the effect of the stronger interactions on the cage molecule's rotation or structure was not discussed there. If we consider [S@M_4@I_{12}] unit as neutral fragment, electronegativity of Cu is more than Zn, Cu has higher tendency to act as Lewis acid with Pn_4Q_3 as Lewis base with pnictogen atom as donor centre. That can be the possible reason for co-ordination interaction between metal halide framework and cage molecule $(Pn_4Q_3)@Cu_7M_3I_{13}$ (M= Zn, Cd, Hg; *Pn* = P, As; Q= S, Se)[49]. In order to establish this theory and to solve the crystal structure with rotating cage molecule the series were extended and thoroughly studied along with $(P_4S_3)@Zn_7SI_{12}$ in this thesis. Because of the crystalline structure of most of the compounds, it became easier to study such phenomenon such as rotation of Pn_4Q_3 molecules inside the metal halide framework. This rotation of the cage molecules is often observed in glass materials[50] in the mixture of corresponding elements but usually not in crystalline compounds.

1.1 References

[1] Ashley, K.; Cordell, D.; Mavinic, D., *Chemosphere*, (2011) **84**, 737.

[2] Schnering, H. G. von; Hoenle, W., *Chem. Rev.*, (1988) **88**, 243.

[3] Rödl, T.; Weihrich, R.; Wack, J.; Senker, J.; Pfitzner, A., *Angew. Chem. Int. Ed.*, (2011) **50**, 10996.

[4] Marggraf, A. S., *Miscell. Berolin.*, (1740) **6**, 54.

[5] Stock, A., *Ber Dtsch Chem Ges.*, (1908) **41**, 558.

[6] Stock, A., *Ber Dtsch Chem Ges.*, (1910) **43**, 150.

[7] Stock, A., *Ber Dtsch Chem Ges.*, (1910) **43**, 41.

[8] Stock, A., *Ber Dtsch Chem Ges.*, (1910) **43**, 1223.

[9] Adolf, A.; Gonsior, M.; Krossing, I., *J. Am. Chem. Soc.*, (2002) **124**, 7111.

[10] Chattopadhyay, T. K.; May, W.; Schnering, H. G. v.; Pawley, G. S., *Z. Kristallogr.*, (1983) **165**, 47.

[11] Leung, Y. C.; Waser, J.; Houten, S. V.; Vos,A., Wiegers, G. A.; Wiebenga, E. H., *Acta Crystallogr.*, (1957) **10**, 574.

[12] Gruber, H.; Müller, U., *Z. Kristallogr.*, (1997) **212**, 662.

[13] Griffin, A. M.; Minshall, P. C.; Sheldrick, G. M., *J. Chem. So., Chem. Commun.*, (1976) **43**, 809.

[14] Minshall, P. C.; Sheldrick, G. M., *Acta Crystallogr., Sect. B*, (1978) **34**, 1326.

[15] Chang, C.-C.; Haltiwanger, R. C.; Norman, A. D., *Inorg. Chem.*, (1978) **17**, 2056.

[16] Vos, A.; Olthof, R.; van Bolhuis, F.; Botterweg, R., *Acta Crystallogr.*, (1965) **19**, 864.

[17] van Houten, S.; Wiebenga, E. H., *Acta Crystallogr.*, (1957) **10**, 156.

[18] Griffin, A. M.; Sheldrick, G. M., *Acta Crystallogr., Sect. B*, (1975) **31**, 2738.

[19] Blachnik, R.; Peukert, U.; Czediwoda, A.; Engelen, B.; Boldt, K., *Z. Anorg. Allg. Chem.*, (1995) **621**, 1637.

[20] Rödl, T.; Pfitzner, A., *Z. Anorg. Allg. Chem.*, (2011) **637**, 1507.

[21] Vos, A.; Wiebenga, E. H., *Acta Crystallogr.*, (1955) **8**, 217.

[22] Dixon, D. T.; Einstein, F. W.; Penfold, B. R., *Acta Crystallogr.*, (1965) **18**, 568.

[23] Blachnik, R.; Matthiesen, J.; Müller, A.; Nowottnick, H.; Reuter, H., *Z. Kristallogr.*, (1998) **213**, 233.

[24] Bjorholm, T.; Jakobsen, H. J., *J. Am. Chem. Soc.*, (1998) **113**, 233.

[25] Nowottnick, H.; . Blachnik, R., *Z. Anorg. Allg. Chem.*, (1999) **625**, 1966.

[26] Nowottnick, H.; Blachnik, R., *Z. Anorg. Allg. Chem.*, (2000) **626**, 611.

[27] Barieux, J. J.; Demarcq, M. C., *J. Chem. So., Chem. Commun.*, (1982) **49**, 176.

[28] Jason, M.; Ngo, T.; Rahman, S., *Inorg. Chem.*, (1997) **36**, 2633.

[29] Li, Y. L.; Stavrou, E.; Zhu, Q.; Clarke, S. M.; Li, Y.; Huang, H.-M., *Phys. Rev. B*, (2019) **99**, 220503.

[30] Baldus, H. P.; Blachnik, R., *Z. Naturforsch*, (1990) **45b**, 1605.

[31] Mizuno, F.; Hayashi, A.; Tadanaga, K.; Tatsumisago, M., *Adv. Mater.*, (2005) **17**, 918.

[32] Lin, Z.; Liu, Z.; Fu, W.; Dudney, N. J.; Liang, C., *Adv. Funct. Mater.*, (2013) **23**, 1064.

[33] Yamamoto, H.; Machida, N.; Shigematsu, T., *Solid State Ion.*, (2004) **175**, 707.

[34] Sun, F.; Zhang, B.; Tang, H.; Yue, Z.; Li, X.; Yin, C.; Zhou, L., *J. Mater. Chem. A*, (2018) **6**, 10104.

[35] Li, S.; Zeng, Z.; Yang, J.; Han, Z.; Hu, W.; Wang, L.; Ma, J.; Shan, B.; Xie, J., *ACS Appl. Energy Mater.*, (2019) **2**, 2956.

[36] Chung, I.; Song, J. H.; Kim, M. G.; Malliakas, C. D.; Karst, A. L.; Freeman, A. J.; Weliky, D. P.; Kanatzidis, M. G., *J. Am. Chem. Soc.*, (2009) **131**, 16303.

[37] Binnewies, M.; Glaum, R.; Schmidt, M.; Schmidt, P., *Z. Anorg. Allg. Chem.*, (2013) **639**, 219.

[38] Blake, A. J.; Brooks, N. R.; Champness, N. R.; Hanton, L. R.; Hubberstey, P.; Schröder, M., *Pure Appl. Chem.*, (1998) **70**, 2351.

[39] Pfitzner, A.; Freudenthaler, E., *Angew. Chem. Int. Ed.*, (1995) **34**, 1647.

[40] Pfitzner, A.; Freudenthaler, E., *Z. Naturforsch. B Chem. Sci.*, (1997) **52**, 199.

[41] Pfitzner, A.; Reiser, S.; Nilges, T., *Angew. Chem. Int. Ed.*, (2000) **39**, 4160.

[42] Pfitzner, A.; Reiser, S., *Inorg. Chem.*, (1999) **38**, 2451.

[43] Deiseroth, H.-J.; Wagener, M.; Neumann, E., *Eur. J. Inorg. Chem.*, (2004) **2004**, 4755.

[44] Hong, J. H., *Dissertation*, (2004), Universität Regensburg.

[45] Bräu, M. F., *Dissertation*, (2007), Universität Regensburg.

[46] Biegerl, A.; Brunner, E.; Gröger, C.; Scheer, M.; Wachter, J.; Zabel, M., *Chem.: Eur. J*, (2007) **13**, 9270.

[47] Bräu, M. F.; Pfitzner, A., *Angew. Chem. Int. Ed.*, (2006) **45**, 4464.

[48] Pearson, R. G., *J. Am. Chem. Soc.*, (1963) **85**, 3533.

[49] Vitzthumecker, C., *Dissertation*, (2017), Universität Regensburg.

[50] Kaseman, D. C.; Gulbiten, O.; Aitken, B. G.; Sen, S., *J. Chem. Phys.*, (2016) **144**, 174501.

[51] https://roempp.thieme.de/include/images/r100/RI-152-0406.gif

2. Experimental

2.1 Chemicals

All the chemicals used for the research work are listed in table 2.1. Copper (I) iodide was purified before further use and phosphorus sesquisulfide and tetraphosphorous triselenide were synthesised in the working laboratory. The applied procedure is described later.

Table 2.1: List of chemicals used for synthesis in this thesis

Name	Formula	Purity	Company
Arsenic	As	99.0%	Chempur
Cadmium	Cd	99.5%	Chempur
Copper iodide	CuI	Recryst. from conc. HI	Merck
Ferric chloride hexahydrate	$FeCl_3.6H_2O$	99.5%	Sigma-Aldrich
Mercury iodide	HgI_2	99.0%	Merck
Iodine	I_2	99.8%	Sigma-Aldrich
Red phosphorus	P	Purified	Riedel-de Haën
Phosphorus sesquisulfide	P_4S_3	--	Synth. in lab.
Tetraphosphorous triselenide	P_4Se_3	--	Synth. in lab.
Sulphur	S	99.5%	Sigma-Aldrich
Selenium	Se	99.999%	Chempur
Tellurium	Te	99.999%	Chempur
Zinc	Zn	99.999%	Merck
Zinc iodide	ZnI_2	99.999%	Sigma-Aldrich

2.1.1 Preparation of P_4S_3

To synthesize P_4S_3, red phosphorus was first mixed with sulphur in the corresponding stoichiometric ratio and annealed at 300 °C for one week. The resulting raw product was dissolved in deionized water under constant stirring until the boiling to remove the higher phosphorus sulphides such as P_4S_7 or P_4S_{10}. As the higher phosphorus sulphides are highly sensitive to hydrolysis, they will be decomposed by refluxing. Only P_4S_3 remains as a molecular species. After filtration a greenish yellow residual solid remained. This residue is dissolved and recrystallized in toluene to get crystalline P_4S_3[1–3].

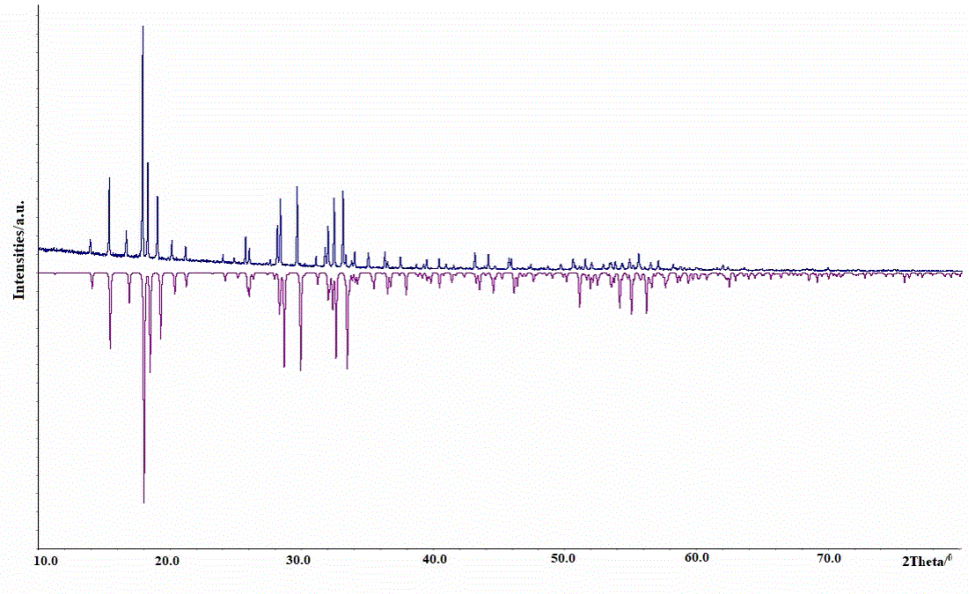

Figure 2.1 Measured powder diffractogram of P_4S_3 (blue) compared to calculated single crystal data with negative intensity (purple).

2.1.2 Purification of CuI

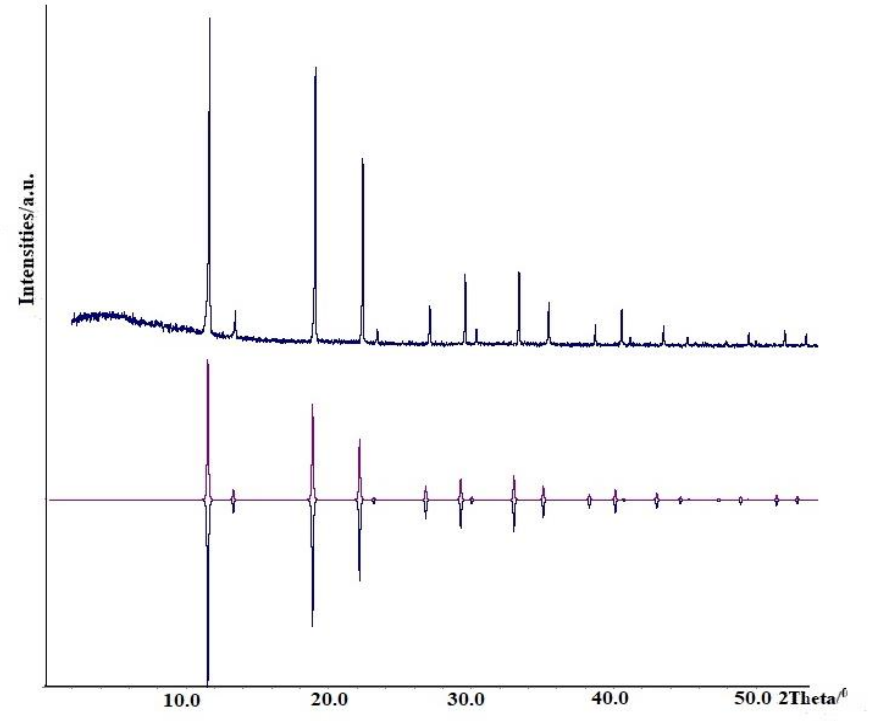

Figure 2.2: First diffractogram, Measured powder diffractogram of raw CuI (blue); second diffractogram, purified and calculated pattern of CuI (in purple and light blue respectivly)

Available copper (I) iodide usually contain impurities. For this reason, the copper (I) iodide first had to be purified. The raw CuI has purple colour. From this reason the copper (I) iodide dissolved in conc. Hydro-iodic acid, quenched with deionized water, washed several times

and under argon. Contact with atmospheric oxygen must be avoided at all costs in order to avoid oxidation reactions with Cu^{1+}. The colourless, pure copper (I)-iodide were obtained in this way[4]. Powder diffractogram of cleaned CuI shown in Figure 2.2.

2.2 Preparation techniques

In the classical solid state synthesis (solid-solid reaction), the finely powdered and well homogenized reactants are reacted with each other at high temperatures, which usually leads to the formation of thermodynamically stable products. A fundamental problem with this synthesis route, however, is the slow diffusion velocity of the atoms or ions in the solid mixture and the resulting relatively long reaction time. Much faster reactions take place when they are carried out in melts. In the process, the reactants are either melted directly or a foreign melt (flux) is added, which would release the reactants. The reaction conditions are comparable to those of the molecular or complex chemistry, where the reactions also take place in solution and where the diffusion velocities are many times higher respectively. Furthermore, very frequently used synthesis routes that avoid the problem of slow diffusion in solids are reactions via the gas phase or transport reactions. As transport agent in this context, a thermally labile precursor compound can be defined as a compound which readily decomposes at relatively low temperatures initiating the reaction. An interesting aspect of such low-temperature methods is that in this way also thermodynamically metastable connections are accessible.

For the synthesis of the polymeric phosphorus sulphides[5] anhydrous $FeCl_3$ was used as mineraliser. But after a thorough screening it was discovered that hexa-hydrated $FeCl_3$ is much better mineraliser in this purpose, possibly because of its much lower melting point 37 °C where the anhydrous one has melting point 307.6 °C. The new mineraliser also helped to synthesis a range of new and interesting phosphorus chalcogenides at 350 °C. So in order to understand why hexa-hydrated compound is better mineraliser than anhydrous one, is only the melting point concerning factor or formation of the intermediate (like HCl) is also important; a series of other material also used as mineraliser for same reactants. Low melting transition metal halides, NH_4Cl, ($NaCl+NaHSO_4$) are used to understand if the role of mineraliser is to promote the reactants to the reaction equilibrium by functioning as transport agent or water and $FeCl_3$ react and form intermediate HCl which in turn catalysed the reaction respectively. But in none of the cases desired product was obtained. One thing can be calculated from here, not only mineraliser (with low m. p.) is important for this reaction

but also Fe^{3+} has some significant effect on it. Control reaction without mineraliser for phosphorus chalcogenides containing selenium resulted into glassy materials and for reactions containing tellurium resulted into mixture of unreacted tellurium and other phosphorus chalcogenide intermediate.

2.2.1 Preparation in ampoules

For the execution of classical solid state syntheses, the starting materials were weighed on an analytical balance (Kern; accuracy 0.1 mg). For air-sensitive samples, an analytical balance (Sartorius; accuracy 0.1 mg) was used in the of an argon glove box for weighing. Then the corresponding reactants were ground thoroughly in an agate mortar and poured into quartz glass ampoules or quartz ampoules for short. The ampoules were heated at 140 °C before use in order to remove the moisture before pouring the reaction mixture in it. The ampoule was then rinsed several times with argon to remove the air completely and finally evacuated to a pressure < 3.5×10^{-2} mbar. Subsequently the ampoules were melted with a hydrogen-oxygen forced-air burner. Annealing of the samples is carried out in tube furnaces according to the specified temperature profiles. After cooling down to room temperature, the ampoules were treated and if necessary under inert gas environment in glove box.

2.3 Instrumental techniques

2.3.1 Single crystal X-ray diffraction measurement

In order to determine the crystal structures of the resulting compounds X-ray examinations were carried out on suitable single crystals. Suitable single crystals were selected under a light microscope and data measurement was carried out on a four-circle diffractometer (supernova) from Rigaku. Also, Xcalibur, AtlasS2, Gemini ultra-diffractometer was used for single crystal measurement. The diffractometer is equipped with a microfocus molybdenum X-ray tube (λ = 0.71073 Å) and an EOS CCD detector. The crystals, surrounded by an inert, colorless transparent mineral oil (Sigma Aldrich, CAS 8042-47-5), were attached to a "CryoLoop" (diameter 0.1 - 1.0 mm) of Hampton Research. The subsequent data collection was carried out either at room temperature or -150 °C or -50 °C. The crystals were cooled with an Oxford cryosystem by a nitrogen stream to prevent the crystals from potential decomposition at air over time during the measurement.

The analysis and integration of the obtained data was performed with the CrysAlisPro software[6] The correction of Lorentz and polarization effects as well as an analytical

absorption correction based on the crystal shape was also performed with the CrysAlisPro software. The spatial groups of the measured compounds were determined directly with the CrysAlisPro software or with the Jana2006 software package[7]. The crystal structures were dissolved using charge flipping methods (Superflip)[8]. The subsequent refinement of the obtained structure models was carried out by successive Fourier syntheses and least-squares methods (full matrix versus F^2) using the programs Jana2006[8] The obtained crystal structures were examined for unconsidered symmetry elements (ADDSYM) and twinnings (TwinRotMat) using the program package PLATON[9] To visualize the crystal structures discussed in this thesis, the program Diamond[10] of Crystal Impact was used and all displacement ellipsoids are shown with a probability factor of 90%.

2.3.2 Powder diffraction

X-ray examinations of finely powdered samples were performed on two STOE Stadi P X-ray powder diffractometers. Alternatively, copper or molybdenum radiation ($\lambda_{(Cu\text{-}K\alpha1)}$ = 1.540598 Å, $\lambda_{(Mo\text{-}\ K\alpha1)}$ = 0.70930 Å) could be used with monochromatized (Ge[111] single crystal) radiation. The intensities of the diffracted X-rays were measured in transmission geometry using a Dectris Mythen 1K detector ($\Delta\theta = 0.015°$, $2° \leq 2\theta \leq 126°$) at variable exposure times. The samples, finely powdered with an agate mortar, were fixed between two Mylar foils with Baysilone paste on flat bed carriers. Air-sensitive samples were measured in sealed glass capillaries (quartz or borosilicate glass; outer diameter 0.5 - 0.3 mm).

The WinXPOW software[11] from STOE & Cie was used to evaluate the diffractograms obtained. The obtained reflexes were indexed by common indexing algorithms (TREOR[12], ITO[13], DICVOL[14]). Fundamental parameters of the diffractometer were used to adjust asymmetries of the measured reflexes caused by grain size and stress effects. During refinement, the parameters of a calculated diffractogram (cell parameters, background, and profile parameters) were varied according to the method of the smallest error squares until the difference between the measured and calculated diffractogram was as small as possible.

2.3.3 Vibration Spectroscopy

To study bonding and non-bonding interaction in the compounds Raman spectroscopy is a very important tool. Air-sensitive samples was powdered and filled in Duran glass capillaries in Glove box and sealed with hydrogen-oxygen flame. The measurements were conducted on a DXR^{TM} SmartRaman spectrometer from Thermoscientific (excitation wavelength λ = 780

nm) with a resolution of 0.5 cm^{-1}. The baseline correction and smoothing of the spectra were performed with the software package OMNIC[15].

The Raman measurements were performed on a self-made Raman spectrometer in cooperation with Prof. Dr. Alkwin Slenczka on piece of crystalline samples for air stable compounds. The spectroscopy is equipped with coaxial guided laser beam and 35 mW HeNe laser was used. Grating spectrograph (1800/mm) equipped with CCD camera (Andor).

2.3.4 UV-vis Spectroscopy

The band gaps of the investigated substances were determined by diffuse reflection spectroscopy (DRS). Therefore, the measurement of the solid-state UV-VIS spectra were performed with an Omega 20 spectral photometer from Bruins Instruments, controlled by the program OMEGA[16]. Diffuse reflection or remission generally describes the sum of the individual phenomena of reflection, refraction, diffraction and absorption of light on a matt surface in all spatial directions. The Kubelka-Munk theory[17] was applied to determine the absorption behavior of the investigated substances. The Kubelka-Munk function (equation 2.1) describes the relationship between R_∞, the remission versus a non-absorbent standard ($BaSO_4$), the absorption coefficient *K*, and the scattering coefficient *S*.

An Omega 20 spectrophotometer from Bruins Instruments was used to record reflectance spectra of the samples. The powdered samples were mixed with a white standard ($BaSO_4$) and pressed on a metal carrier to a thin layer (2 mm). The reference substance (100 % reflection) was pure $BaSO_4$. The light reflected from the sample surface was collected by an integrating sphere and transmitted to the detector. The photometer was controlled using the OMEGA program. The obtained reflectance spectra were transformed into absorption spectra by the Kubelka-Munk transformation. To characterize air-sensitive samples, the spectrometer was placed in a Plexiglas box flooded with nitrogen. From the root of the product of the Kubelka-Munk function and the photon energy E plotted against the photon energy (modified Kubelka-Munk function[18], equation 2.2), the optical band gaps E_g could finally be determined by extrapolation of the linear tangent.

$$\frac{K}{S} = \frac{(1 - R\infty)^2}{2R\infty} = f\,(\mathrm{R}\infty) \qquad 2.1$$

$$\sqrt{(f(\mathrm{R}\infty) * E)} = E\ -\ E\mathrm{g} \qquad 2.2$$

2.3.5 Thermal analysis

Various methods of thermal analysis were used to analyse the thermal behaviour of the samples. Differential thermal analysis (DTA) was used to determine the melting point. The temperature difference between the sample and a reference substance (Al_2O_3) during heating and cooling was measured. When a melting process occurs, a temperature difference occurs, which is registered as a measurement signal. Thermo-gravimetric detects the mass of a sample during heating. The mass of the sample decreases, for example, when water is lost or organic components decompose. Both analysis methods were performed on a SETARAM TG-DTA 92.16.18. The samples of the thermogravimetric analysis were placed in a corundum crucible while the weak current heating the crucible. For differential thermal analysis, the samples were melted into thin quartz ampoules (inner diameter 2 mm). The measurements were made in the temperature range 25-900 °C with variable heating rates (standard: 10 °C/min).

2.3.6 Scanning Electro-Microscopy (SEM) and Electron Dispersive X-ray spectroscopy (EDS)

Using a Zeiss DSM 950 scanning electron microscope (SEM), the surface morphology of selected crystallites compounds was investigated in special cases. The EDS was measured for all the compounds with the same instrument. In the inclusion compounds to support the composition from XRD data for the cage molecules and for phosphorus chalcogenides to determine the ratio of phosphorus and sulphur EDS measurement was an important technique. The acceleration voltage at a variable distance to the sample was 25 kV in all cases. In order to ensure a continuous conductivity of the samples, they were previously coated with carbon.

2.3.7 Solid State NMR Spectroscopy

Solid State NMR of $(P_4S_3)@Zn_7SI_{12}$ was measured and evaluated in collaboration with Prof. Jörn Schmedt auf der Günne. The experiments were conducted in the Chair of Prof. Schmedt auf der Günne. For all the solid-state NMR measurements the ^1H resonance of 1 % $Si(CH_3)_4$ in $CDCl_3$ served as an external secondary reference using the Ξ values for ^{31}P as reported by the IUPAC[19]. The magic angle spinning (MAS) rotors (3.2 mm, ZrO_2) were packed in a glove box under argon atmosphere. The ^{31}P MAS NMR measurements were carried out on a Bruker Avance Neo NMR spectrometer at a frequency of 242.96 MHz (B_0 = 14.1 T) with a

commercial 3.2 mm MAS probe at spinning frequencies of ν_{rot} = 20 kHz and ν_{rot} = 1.8 kHz. The static variable temperature (VT) ^{31}P NMR measurements were carried out on a Bruker Avance Neo NMR spectrometer at a frequency of 242.96 MHz (B_0 = 14.1 T) with a commercial static SOL5 probe in an evacuated quartz ampule (d = 3 mm). The analysis and fitting of the spectra was done with Deconv2Dxy-0.4[20] and Simpson-3.1.2[21].

In cooperation with Prof. Dr. Jürgen Senker solid state NMR spectra of P_2S_6Te were recorded and evaluated at the Chair of Prof. Senker. The spectra were recorded on a Bruker Avance-III HD spectrometer. The Fourier transform of this measurement results in a spikelet spectrum similar to an ordinary MAS-NMR spectrum.

2.4 References

[1] Leung, Y. C.; Waser, J., *Acta Cryst*. (1957) **10**, 574.

[2] Blachnik, R.; Hoppe, A., *Z. Anorg. Allg. Chem.*, (1979) **457**, 91.

[3] Brauer, G., *Handbuch der Präperativen Anorganischen Chemie*, (1975).

[4] Pfitzner, A., *Chem. Eur. J.*, (2000) **6**, 1891.

[5] Rödl, T.; Weihrich, R.; Wack, J.; Senker, J.; Pfitzner, A., *Angew. Chem. Int. Ed*, (2011) **50**, 10996.

[6] CrysAlisPro, Agilent Technologies, Version 1.171.38.37b.

[7] Petříček, V.; Dušek, M.; Palatinus, L., *Z. Kristallogr. Cryst. Mater.*, (2014) **229**.

[8] Palatinus, L.; Chapuis, G., *J. Appl. Crystallogr.*, (2007) **40**, 786.

[9] Spek, A. L., *J. Appl. Crystallogr.*, (2003) **36**, 7.

[10] Diamond Version 4, *Crystal Impact GbR, Bonn*, (2010).

[11] "STOE WinXPOW, Version 1.08, STOE & Cie GmbH, Darmstadt", (2000).

[12] Werner, P. E.; Eriksson, L.; Westdahl, M., *J. Appl. Crystallogr.*, (1985) **18**, 367.

[13] Visser, J. W., *J. Appl. Crystallogr.*, (1969) **2**, 89.

[14] Boultif, A.; Louër, D., *J Appl Crystallogr*, (1991) **24**, 987.

[15] V. OMNIC 9, Thermo Fisher Scientific, Waltham, (2012).

[16] V. OMEGA, Bruins Instruments, Puchheim, (2004).

[17] Kubelka, P.; Munk, F., *Z. Techn. Physik*, (1931) **12**, 593.

[18] Kisch, H., *Angew. Chem. Int. Ed*, (2013), **52**, 812.

[19] Harris, R. K.; Becker, E. D.; Menezes, S. M. C.; Granger, P.; Hoffman, R. E.; Zilm, K. W.; *Magn. Reson. Chem.*, (2008) **46**, 582.

[20] Jardón-Álvarez, D.; Schmedt auf der Günne, J.; *Solid State Nucl. Magn. Reson.*, (2018) **94**, 26.

[21] Bak, M.; Rasmussen, J. T.; Nielsen, N. C.; *J. Magn. Reson.*, (2000) **147**, 296.

3. Phosphorus polychalcogenides

Century-old phosphorus chalcogenide chemistry is always an unpredictable and messy yet a fascinating affair. Marggraf[1], in 1740, first performed the reaction between elemental phosphorus and sulphur at an elevated temperature. Stock first rationalise these vigorous, and almost explosive reactions by synthesising P_4S_3, P_4S_7, P_4S_{10}. Later, various other P_4S_n (n=4, 5, 6, 8 and 9) compounds were synthesised. But all these structures can be derived from P_4 tetrahedra structure by introducing S in the P-P bonds, or exocyclic addition of sulphur on P atoms. $P_{14}S$[2] and P_2S_7[3] are only two compounds that posses diverse structure in comparison to traditional cage like structure of phosphorus sulphides. Phosphorus chalcogenide compounds are well-studied due to their use in potential materials in catalysis, energy applications, semiconducting devices, phase-change materials, and nonlinear optics[4]. Selenium and tellurium are getting attention for their potential use in photoelectric cells[5,6]. Phosphorus doped sulpho-selenides are being extensively used in nanotechnology, for example quantum dots of CdSSe in thin film[7] or as photo-voltaic absorber[8]. Additionally, selenium reduces the toxicity of many metals such as lead, silver, copper, mercury, cadmium, and arsenic. In order to synthesise phosphorus mix chalcogenides, Havel and co-workers used laser ablation technology[9]. They synthesised various ternary species containing phosphorus, sulphur and selenium starting from various precursors. P_4S_3 and grey Se were the most successful starting materials. Although these experiments are only successful to produce few molecules for mass spectrometry, there is only one mix phosphor-seleno-sulphide solid solution system exists to our knowledge[10] and no report about phosphorus mix-chalcogenides containing tellurium. Few phosphorus polychalcogenide ionic species[11,12][13][14][15] stabilised by cations or anions in stable or meta-stable compounds were found in the literature. However, we were able to synthesise and characterise a range of stable and neutral phosphorus poly-chalcogenides containing sulphur, selenium, and tellurium.

3.1 Phosphorus selenium sulphide, P_2S_6Se

Starting from P_4Se_3 and sulphur as precursor, with catalytic amount of hexa-hydrated $FeCl_3$ three compounds were prepared; α-P_2S_6Se and β-P_2S_6Se and $P_2S_{6.4}Se_{0.6}$. α-P_2S_6Se and β-P_2S_6Se are always derived as mixture from a single reaction.

3.1.1 Synthesis

For synthesis of α-P_2S_6Se and β-P_2S_6Se stoichiometric quantities of P_4Se_3 and sulphur, and catalytic amounts of $FeCl_3$•$6H_2O$ (5 wt% of reactants) were grinded and heated to 350°C with a heating rate 0.2°C/min in an evacuated quartz ampoule and annealed at the same temperature for 10 days. Reaction at 250°C yielded very few crystals of the products. Then the ampoule was cooled down slowly. Optically indistinguishable orange colour crystals of α-P_2S_6Se and β-P_2S_6Se were obtained as a mixture from the ampoule. This compound is stable in air for 1-2 days. These crystals are insoluble in almost all organic solvent and dissociate in water. P_2S_6Se is stored in glove box under argon gas environment. $FeCl_3$•$6H_2O$ most probably servers the role of mineraliser[16–18]. Reaction using anhydrous $FeCl_3$ as mineraliser resulted into nothing but glassy mixture. Other hydrated transition metal halides

Figure 3.1.1: Crystals of P_2S_6Se under microscope

with melting point in same range as $FeCl_3$•$6H_2O$ (m.p. 37°C[19]) did not yield any product. Metal halide as mineraliser usually act as reaction promoter[20]. It promotes kinetically-controlled gas phase interactions and short range transport reactions[21]. Melting point of anhydrous $FeCl_3$ is 307.6°C where melting point of hexahydrate $FeCl_3$ is only 37°C. So product formation at 250°C established that low melting mineraliser initiate the reaction by transporting precursor species to gas phase. Melting point must not be the only factor in this case. Otherwise other low melting point mineraliser should also work for the reaction.

3.1.2 Single crystal measurement

Crystals of α-P_2S_6Se and β-P_2S_6Se were separated only by screening under single crystal x-rays. Needle like crystals are stack together to form a big transparent crystal. Similar to P_2S_7, α-P_2S_6Se crystallises in monoclinic space group $P2_1/c$ (no. 14) with a = 6.4779(3) Å, b = 10.5778(9) Å, c = 12.7251(7) Å, β = 93.47(0)°, V= 870.35(10) Å^3, and Z = 4 where β-P_2S_6Se crystallises in triclinic space group $P\bar{1}$ with a = 6.0620(7) Å, b = 6.4765(6) Å, c = 11.2665(15) Å, α = 83.31(1)°, β = 89.29(1)°, γ = 85.06(1)°, V= 437.69(9) Å^3 and Z= 2. The exact composition of α-P_2S_6Se is $P_2S_{5.85}Se_{1.15}$ where β-P_2S_6Se is $P_2S_{5.93}Se_{1.07}$ calculated from single crystal XRD data. All the crystallographic data and measurement parameters are listed in Table 3.1.1. The atom coordinates and equivalent isotropic displacement parameters for the final structure solution are listed in Table S3.1 and Table S3.4. The anisotropic displacement parameters are listed in Table S3.2 and Table S3.5. There is also an overview of the bond lengths and angles are given in Table S3.3 and Table S3.6. All crystallographic data in the appendix are derived from the refinement in the $P2_1/c$ space group for α-P_2S_6Se and $P\bar{1}$ for β-P_2S_6Se at 123 K. Crystal structures of two phases of P_2S_6Se were isostructural with two corresponding modifications of P_2S_7. The basic crystal structures for both compounds are shown in Figure 3.1.2.

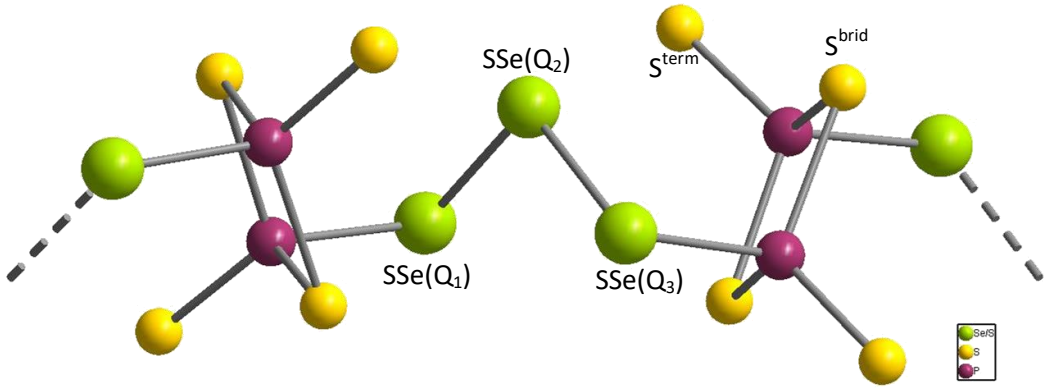

Figure 3.3.2: Repeating unit of α-P_2S_6Se and β-P_2S_6Se. Q_1, Q_2, and Q_3 are occupied by selenium by 20%, 79% and 17% of total occupancy in α-modification and 15%, 72% and 21% in β-modification.

In P_2S_7 the P atom is tetrahedrally coordinated to S atoms and 2 of these PS_4 unit share one edge forming P_2S_6 unit which are connected by one S atom ultimately forming S-S-S bridge. In P_2S_6Se**,** this poly chalcogen bridge, between two P, is mixed occupied by two sulphur and one selenium atoms, can be denoted by Q_1-Q_2-Q_3. Comparing with P_2S_7, substitution of S

Table 3.1.1: Crystallographic data and measurement parameters of α-P_2S_6Se and β-P_2S_6Se

Compound name	**α-P_2S_6Se**	**β-P_2S_6Se**
Empirical formula	$P_2S_{5.85}Se_{1.15}$	$P_2S_{5.93}Se_{1.07}$
Formula weight, g mol^{-1}	333.30	333.30
Crystal colour and shape	Orange, needle-like	Orange, needle-like
Crystal system	monoclinic	triclinic
Space group	*$P2_1/c$ (No. 14)*	*$P\bar{1}$ (No. 2)*
a, Å	6.4779(3)	6.0620(7)
b, Å	10.5778(9)	6.4765(6)
c, Å	12.7251(7)	11.2665(15)
α/^{o}		83.313(9)
β/^{o}	93.469(4)	89.295(10)
γ/^{o}		85.063(9)
V, Å^3; *Z*	870.4(1), 4	437.7(1), 2
Absorption coefficient , mm^{-1}	6.031	5.996
ρ_{calc} , g cm^{-3}	2.543	2.528
Diffractometer	Rigaku Super Nova	
Radiation	MoK_α, λ = 0.71073 Å	
Temperature, K	125	125
θ-range, ^{o}	3.15-31.15	3.62-28.66
hkl-range	$-8 \le h \le 9$	$-8 \le h \le 8$
	$-15 \le k \le 15$	$-8 \le k \le 8$
	$-17 \le l \le 18$	$-14 \le l \le 14$
Absorption correction	numerical (gaussisan)	
Number of reflections	14022	3787
Independent reflections	2611	1977
R_{int}	0.04	0.05
Structure solution	Charge flipping, Superflip	
Structure refinement	*JANA2006*	
Completeness to θ_{max}	96.9%	80%
Parameters	82	82
GooF	1.54	1.56
R_1, wR_2 *[I>2σ(I)]*	0.0250, 0.0309	0.0420, 0.0521
R_1, wR_2 [all reflections]	0.0385, 0.0329	0.0477, 0.0502
Residual electron density, e Å^{-3}	-0.52/0.58	-0.53/0.85

atoms with selenium took place only in the bridging segment in P_2S_6Se, resulting two types of pure sulphur atom in the structure, S^{brid} (bridging sulphur between two phosphorus atoms) and S^{term} (terminal sulphur attached to phosphorus atom). See Figure 3.1.1. The oxidation state of S^{brid} and S^{term} are –I and –II respectively. In the bridging unit Q_1-Q_2-Q_3, $Q_1 = Q_3 = –I$ and $Q_2 = 0$ and phosphorus has an oxidation state of +V. Phosphorus atom, S^{brid} and S^{term} are refined freely where the three positions in the bridge were refined by splitting each position between sulphur and selenium. After refinement, in α-P_2S_6Se one terminal position(Q_1) of the bridge is around 80% and 20% occupied by S and Se respectively when the other end of the bridge(Q_3) it is 83% occupied by sulphur and rest by selenium. And the central position (Q_2), occupation is reversed i.e. 79% by Se and 21% by S. In β–modification Q_1 position is occupied by 85% and 15% by S and Se; Q_2 by 28% and 72% of S and Se and Q_3 by 79% and 21% by S and Se respectively. The Polymeric strands are stack with each other by week van der waal interaction. Except for minimal differences in the bond lengths and angles the polymers in α-P_2S_6Se and β-P_2S_6Se are identical. Bond distance and bond length of $P_2(S^{brid})_2(S^{brid})_2$ [P_2S_4 unit] unit is comparable to P_2S_7 as shown in Table 3.1.2.

Table 3.1.2: Selected bond distances (Å) and bond angle (^{o}) of α- and β- modifications and their comparison with phases of P_2S_7

	α-P_2S_6Se	**β-P_2S_6Se**	**α-P_2S_7**	**β-P_2S_7**
P-S^{term}	1.919(1)-1.926(1)	1.911(1)-1.922(1)	1.914(2)- 1.916(2)	1.912(1)- 1.919(1)
P-S^{brid}	2.122(1)-2.126(1)	2.114(1)- 2.120(1)	2.110(2)- 2.122(2)	2.113(1)- 2.122(1)
P-Q_1	2.135(1)	2.119(1)- 2.134(1)	2.099(2)- 2.101(2)	2.100(1)- 2.102(1)
Q_1-Q_2	2.217(8)	2.201(1)	-	-
Q_3-Q_2	2.204(5)	2.196(1)	-	-
S^{term}-Q_2 (inter-polymeric)	3.229(1)	3.277(3)	3.30	3.30
∠Q_1-Q_2-Q_3	102.37(1)	102.58(5)	106.87(7)	105.84(5)

Maximum similarity of Q_1-Q_2-Q_3 unit is with S_6Se_2[22] with crown structure. Mixed-chalcogen bond distance in Q_1-Q_2-Q_3 unit of both structures is between 2.200(6)-2.217(6) Å which in good agreement with mix SSe-SSe[22,23] distances. The ∠Q_1-Q_2-Q_3 is 102.37(1)^o for α-P_2S_6Se and 102.58(5)^o for β-P_2S_6Se. Though similar bond angle in S_6Se_2 is much higher,

105.45(29)°. P-Q_1 and P-Q_3 distances are 2.136(1) Å and 2.135(1) Å in α-P_2S_6Se and 2.120(3) Å and 2.134(3) Å in β-P_2S_6Se respectively. As expected, the distances between phosphorus and terminal sulfur atoms are d(P-S^{term}) significantly shorter than those between phosphorus and bridging sulfur atoms d(P-S^{brid}). They are $1.919(1) \leq d(P\text{-}S^{term}) \leq 1.926(2)$ Å and $2.114(2) \leq d(P\text{-}S^{brid}) \leq 2.126(2)$ Å, corresponding to a formal phosphorus-sulphur double bond or of a single bond. The slight decrease in bond distances in β-modification is expected because of reduce in amount of selenium, as seen in Table 3.1.2. Even though the polymeric

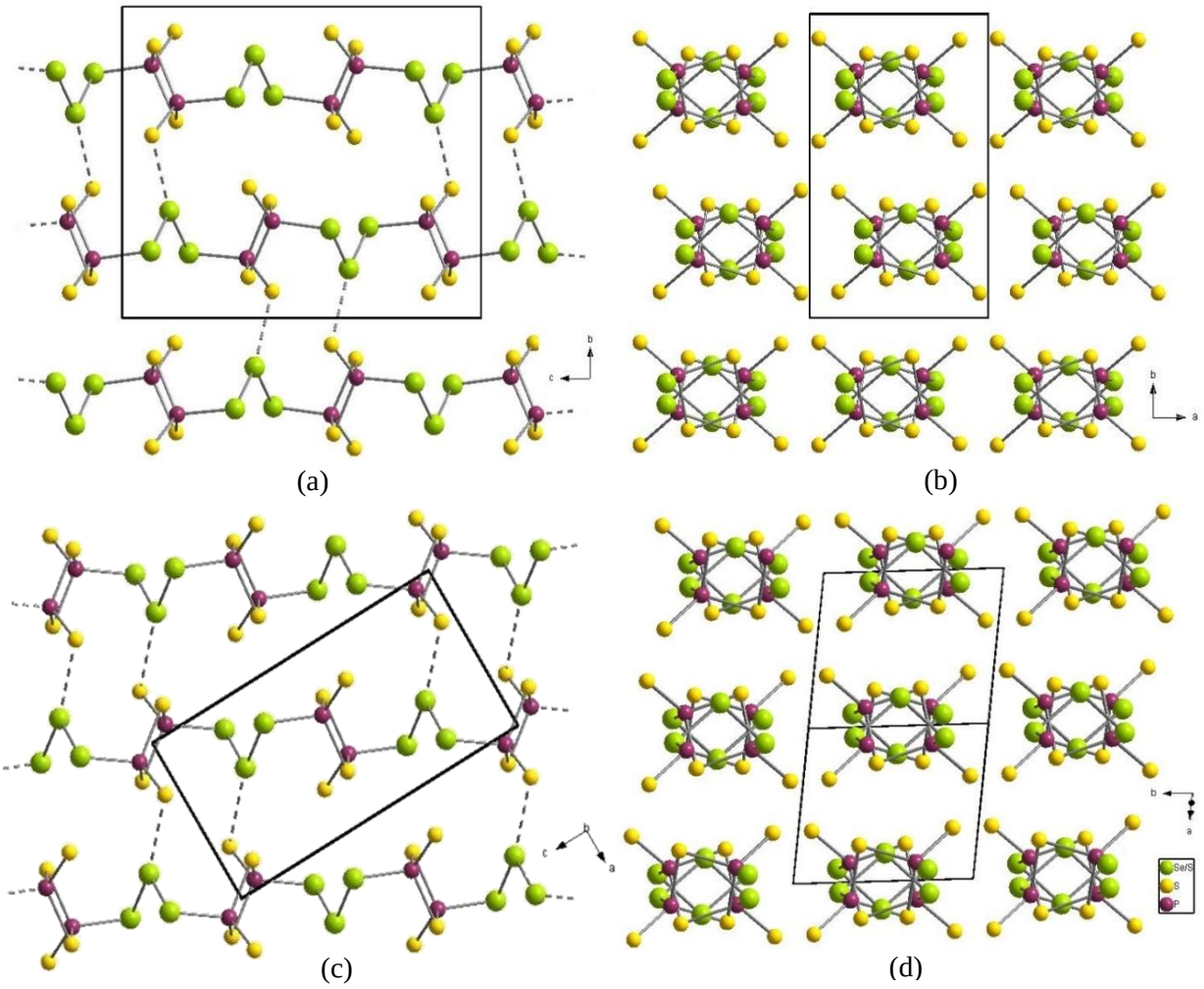

Figure 3.1.3: Crystal structures with parallel view of the polymer axis where long dashed lines represent short inter-polymeric distances between S^{term}-Q_2 which is 3.229 Å and 3.277(8) Å for (a) α-P_2S_6Se and (c) β-P_2S_6Se. (b) and (d) show the non ideal tetragonal packing of α-P_2S_6Se and β-P_2S_6Se respectively

strands of two modifications are almost identical but there is one difference. Unlike α-P_2S_7 and β-P_2S_7 both modifications of P_2S_6Se show same distorted or non-ideal tetragonal packing shown in Figure 3.1.3. No packing polymorphism is observed here. In both modifications the polymer rods are packed in non-ideal tetragonal packing. The introduction of the selenium in the structure is responsible for this. The heavier chalcogen atom- selenium has significant effect on inter-polymeric interaction. With the increase in amount of heavier chalcogen atom in the bridging unit inter-polymeric distance decreases which ultimately also affects packing effectively. The minimum inter-polymeric distance (S^{term}-Q_2) is 3.229(1)-3.277(3) Å which is shorter than P_2S_7 even though bigger selenium atom in Q_2 position which can be described as non-formal chalcogen bond. This Phenomenon is discussed in details later in Section 3.5. In P_2S_4 unit, one S^{term} has this chalcogen bond with the neighbouring polymer where other S^{term} does not as can be seen in Figure 3.1.3(a) and (c). S^{term} atom with chalcogen bond has little longer P-S^{term} distance than the other one. α-P_2S_6Se shows a little higher calculated density ($\rho_{X\text{-}ray}$=2.5434 gcm^{-3}) and translational periodicity (d_{mean}), 12.725 Å than β-P_2S_6Se with calculated density ($\rho_{X\text{-}ray}$=2.5288 gcm^{-3}) and translational periodicity (d_{mean}), 12.720 Å. All these are also explained explicitly in 3.5.

3.1.3 Powder XRD

α-P_2S_6Se and β-P_2S_6Se can not be separated for powder XRD measurement synthesis route. The corresponding powder diffractogram is shown in Figure 3.1.4 of mixture of both modifications. For comparison, the single crystal data were used to create a calculated

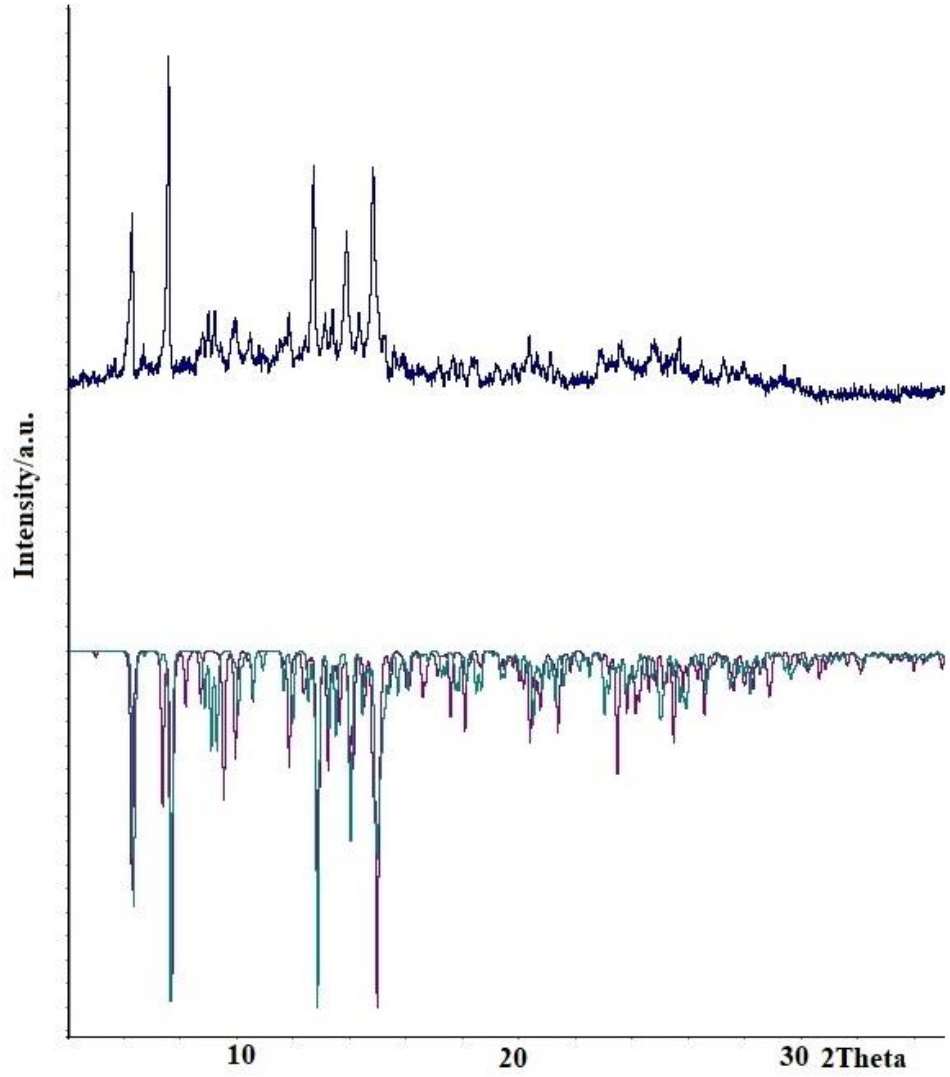

Figure 3.1.4: Measured powder diffractogram of mixture of α-P_2S_6Se and β-P_2S_6Se (positive intersities); blue diffractogram for calculated pattern of α-P_2S_6Se and purple diffractogram for the calculated pattern of β-P_2S_6Se derived from SCXRD data (negative intensities)

diffractogram. The measured diffractogram has very high background due of fluorescence. It can be seen, apart from the phosphorus selenium sulphides, no other crystalline products were created. However, the indexing of the diffractogram is somewhat problematic due to numerous overlapping reflections and high background. Especially at larger diffraction angles, the assignment of individual reflections to the respective compound significantly more difficult.

3.1.4 Thermal analysis

Thermal analysis (DTA) was done for mixture of α and β modifications. This analysis gives incite about the importance of the mineraliser and melting point of the compound. The 1st heating cycle showed a broad endothermic peak at 283°C as shown in Figure 3.1.5. Although subsequent heating cycle does not show any endothermic change upto 800°C indicating no compound formation after the cooling of the melted substance because of the absence of the mineraliser. Evidently in the second heating there is no endothermic peak.

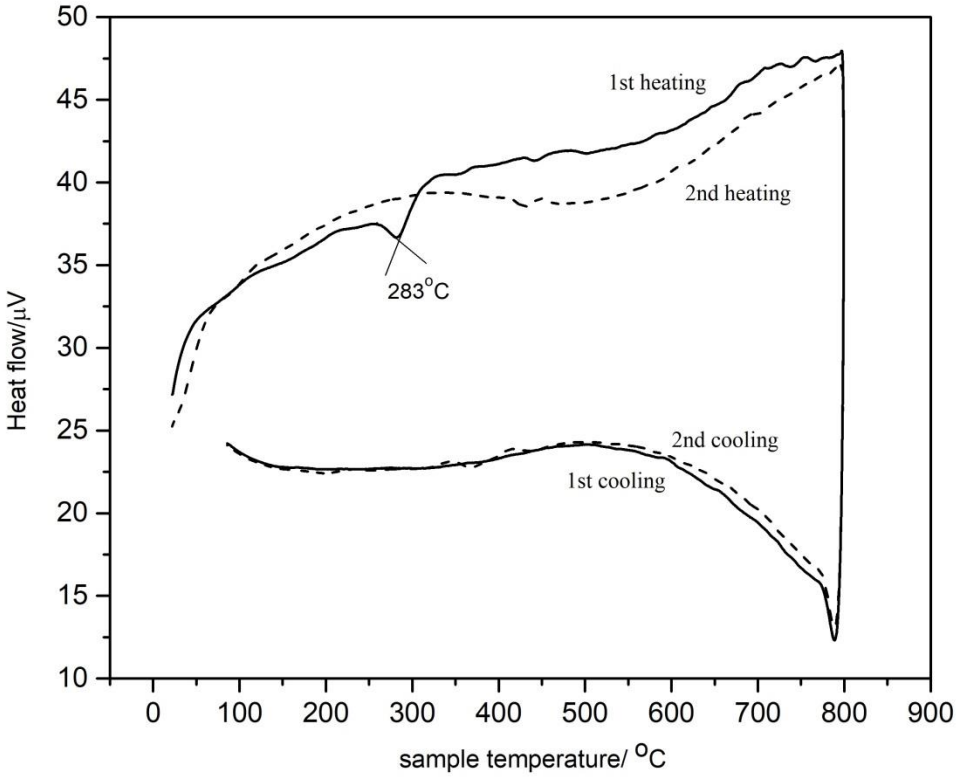

Figure 3.1.5: DTA measurement of mixture of α-P_2S_6Se and β-P_2S_6Se. The measurement was in the temperature range from 25 °C to 800 °C with a heating rate of 10 °C/min. Curves with full line denote first heating and cooling cycle and curves with dotted line denote second heating and cooling cycle.

3.1.5 SEM-EDS measurement

Scanning electron microscopy shows same fibrous morphology for all the compounds like P_2S_7. See Figure 3.1.6. The elemental analysis was done with crystals of α-P_2S_6Se which were screened by single crystal XRD measurement. The theoretical calculation of chemical composition from SCXRD matched almost perfectly with measured composition by elemental analysis of EDS. As shown in Table 3.1.3. The standard deviation is within 5%.

Table 3.1.3 Atomic percentage of α-P_2S_6Se from SEM-EDS measurement and theoretical value calculated from SCXRD

Elements (atom %)	P	S	Se
Calculated (SCXRD)	22.22	65.00	12.78
Measured (EDS)	22.42	64.84	12.73

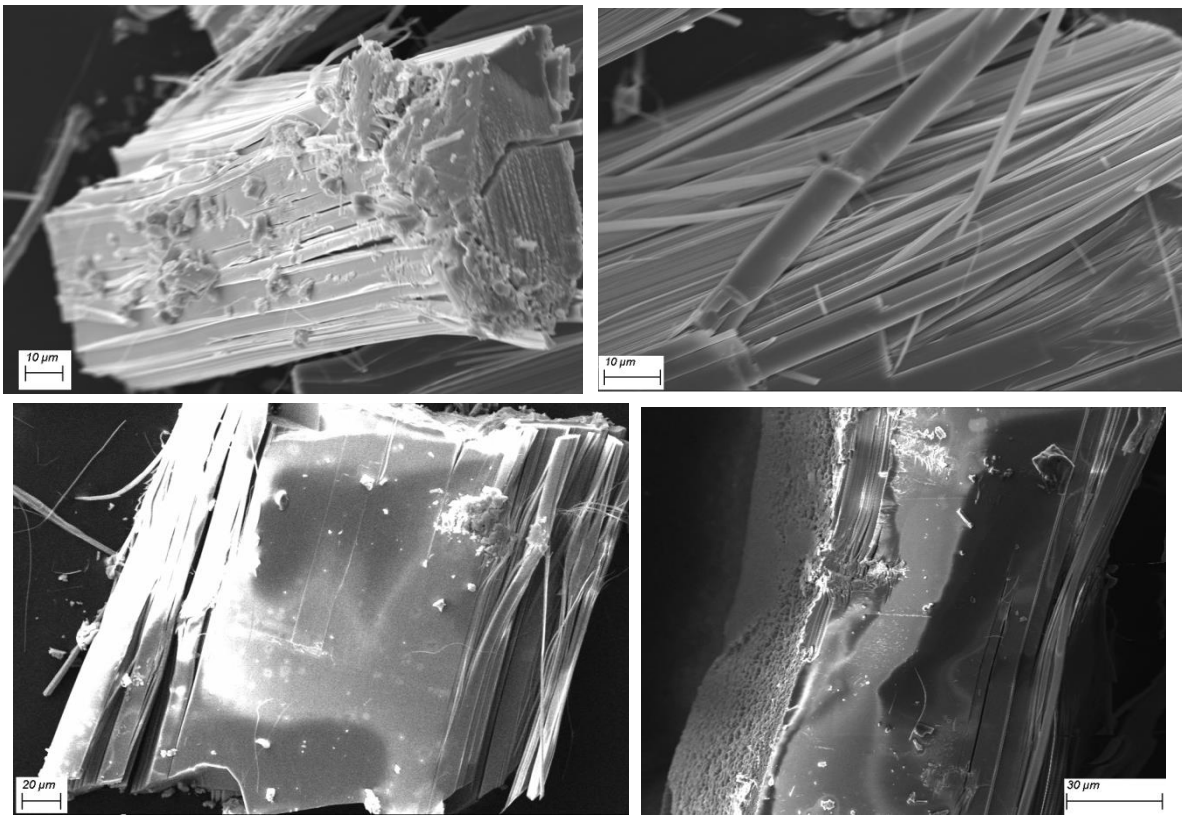

Figure 3.1.6: SEM pictures of P_2S_6Se showcasing fibrous morphology of the compound. The pictures showed that a big crystal is actually association of numerous polymeric units

3.1.6 Raman Spectroscopy

Mixture of the both modifications was measured for Raman spectroscopy. The measured data in Figure 3.1.7 and possible assignment of the Raman bands is demonstrated in Table 3.1.4. Numerous sharp bands are evidence of the high level of crystallinity of the sample and again

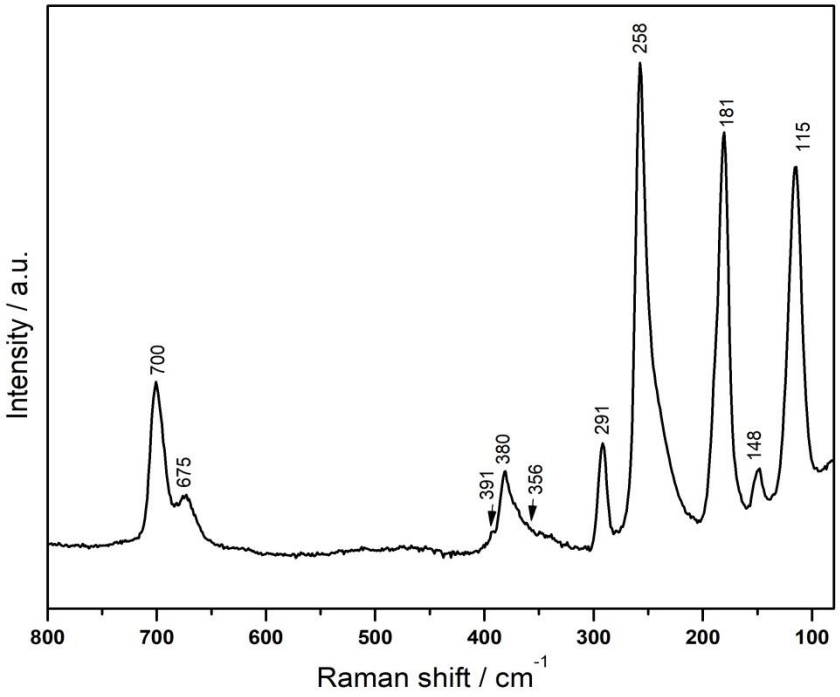

Figure 3.1.7: Raman spectrum of mixture of α-P_2S_6Se and β-P_2S_6Se

Table 3.1.4: List of peaks of Raman spectrum of mixture of α-P_2S_6Se and β-P_2S_6Se

Wavenumbers (cm^{-1})	**Intensity**	**P_2S_6Se**
700	s	ν(P-S^{term})
675	w	ν (P-S^{term})
391	w	ν (P2S2-Ring)
380	ms	ν (Q_1-Q_2-Q_3 bridging unit)
356	sh	ν (Q_1-Q_2-Q_3 bridging unit)
291	vs	ν (Q_1-Q_2-Q_3 bridging unit)
258	S, broad	ν (Q_1-Q_2-Q_3 bridging unit)
181	s	δ
148	w	δ
115	s	δ

w= weak, ms= medium strong, s= strong, vs=very strong, sh=shoulder

illustrate the influence of the mineralizer. The spectrum can be roughly divided into four areas: firstly, from 700-675 cm^{-1} with the P-S stretching oscillations of terminal bound sulphur atoms, secondly, at 391 cm^{-1} for P2S2 ring; thirdly, 380-258 cm^{-1} for Q_1-Q_2-Q_3 bridging unit and finally the range of the deformation oscillations below 258 cm^{-1}. The peak from interaction between P an S of the bridging unit is expected to be appeared around 510-495 cm^{-1} from theoretical calculations but those peaks are absent or a little hump can be observed which may be caused by very high intensity of other peaks at lower frequencies. Further explanation on peak shift and effect of heavier atoms are described in Section 3.5.

3.1.7 UV-vis spectroscopy

The UV-vis measurement was performed for mixture of both modifications of P_2S_6Se. Calculated band gap for α–P_2S_6Se and β–P_2S_6Se are 1.52 eV and 1.32 eV where the measured value is 2.1 eV. This discrepancy in calculated and measured value was also observed in P_2S_7[3].The orange colour of the crystals indicates smaller band gap than green coloured crystals of P_2S_7 which is supported by measured data.

3.2 Phosphorus selenium sulphides, $P_2S_{6.36}Se_{0.64}$

$P_2S_{6.36}Se_{0.64}$, the selenium poor compound was prepared to examine ordered S-Se bond and for better understanding of the phosphorus chalcogen bonding behaviour compared to P_2S_6Se so that instead of distributed along the three member chalcogen bridge selenium only confined to the middle position of the bridge.

3.2.1 Synthesis

For synthesis of $P_2S_{6.36}Se_{0.64}$, excess amount of sulphur (0.32 gm, 0.01 mole) is grinded with 0.18gm of P_4Se_3 (0.0005 mole) and catalytic amounts of $FeCl_3 \cdot 6H_2O$ (5 wt% of reactants) heated to 350°C with a heating rate 0.2°C/min in an evacuated quartz ampoule. After 10 days few light orange colour crystals were obtained. Obtained product is enough for only SCXRD and SEM-EDS measurement.

3.2.2 Single crystal measurement

$P_2S_{6.36}Se_{0.64}$ crystallises in monoclinic space group $P2_1/c$ like α-P_2S_6Se only with slightly reduced cell parameters which is obvious because of lower selenium contain. Cell parameters of $P_2S_{6.4}Se_{0.6}$ are a = 6.4636(5) Å, b = 10.5197(7) Å, c = 12.5751(7) Å, β = 93.47(0)°, V= 870.35(10) Å^3, and Z = 4 . All the crystallographic data and measurement parameters are listed in Table 3.2.1. The atom coordinates and equivalent isotropic displacement parameters for the final structure solution are listed in Table S3.7. The anisotropic displacement parameters are listed in Table S3.8. There is also an overview of the bond lengths and angles are given in Table S3.9.

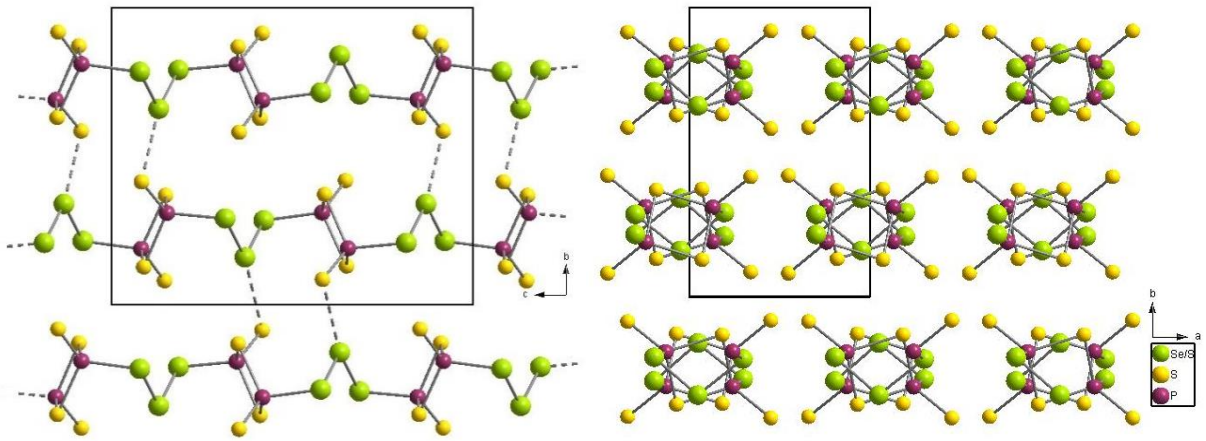

Figure 3.2.1: Crystal structures with parallel view of the polymer axis where long dashed lines represent short inter-polymeric distances between S^{term}-Q_2 (picture on left), Packing of the polymers in distorted tetragonal rod packing (picture on right)

Table 3.2.1: Crystallographic data and measurement parameters of $P_2S_{6.4}Se_{0.6}$

Compound name	**$P_2S_{6.4}Se_{0.6}$**
Empirical formula	$P_2S_{6.365}Se_{0.635}$
Formula weight, g mol^{-1}	314.5
Crystal colour and shape	Orange, needle-like
Crystal system	monoclinic
Space group	*$P2_1/c$ (No. 14)*
a, Å	6.4636(5)
b, Å	10.5197(7)
c, Å	12.5751(9)
β/°	93.583(6)
V, Å^3; *Z*	853.37(11), 4
Absorption coefficient , mm^{-1}	4.542
ρ_{calc} , g cm^{-3}	2.4479
Diffractometer	Rigaku Super Nova
Radiation	MoK$_\alpha$, λ = 0.71073 Å
Temperature, K	123
θ-range, °	3.69-30.49
hkl-range	$-9 \le h \le 9$ $-14 \le k \le 14$ $-17 \le l \le 17$
Absorption correction	numerical (gaussisan)
Number of reflections	2436
Independent reflections	1799
R_{int}	0.049
Structure solution	Charge flipping, Superflip
Structure refinement	*JANA2006*
Completeness to θ_{max}	99.7%
Parameters	83
GooF	1.11
R_1, wR_2 *[I>2σ(I)]*	0.0278, 0.0278
R_1, wR_2 [all reflections]	0.0455, 0.0320
Residual electron density, e Å^{-3}	-0.59/0.59

The triclinic modification was not found for this compound even after checking 30 crystals. This compound is isostructural with α–P_2S_6Se. In this compound the Q_2 position is 53% occupied by selenium and Q_1 and Q_3 positions are 94% and 95% occupied by sulphur respectively. Though selenium is distributed in a little amount in the terminal positions of the bridge but the P-Q_1 and P-Q_3 distances are 2.099(1) Å and 2.103(1) Å much lower than P_2S_6Se. The $\angle Q_1$-Q_2-Q_3 angle is 102.78(3)^o owing to reduced amount of selenium Q_2 position. Q_1-Q_2 and Q_3-Q_2 distances are 2.160(1) Å and 2.151(1) Å respectively, much lower than in α–P_2S_6Se indicating lower selenium contain in the bridging unit in $P_2S_{6.4}Se_{0.6}$. Apart from very small diversion in bond distances and bond angles the repeating unit, orientation of the polymers with respect to unit cell axis and packing of the polymers of $P_2S_{6.4}Se_{0.6}$ are same to that of α–P_2S_6Se as shown in Figure 3.2.1.

A detailed structural comparison with other related compounds is illustrated in 3.5.

3.2.3 SEM-EDS measurement

The composition of this selenium-deficient compound is supported by SEM-EDS measurement as demonstrated in Table 3.2.2. The standard deviation is within 5%.

Table 3.2.2: Atomic percentage of α-$P_2S_{6.36}Se_{0.64}$ from SEM-EDS measurement and calculated value from SCXRD

Elements (atom %)	**P**	**S**	**Se**
Calculated (SCXRD)	22.22	70.67	7.11
Measured (EDS)	22.29	70.85	6.86

3.3 Phosphorus tellurium sulphides, P_2S_6Te

Tellurium has been used extensively in metallurgy as alloying agent to different applications in organic, inorganic chemistry and materials science especially in electronic industry[24]. Speculations on synthesis of phosphorus chalcogenide containing tellurium have been there for many decades and many conceptual structures were predicted in the literature though any of such compounds is yet to be found. Seifert and co-workers[25] calculated geometry and stability of cage phosphorus sulphide tellurides and phosphorus telluride. And Blachnik and co-workers [26] claimed to synthesise the phosphorus sulphide tellurides from the melt of the corresponding elements but any crystallographic structure or solid evidence to these compounds are missing. The lack in research of phosphorus chalcogenides containing tellurium was partly because of low abundance of tellurium on earth and also due to instable Te-P bond. Phosphorus telluride or miscellaneous compound like phosphorus sulphide telluride were always tried to be synthesised analogous to cage molecules like P_4S_3 but no way the weak P-Te bond formation can be avoided in such cage structure though binary phosphorus telluride anions are stabilised by alkali metal ion e.g. BaP_4Te_2 [27] [28]. Recently Te_xS_{1-x} was used with carbon nanotube in a composite form as cathode material[29] in carbonate based electrolytes for lithium chalcogen batteries. This kind of sulphur tellurium components are getting the interest of the scientists because of opposite but complementary properties between sulphur and tellurium in heteroatomic chalcogen moiety. The major reason for chalcogen-based cathode materials has focused on S/Se/Te hosts as molecular modification of such composite compounds could open a new method to improve the Li–chalcogen battery performance. Also tellurium has higher utilization rate and better and faster electrochemical interaction with lithium than sulphur[30]. So it can be predicted that phosphorus chalcogenide compounds containing Te-S bond can show higher polarizability for battery applications than P_2S_5 or P_2Se_5. Herein the first metal free ternary phosphor-chalcogenide compound P_2S_6Te containing Te is reported here. This compound can be synthesised starting from elements and stable for weeks in air. An extensive study for P_2S_6Te was performed by crystal structural analysis, scanning microscopy, UV-vis spectroscopy and Raman spectroscopy.

3.3.1 Synthesis

P_2S_6Te was synthesised from both P_4S_3 and Te and mixture of elemental precursors but the necessity of $FeCl_3.H_2O$ as mineraliser inevitable and without the mineraliser the result was

pure glass. To synthesize P_2S_6Te from elements stoichiometric amount of elemental phosphorus and sulphur and little excess tellurium with catalytic amounts of $FeCl_3 \cdot 6H_2O$ (5 wt% of reactants) were grinded and sealed in an evacuated quartz ampoule. Total 1 gm of reaction mixture was taken in 8 cm long quartz tube and then melted and annealed at 350°C with a heating rate 0.2°C/min for 10 days. After the annealing period the quartz tube was cooled down at the same rate as heating. The resultant product has more than 92% yields. A little bit of excess elemental tellurium can be separated from the product by help of tweezers. Bright wine red colour crystals as shown in Figure 3.3.1, are air and moisture stable. All measurement and analysis were performed with this compound without further purification.

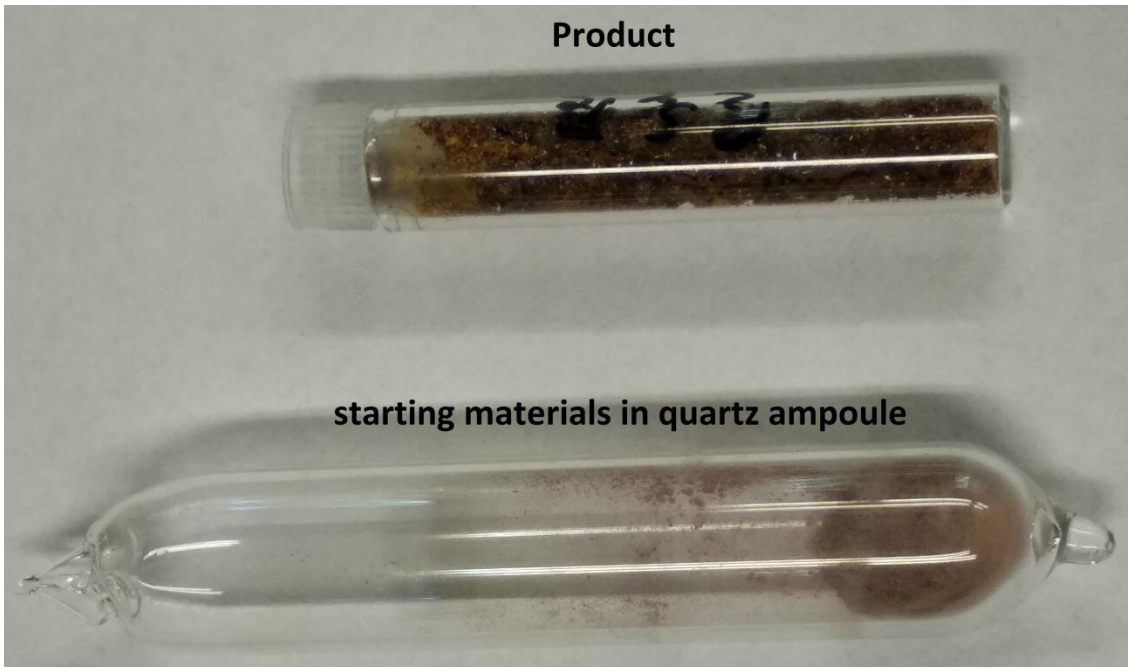

Figure 3.3.1: unreacted starting materials in quartz ampoule and the air stable crystalline product in a snappy.

3.3.2 Single crystal measurement

The measured crystal at 123 K showed a monoclinic crystal system like α-P_2S_7 but completely different cell parameters and packing, adopting space group *C2/c* (No. 15) with lattice parameters a = 10.5448(7) Å, b = 7.5851(5) Å, c = 12.1630(7) Å, β = 114.37(1)°. All the crystallographic data is listed in Table 3.3.1. The atom coordinates and equivalent isotropic displacement parameters for the final structure solution are listed in Table S3.10. The anisotropic displacement parameters are listed in Table S3.11. There is also an overview

Table 3.3.1: Crystallographic data and measurement parameters of P_2S_6Te

Compound name	**P_2S_6Te**
Empirical formula	P_2S_6Te
Formula weight, g mol^{-1}	381.9
Crystal colour and shape	Red, needle-like
Crystal system	monoclinic
Space group	*C2/c* (No.15)
a, Å	10.5448(7)
b, Å	7.5851(5)
c, Å	12.1630(7)
β/°	114.374(6)
V, Å^3; *Z*	886.13(11), 8
Absorption coefficient , mm^{-1}	10.086
ρ_{calc} , g cm^{-3}	5.7253
Diffractometer	Rigaku Super Nova
Radiation	MoK_α, λ = 0.71073 Å
Temperature, K	123
θ-range, °	3.42-29.90
hkl-range	$-13 \leq h \leq 14$ $-10 \leq k \leq 10$ $-15 \leq l \leq 16$
Absorption correction	numerical (gaussisan)
Number of reflections	5560
Independent reflections	1093
R_{int}	0.040
Structure solution	Charge flipping, Superflip
Structure refinement	*JANA2006*
Completeness to θ_{max}	99.9%
Parameters	42
GooF	1.09
R_1, wR_2 *[I>2σ(I)]*	0.0175, 0.0232
R_1, wR_2 [all reflections]	0.0191, 0.0238
Residual electron density, e Å^{-3}	-0.29/0.25

of the bond lengths and angles are given in Table S3.12. A short overview of bond length and bond angle is given in Table 3.3.1. The composition calculation from crystallographic software does not show any excess tellurium contain than one like P_2S_6Se. The crystals are assembly of polymeric strand like all the previous structure but no further modifications were found of this compound. P atom is tetrahedrally coordinated to S atoms and two of these PS_4 unit share one edge forming P_2S_6 unit which are connected by one tellurium atom making S-Te-S Bridge to give rise to a one dimensional polymeric structure. And these S-Te bonds are very ordered possibly because of positioning of phosphorus atom adjacent to the S. The structural motif of the polymer is similar to P_2S_6Se but relative orientation or position of the PS_4 tetrahedron with respect to the bridging unit is different in order to avoid Te-P interaction through space as shown in Figure 3.3.2. In the structure there are three types of sulphur atoms; S^{term}, terminal S atom connected to P atom; S^{brid1}, connecting two P atoms in P_2S_6 unit and S^{brid2}, S atom of the bridging unit connecting P and Te atoms.

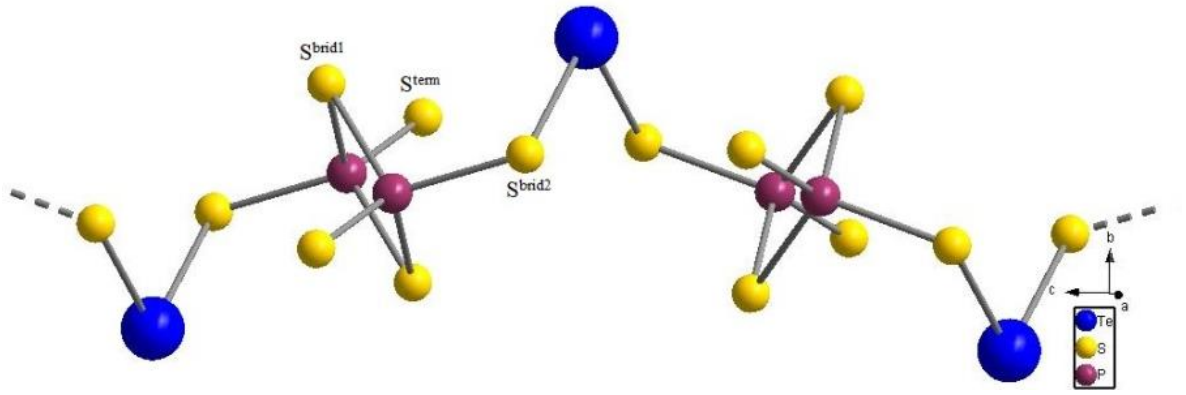

Figure 3.3.2: Repeating unit of polymer of P_2S_6Te with three types of sulphur atoms and one connecting tellurium atom

The P-S^{brid1} bond distance is same as in P_2S_7 but P-S^{term} bonds and P- S^{brid2} bonds show significant deviation in bond length. P-S^{term} bond length is 1.949(9) Å, around 0.035 Å longer which is explained later and P- S^{brid2} is 2.079(4) Å, around 0.021 Å shorter than corresponding bonds in P_2S_7. Usually co-valent bonds between Te and S atoms are longer than the sum of their standard co-valent radii. In compound CuClSTe Te-S distance (covalent) is 2.437 Å and in CuBrSTe it is 2.450 Å [31]. Here Te-S bonds are almost of same length i.e. 2.439(10) Å to the summation of mean of the S-S bond in S_8 (2.10 Å) and covalent radius of Te (1.38 Å)[32]. The ∠S-Te-S angle is 100.8°, lower than the ∠S-S-S angle because of increase in size of the Te atom. The ∠S^{term}-P-S^{brid1} bond angle is between that in P_2S_7 and in P_2S_5, i.e. 115°. The bond length of Te-S can vary from 2.3 Å to 3.2 Å in organometallic

coordination complexes but the longer bonds are quite rare in pure inorganic complexes[38]. This elongated secondary bond we observed in P_2S_6Te between Te and S^{term} of two neighbouring polymeric chain along b-axis or along 010-plane (Figure 3.3.3) as tellurium shows a higher tendency to form secondary bond then S or Se. The interchain Te - S^{term} nonbonding distance is 3.10(11) Å which longer than the standard co-valent bond length of Te-S(~2.44 Å) but much shorter than sum of their van der waal radii (~3.9 Å)[33]. This secondary or semi bond is a result of partially polar interaction between S^{term} which is in -2 oxidation state and Te which contains a +δ charge because of large size difference and polarizability between Te and S^{brid2}. All 4 Te-S bonds of this TeS_4 unit lay in the same plane forming a distorted square planer structure with two elongated Te-S bonds. The lone pairs of tellurium located in the p-orbital perpendicular to the Te-S bond plane. As Te is in zero oxidation state and has co-ordination number 4 so it can be assumed that the lone pairs of the Te are stereo chemically active[31] and it influences the coordination of tellurium in significant manner resulting into distorted square-planner geometry of TeS_4 unit.

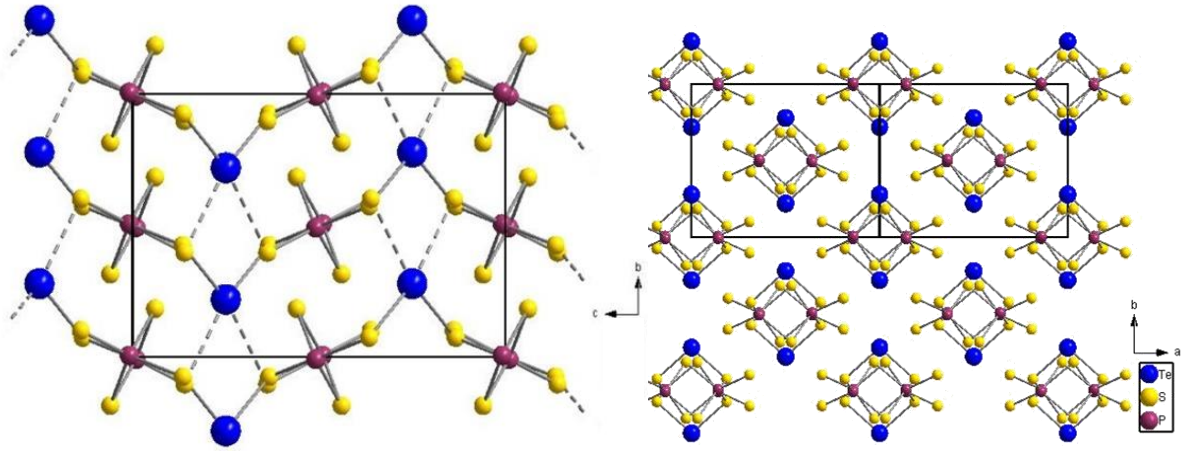

Figure 3.3.3: Unlike P_2S_6Se, in P_2S_6Te all the S^{term} atoms are connected to tellurium atoms of neighbouring polymers (picture in left). Perfect tetragonal rod-packing of the polymers (picture in the right)

And this strong secondary Te-S interaction, not only reduce the inter-chain distance but also change the crystal packing completely than P_2S_7 or P_2S_6Se. Where P_2S_7 shows hexagonal rod packing and P_2S_6Se shows non-ideal tetragonal rod packing, P_2S_6Te shows perfect tetragonal rod packing. In P_2S_6Te, the polymers are stacked on each other in alternative layer (Figure 3.3.3) to avoid strong interaction between Te atoms. The dihedral angle in ploychalcogenide rings are usually around 90^0 [34] and for S-Te-S system around 87^O but in P_2S_6Te this angle between S-Te-S-P reduced to 80° resulting into better overlap between p-orbitals of the S atoms.

3.3.3 Powder XRD

By comparing the powder diffractograms of the synthesised compound with calculated data from SCXRD measurement, cell parameters and purity of the compound was verified. Measured powder diffractogram along with calculated data is shown in Figure 3.3.4. Six small peaks which were unindexed were identified as starting material phosphorus and tellurium. As the reaction takes place at 350^{O}C and melting point of elemental phosphorus and tellurium are 597^{O}C and 450^{O}C, so possibly a little bit of unreacted precursors are present in the sample. The measured cell parameters are a = 10.549(5) Å, b = 7.647(4) Å, c = 12.226(7) Å, β = 114.53(1)°, V= 897.2(12) Å^3. This little incrase in cell parameter than SCXRD value is due to elevated powder measurement temperature than single crystal. Indexing and refinement data is listed in Table S3.13 in supporting information section.

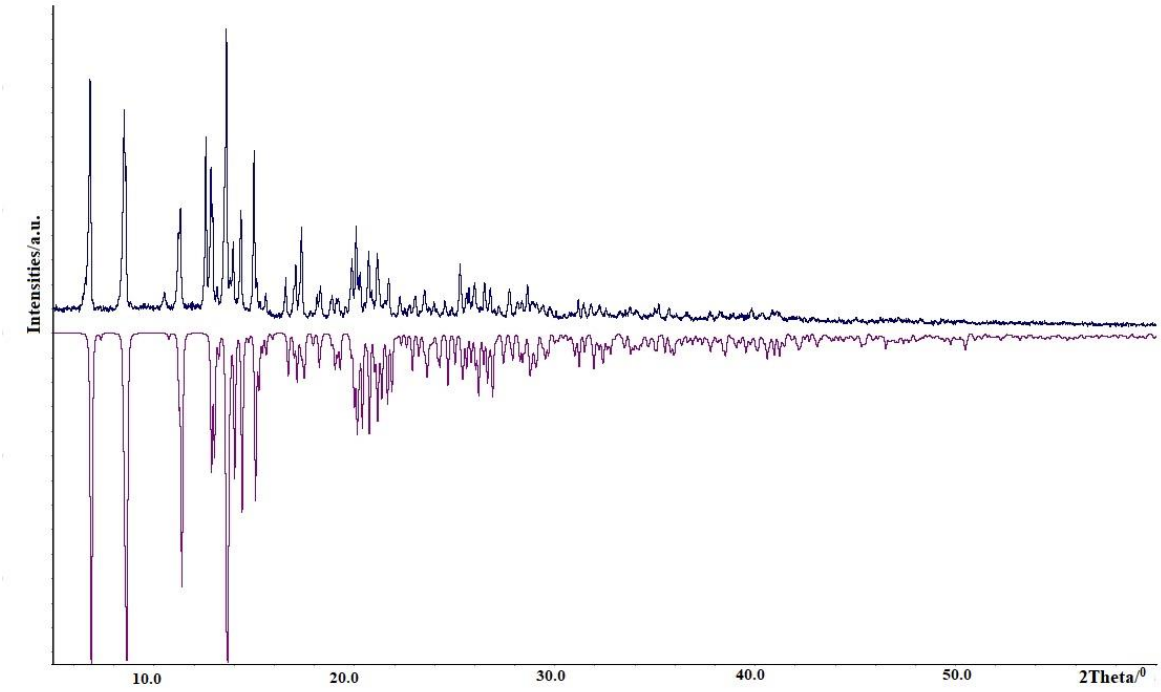

Figure 3.3.4: Measured powder diffractogram of mixture of P_2S_6Te (positive intersity); and purple diffractogram for calculated pattern of P_2S_6Te derived from SCXRD data (negative intensity)

3.3.4 Thermal analysis

Similar to P_2S_6Se thermal analysis (DTA) supports the necessity of mineraliser also for P_2S_6Te as endothermic peak for melting of crystalline compound appeared only in 1st heating but not in 2nd heating. The melting point of the compound is 337°C, higher than P_2S_6Se indicating stronger inter-polymer interaction.

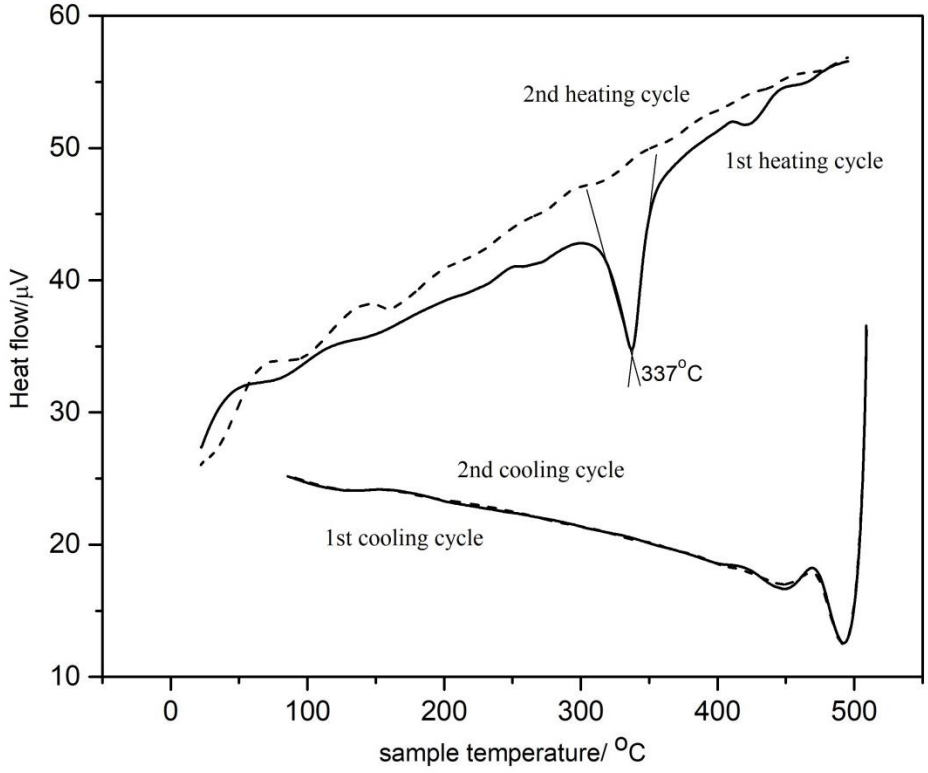

Figure 3.3.5: DTA measurement of P_2S_6Te. The measurement was in the temperature range from 25 °C to 500 °C with a heating rate of 10 °C/min. Curves with full line denote first heating and cooling cycle and curves with dotted line denote second heating and cooling cycle.

3.3.5 SEM-EDS measurement

The SEM pictures (Figure 3.3.6) of P_2S_6Te show bit fibrous morphology but mostly smoother surface than P_2S_6Se. This can be an indication of stronger inter-polymeric interaction. The EDS measurement supports the composition calculated from SCXRD measurement, showed in Table 3.3.2.

Table 1.3.2: Atomic percentage of P_2S_6Te from SEM-EDS measurement and theoretical value calculated from SCXRD

Elements (atom %)	P	S	Te
Calculated (SCXRD)	22.22	66.67	11.11
Measured (EDS)	21.75	66.86	11.37

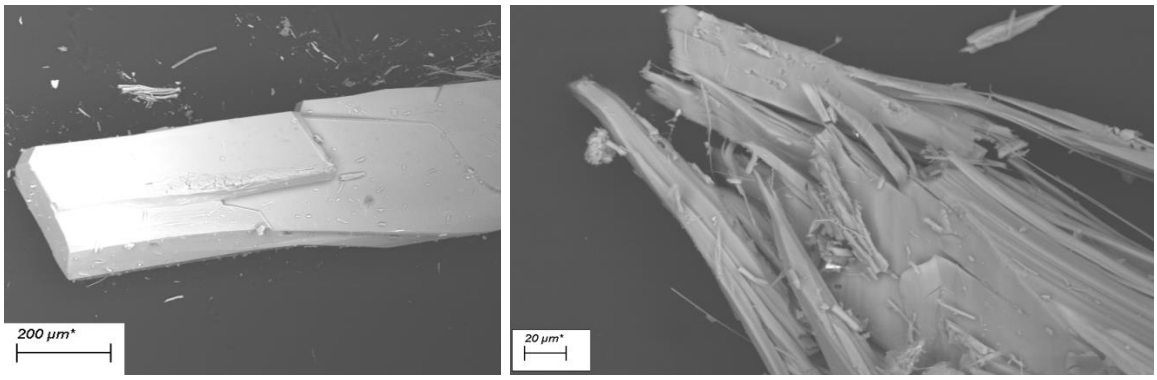

Figure 3.3.6: SEM pictures of P_2S_6Te

3.3.6 Raman Spectroscopy

Raman spectra of P_2S_6Te have a high noise and background mostly because the measurement was done on a single crystal in an open-air condition. Still the data is good enough for analysis. The spectra (in Figure 3.3.7) evident not only direct Te-S bond but also support inter-chain Te-S interaction. The average value for Te-S stretching vibration[35,36] is 350 cm^{-1} but in the measured data, stretching frequencies between Te and S of the bridging unit are observed between 328 and 255 cm^{-1}. This red shift took place due to additional interaction between Te and S^{term} of the neighbouring chains in 3.1 Å distances which is much smaller than so-called non-bonding distance i.e. 4.1 Å. In the region 238-222 cm^{-1} this long distance inter-chain interaction can also be observed directly. Also, when compared to P_2S_7, the P-S^{term} stretching is observed around 703-690 cm^{-1} but in P_2S_6Te it is observed around 650-638 cm^{-1}. This red shift evident the S^{term}-Te inter-chain interaction. The other peak at 520 cm^{-1} is assigned to the interaction between P and S of the bridging unit, 415-396 cm^{-1} is assigned to P_2S_2 ring by comparing the literature data[37, 39] and from theoretical calculations. The peak details are listed below in Table 3.3.3.

Table 3.3.3: List of peaks of Raman spectrum of mixture of P_2S_6Te

Wavenumbers (cm^{-1})	**Intensity**	**P_2S_6Te**
650-638	ms	$\nu(P\text{-}S^{term})$
522	s	$\nu(P\text{-}S^{brid})$
414-396	vs	ν (P2S2-Ring)
328	s	ν (S-Te-S bridging unit)
317	s	ν (S-Te-S bridging unit)
255	vs	ν (S-Te-S bridging unit)
238	s	δ
222	s	δ

ms= medium strong, s= strong, vs= very strong

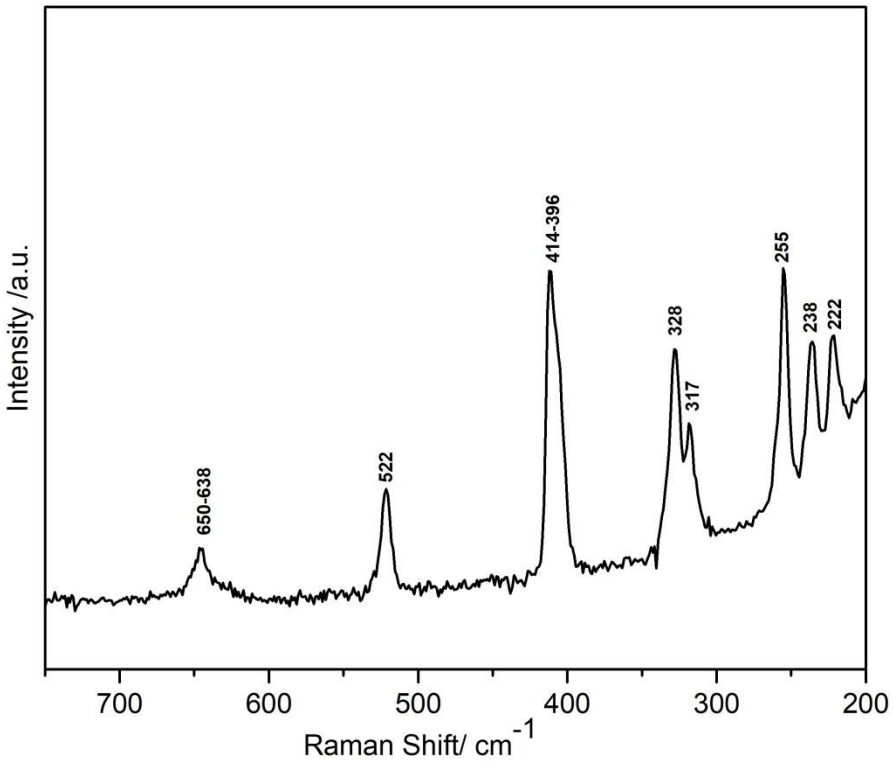

Figure 3.3.7: Raman spectrum of mixture P_2S_6Te

3.3.7 UV-vis spectroscopy

The measured optical band gap is 1.65 eV (Figure 3.3.8). The calculated value for band gap by using the LDA (PBE) function is 1.343 eV. The inherent uncertainties of DFT calculations or band-gap problem[40] can be accountable for this disparity in measured and calculated value.

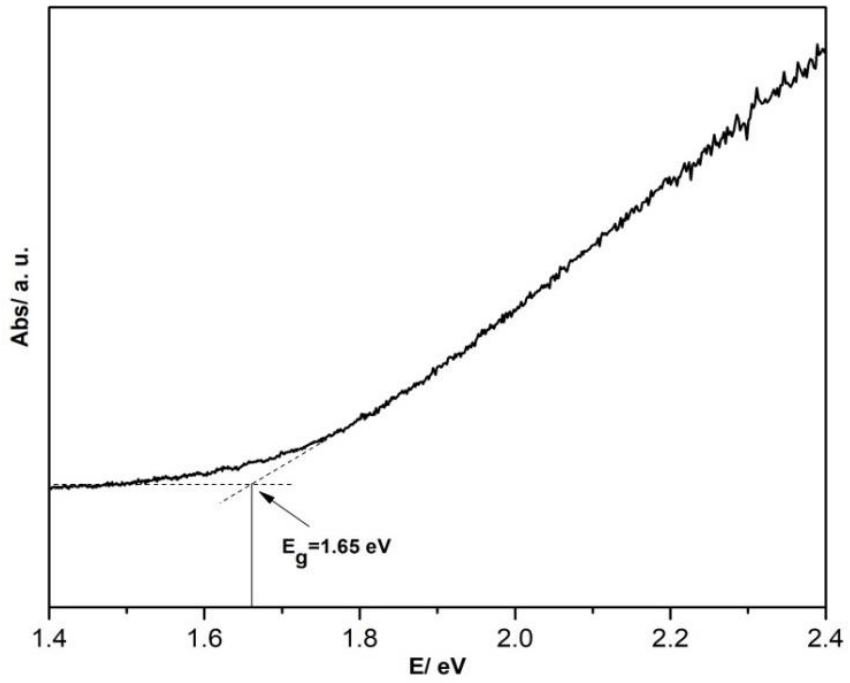

Figure 3.3.8: UV/Vis spectrum of P_2S_6Te. The band gap of 1.65 eV was determined by extrapolating the linearly decreasing part of the Kubelka-Munk function to the baseline (dotted lines).

3.1.9 NMR spectroscopy

Pure sample of P_2S_6Te was also analysed by ^{31}P-NMR-spectroscopy. However, due to their insolubility in any ordinary solvent NMR spectroscopy was measured on a polycrystalline sample. The recorded ^{31}P-MAS-NMR spectrum is available in Figure 3.3.9. The signal deconvolution results in a total of seven signals, of which the signal at 65 ppm can be accounted for phosphorus of P_2S_6Te and all other six signals are resulted from spinning side band. Contradicting to P_2S_7[39], here, only one peak for two phosphorus atoms is generated for the formula unit P_2S_6Te, indicating both phosphorus atoms in the P_2S_6 unit are same from symmetrical and chemical viewpoint. The crystallographic data also supports this interpretation. Also, there is down field shift in the peak position (65 ppm) when compared to

P_2S_7 (peaks are at 60.1 and 57.9 ppm for α-P_2S_7). This can be associated with the effect of electron withdrawing group or atom on phosphorus. As tellurium is less electronegative or stronger electron withdrawing than sulphur, and S^{term} and S^{brid2} both have significant interaction with tellurium (Figure 3.2.3 and Figure 3.3.3), there is compelling electron withdrawing effect on phosphorus through bonds which results in down field shift of the peak position. Solid-state NMR spectroscopy thus confirms the structural interpretation from SCXRD study.

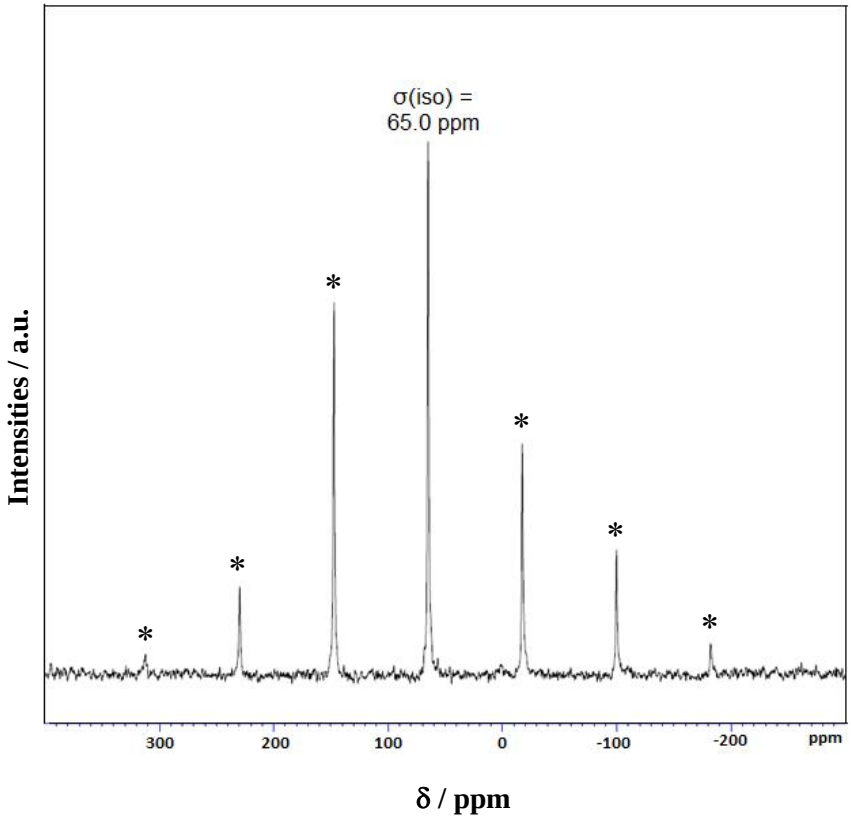

Figure 3.3.9: ^{31}P-MAS-NMR spectrum of P_2S_6Te. There are 7 peaks but the one at 65 ppm can be accounted for the compound. The other peaks are spinning side bands and positioned at beyond reasonable region **(**∗ represents spinning sidebands).

3.4 Phosphorus tellurium selenium sulphides, P_2S_5SeTe

This phosphorous chalcogenide compound contains all non- radioactive chalcogen except oxygen. In this compound competitive occupancy of the chalcogens is observed in the three membered bridge and little bit of selenium in P2S2 4-membered ring. A detailed study of the compound showed effect of even small amount tellurium on the crystal packing and inter-polymeric distance. Raman measurement also gave an elaborated insight this long distance interaction.

3.4.1 Synthesis

P_2S_5SeTe was synthesised by same procedure like the previous compounds only by using P_4Se_3 with elemental sulphur and tellurium. Starting from elemental precursors for all components of the compound resulted in glass. This one is also air and moisture stable. The end product was mixture of desired compound with some intermediate and unreacted starting materials. So the crystalline product was separated from the rest of mass by tweezers for further experiments.

3.4.2 Single crystal measurement

Orange colour crystal of P_2S_5SeTe is measured at 123 K by SCXRD. It crystallised in *C*2/*c* space group with cell parameters a = 10.6159(7) Å, b = 7.6193(5) Å, c = 12.2726(8) Å, β = 114.25(1)°, V=905.11(11)Å^3 and Z=4. The compound is isostructural to P_2S_6Te. No other modification was observed for this compound. It has same repeating unit (Figure 3.4.1) as P_2S_6Se but instead of Q_1-Q_2-Q_3 unit it has Q_1-Q_2-Q_1 unit which is mixed occupied by sulphur, selenium and tellurium.

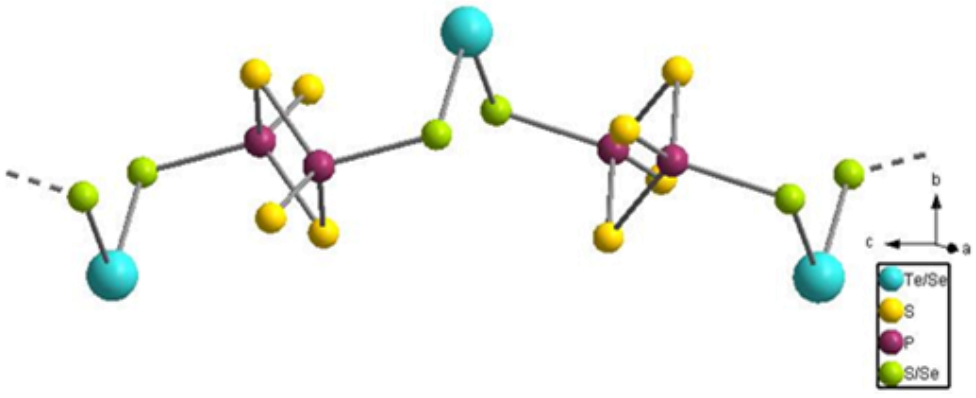

Figure 3.4.1: Repeating unit of polymer of P_2S_5SeTe with three types of sulphur atoms and one connecting tellurium atom

Table 3.4.1: Crystallographic data and measurement parameters of P_2S_5SeTe

Compound name	**P_2S_5SeTe**
Empirical formula	$P_2S_{5.29}Se_{0.932}Te_{0.866}$
Formula weight, g mol^{-1}	428.80
Crystal colour and shape	Red, needle-like
Crystal system	monoclinic
Space group	*C2/c* (No.15)
a, Å	10.6159(7)
b, Å	7.6193(5)
c, Å	12.2726(8)
β/^{o}	114.247(6)
V, Å^3; *Z*	905.11(11), 8
Absorption coefficient , mm^{-1}	17.456
ρ_{calc} , g cm^{-3}	6.2936
Diffractometer	Rigaku Super Nova
Radiation	MoK$_\alpha$, λ = 0.71073 Å
Temperature, K	123
θ-*range*,^{o}	3.15-31.15
hkl-range	$-8 \le h \le 9$ $-15 \le k \le 15$ $-17 \le l \le 18$
Absorption correction	numerical (gaussisan)
Number of reflections	8757
Independent reflections	1310
R_{int}	0.04
Structure solution	Charge flipping, Superflip
Structure refinement	*JANA2006*
Completeness to θ_{max}	99.9%
Parameters	42
GooF	1.86
R_1, wR_2 $[I>2\sigma(I)]$	0.029, 0.034
R_1, wR_2 [all reflections]	0.033, 0.035
Residual electron density, e Å^{-3}	-0.97/1.63

Tellurium and selenium occupy the bridging position. Tellurium has occupied (87%) the central position i.e. Q_2 along with little bit of selenium (13%) and sulphur is the main component (68%) for Q_1 position along with selenium (32%). The composition calculated from SCXRD, $P_2S_{5.29}Se_{0.93}Te_{0.86}$. All the crystallographic data is listed below in Table 3.4.1. Q_1-Q_2 distance is 2.484(6) Å which is in between standard S-Te distance[23], 2.437 Å and Se-Te distance, 2.55 Å with $\angle Q_1$-Q_2-Q_1 angle 100.83°. After refinement of the single crystal data the connecting sulphur (S^{brid}) between two phosphorus atoms (S2), showed occupancy of 1.057 and the EDS measurement also indicates a little higher amount of selenium. However S2 position was refined only with sulphur occupancy. P-S^{brid} distances are 2.127(1)-2.136(2) Å and $\angle$P-S^{brid}-P angle is 85.54(4)°. EDS measurement and high *GOF* value indicated more selenium contain in the structure. The atom coordinates and equivalent isotropic displacement parameters for the final structure solution are listed in Table S3.14. The anisotropic displacement parameters are listed in Table S3.15. There is also an overview of the bond lengths and angles are given in Table S3.16.

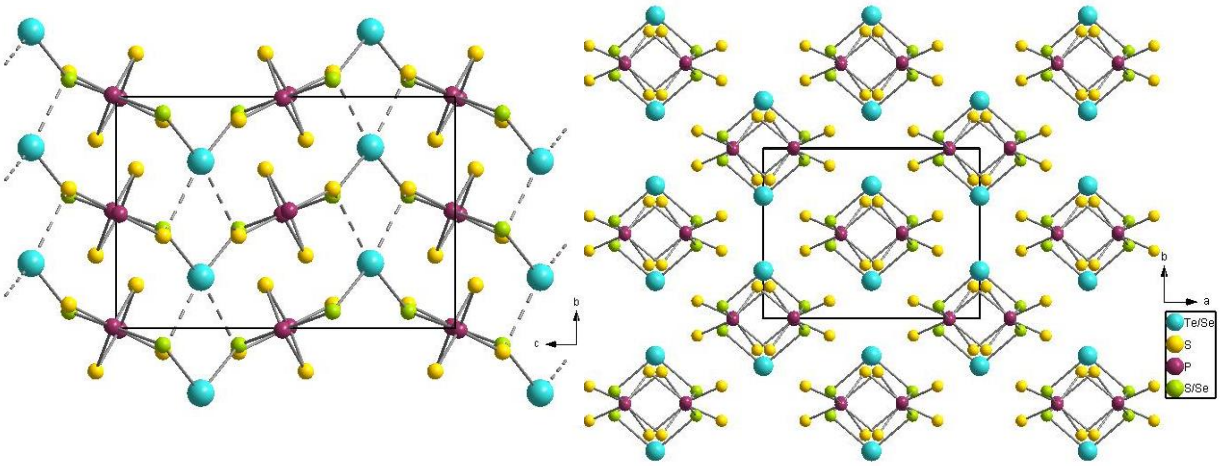

Figure 3.4.2: Similar to P_2S_6Te, in P_2S_5SeTe all the S^{term} atoms are connected to tellurium atoms of neighbouring polymers (picture in left). Perfect tetragonal rod-packing of the polymers (picture in the right)

The packing of the compound is similar to P_2S_6Te i.e. perfect tetragonal packing. This interprets that even very little amount tellurium incorporation in the structure can influence packing of the structure. Further structural details are discussed in Section 3.5. The inter-polymeric distance between Q_2-S^{term} is 3.130(1) Å. The polymeric arrangement and rod packing of the polymers are shown in Figure 3.4.2.

3.4.3 Powder XRD

Powder XRD pattern of this compound (Figure 3.4.3) matched reasonably with calculated data only with few extra peaks from starting material impurity like elemental tellurium (marked by ∗). Though the powder data has quite high back ground.

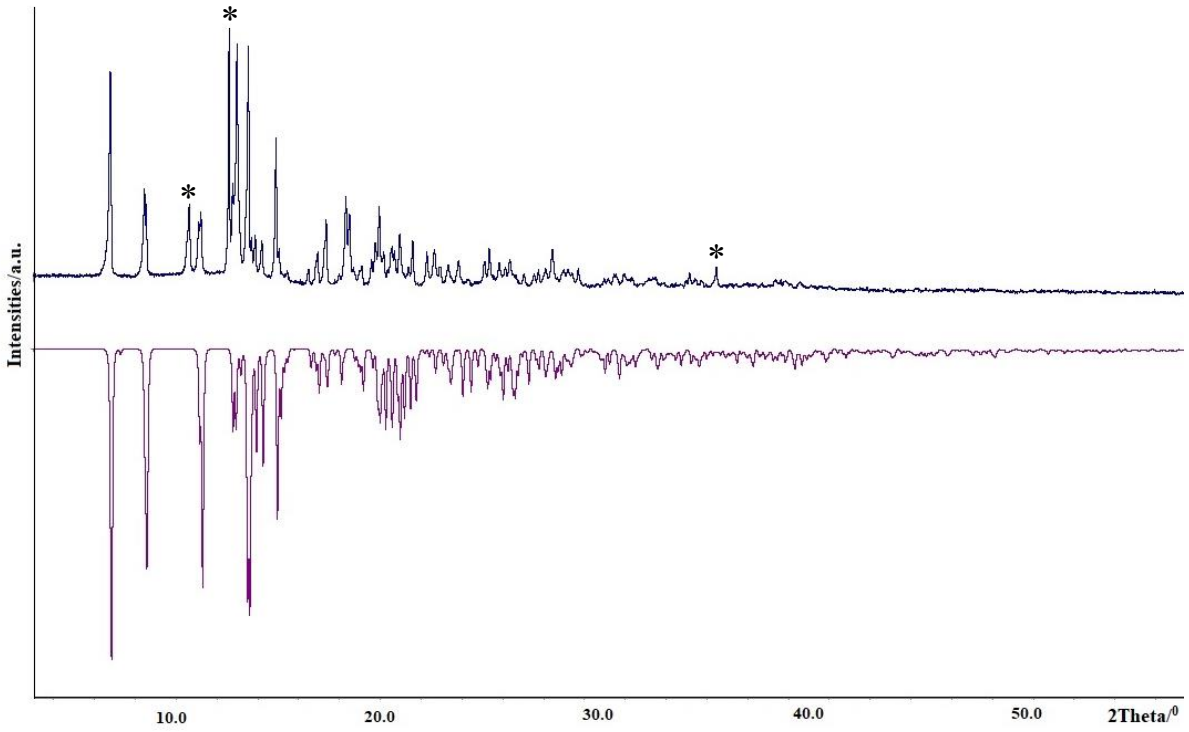

Figure 3.4.3: Measured powder diffractogram of mixture of P_2S_5SeTe (positive intensity) with impurities (marked by ∗); and purple diffractogram for calculated pattern of P_2S_5SeTe derived from SCXRD data (negative intensity)

3.4.4 SEM-EDS measurement

EDS measurement actually gave incite about the presence of selenium in other position than only bridging unit. For all the other compounds measured data matches almost perfectly with calculated data. Even after selenium incorporation in P_2S2 ring the composition does matches well with measured value as the standard deviation is more than 5%. The comparison is listed below in Table 3.4.2.

Table 3.4.2: Atomic percentage of P_2S_5SeTe from SEM-EDS measurement and theoretical value calculated from SCXRD

Elements (atom %)	P	S	Se	Te
Calculated (SCXRD)	22.01	58.20	10.26	9.52
Measured (EDS)	22.25	55.95	12.05	9.75

3.4.5 Raman Spectroscopy

As the bridging unit Q_1-Q_2-Q_1 is occupied by sulphur, selenium and tellurium, four different types of interaction can be observed, S-Se, Se-Se, Se-Te, S-Te. The band in the range 384-218 cm^{-1} is assigned for this mix-chalcogen bridging unit. Because of the presence of three types of chalcogen atoms in the bridging unit, the spectra contain more peaks than the compounds discussed above. All the assigned peaks are compared with the literature reports and evident by theoretical calculations. The measured Raman spectra and peaks assigned to the bonds are listed in Figure 3.4.4 and Table 3.4.3 respectively. A comparative study of all the compounds is discussed in Section 3.5.2.

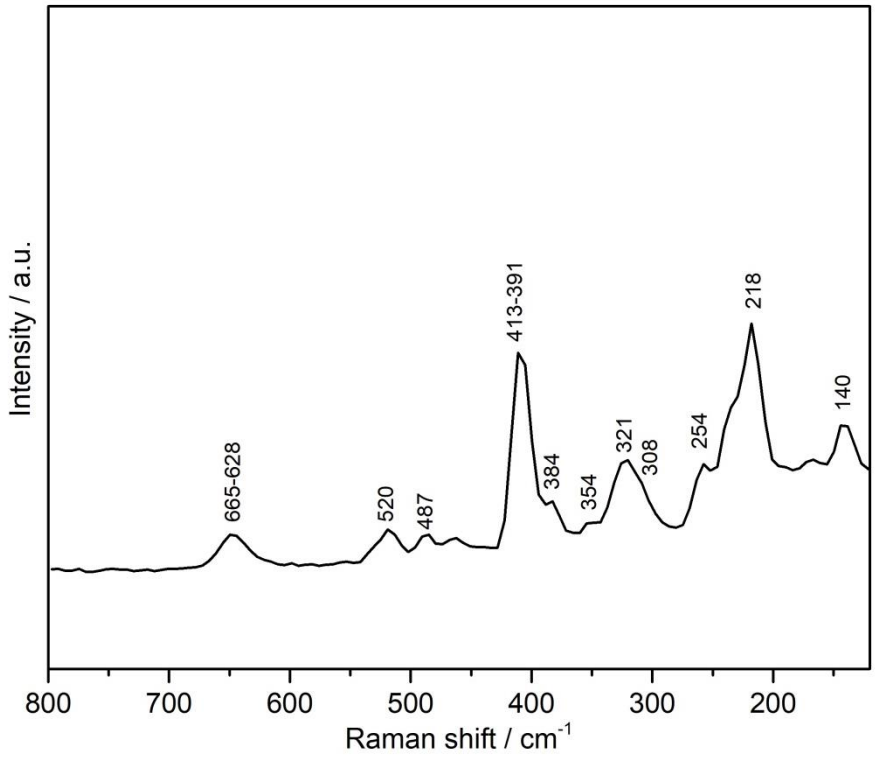

Figure 3.4.4: Raman spectrum of mixture P_2S_5SeTe

Table 3.4.3: List of peaks of Raman spectrum of mixture of P_2S_5SeTe

Wavenumbers (cm^{-1})	**Intensity**	**P_2S_5SeTe**
665-628	w	$\nu(P\text{-}S^{term})$
520	w	$\nu(P\text{-}S^{brid})$
487	vw	$\nu(P\text{-}S^{brid})$
413-391	s, sh	$\nu(P_2S_2\text{-Ring})$
354	vw	$\nu(Q_1\text{-}Q_2\text{-}Q_1$ bridging unit)
321	ms	$\nu(Q_1\text{-}Q_2\text{-}Q_1$ bridging unit)
308	w	$\nu(Q_1\text{-}Q_2\text{-}Q_1$ bridging unit)
254	ms	$\nu(Q_1\text{-}Q_2\text{-}Q_1$ bridging unit)
218	s	δ
140	ms	δ

ms= medium strong, s= strong, w= weak, vw=very weak, sh= shoulder

3.5 Comparison between the compounds

P_2S_7 synthesised by Rödl[39] and compounds discussed in this chapter have similar basic polymeric structure with P2S4 units which are connected by a 3-membered chalcogen bridge. Starting from P_2S_7 with all-sulphur bridge to P_2S_6Se with selenium distributed all along the bridging unit to P_2S_6Te where tellurium is the heteroatom with two sulphurs in the bridge to P_2S_5SeTe with all three types of chalcogens in the bridge, the cell parameters, crystal structure, bond distances, polymer packing and physical properties showed interesting trend which is important for better understanding of bonding between chalcogens and phosphorus – tellurium interaction. In this section a comparative study is done between α-P_2S_7, α-P_2S_6Se, $P_2S_{6.4}Se_{0.6}$, P_2S_6Te, P_2S_5SeTe. The β– modifications of first two compounds were not considered for structural comparison as they have triclinic symmetry when all other structure has monoclinic symmetry.

3.5.1 Structural comparison

α-P_2S_7, $P_2S_{6.4}Se_{0.6}$, and α-P_2S_6Se crystallise in space group $P2_1/c$ where introduction of tellurium in the crystal structure changes the space group to $C2/c$ for P_2S_6Te and P_2S_5SeTe. As all four structures do not have the same space group, it would be difficult to compare the cell parameters. A comparison between structural aspects is listed in Table 3.5.1.

Table 3.5.1: A comparison between structural aspects of α-P_2S_7, α-P_2S_6Se, $P_2S_{6.4}Se_{0.6}$, P_2S_5SeTe and P_2S_6Te

	α-P_2S_7	**$P_2S_{6.4}Se_{0.6}$**	**α-P_2S_6Se**	**P_2S_5SeTe**	**P_2S_6Te**
Space group	$P2_1/c$	$P2_1/c$	$P2_1/c$	$C2/c$	$C2/c$
Density (g cm^{-3})	2.145	2.4479	2.5434	6.2936	5.7253
Mini. inter-polymeric distance(Å)	3.30	3.235	3.229	3.130	3.10
P-S^{term} (Å)	1.916(2)	1.921(1)	1.926(1)	1.954	1.949(9)
$\angle Q_1$-Q_2-Q_1	106.87(1)°	102.78(2)°	102.38(1)°	100.83(3)°	100.82(2)°
Rod-packing of polymers	Hexagonal or honeycomb	Non-ideal or distorted tetragonal	Non-ideal or distorted tetragonal	tetragonal	tetragonal
Periodicity of the polymeric unit(Å)	12.565	12.575	12.725	12.270	12.163

It can be seen from the Table that the effect of chalcogens are maximum on inter-polymeric distance and crystal packing. With increase in amount of heavier chalcogen in the central position (Q_2) of the bridging unit, inter-polymeric distance decreases. It does not depend on the total molecular weight. This can be explained by chalcogen bond formation between S^{term} and Q_2 of two polymeric chains. These distances are smaller than van der Waal distance of corresponding atoms even for α-P_2S_7. And the bond became stronger with increase in amount of tellurium in bridging unit. Because of increase in electrophilicity in Q_2 position (higher selenium/tellurium contain) owing to polarizability difference with neighbouring positions Q_1 and/or Q_3 (higher sulphur contain), Q_2 attacks the S^{2-} of the neighbouring polymer forming a non-covalent bond or chalcogen bond. This also elongated P-S^{term} bond distance as can be seen in Table 3.5.1. With smaller chalcogen bond, P-S^{term} bond increases. Ultimately this non-formal bond affects the packing of the polymers, see Figure. 3.5.1. It can be seen in Table 3.5.1 from α-P_2S_7 to P_2S_6Te, $\angle Q_1$-Q_2-Q_1 angle decreases. As the Q_2 position

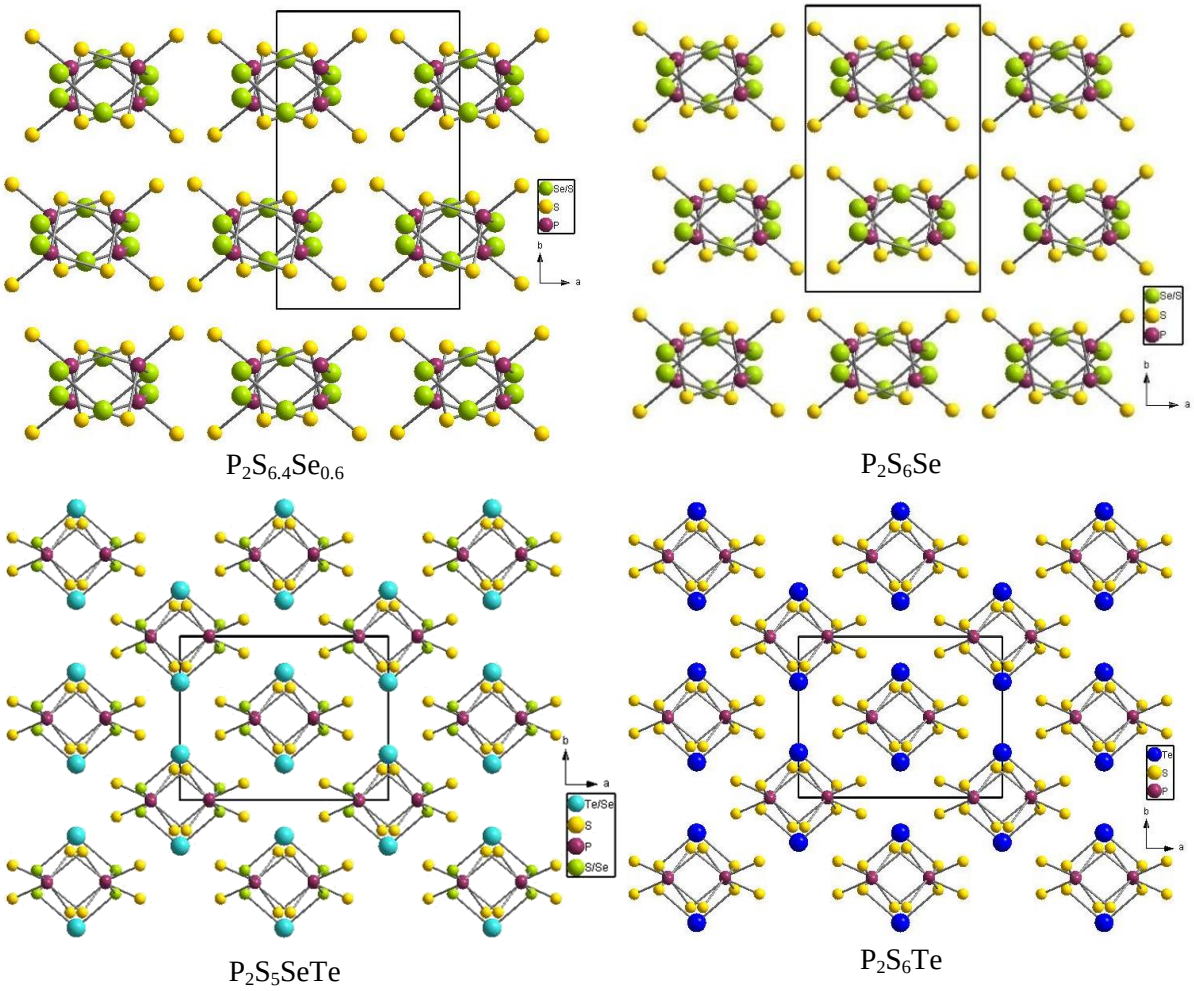

Figure 3.5.1: Rod-packing of polymers in different compounds

is occupied by a heavier chalcogen, due to the increase in the atomic size from S to Te the bond angle gradually decreases from α-P_2S_7 to P_2S_6Te. The packing of the polymer shows a systematic change from lower to higher selenium contain to tellurium compounds. Unlike α-P_2S_7, P_2S_6Se shows same distorted or non-ideal tetragonal packing arrangement of the polymers and compound $P_2S_{6.4}Se_{0.6}$ too. Interestingly P_2S_6Te and P_2S_5SeTe have perfect

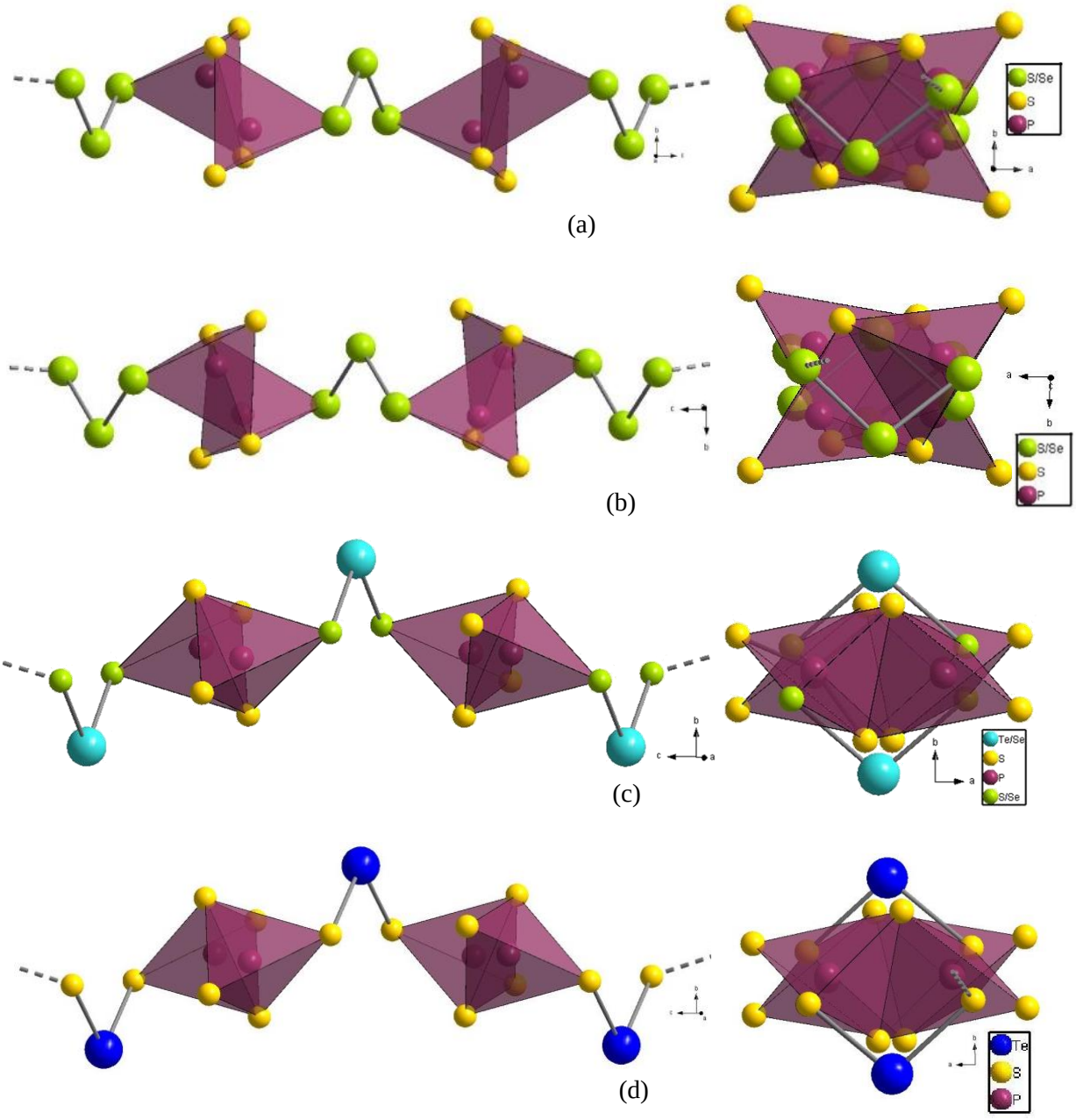

Figure 3.5.2: Orientation of the polymeric chains in compounds along the polymeric axis and perpendicular to the axis in (a) $P_2S_{6.4}Se_{0.6}$, (b) P_2S_6Se, (c) P_2S_5SeTe and (d) P_2S_6Te. In (c) and (d) tellurium is coming out from the plane of PS4 tetrahedron.

tetragonal packing. Further an interesting trend is also observed for length of the repeating unit of the polymers. From α-P_2S_7 to $P_2S_{6.4}Se_{0.6}$ to α-P_2S_6Se it gradually increases with increase in amount of selenium in the structure but with introduction of tellurium it decreases significantly, even lower than α-P_2S_7. With increase in tellurium in the Q_2 position this distance decreases. This happens because of the structure of the polymeric chain. P_2S_6Te and P_2S_5SeTe have a zigzag structure of the polymer to reduce tellurium-phosphorus interaction where all the other compounds have straight chains (Figure 3.5.2). In P_2S_6Te and P_2S_5SeTe, orientation of the PS_4 polyhedrons changed because of presence of tellurium in Q_2 position as it is coming out of the chain to avoid interaction with phosphorus. In P_2S_6Te, with highest tellurium content this repulsive interaction between tellurium and phosphorus is strongest resulting into smaller chain length.

3.5.2 Comparison between the Raman spectra corresponding compounds

The effect of chalcogen bonding is quite evident by Raman spectroscopy also. By comparing raman data of P_2S_7[3,39], P_2S_6Se, P_2S_6Te and P_2S_5SeTe, it is observed that there is regular and logical shift in spectra as can be seen in Figure 3.5.3. A comparative study for position of the peaks assigned for formal interactions between similar moieties is listed in Table 3.5.2. Position of the peak for P-S^{term} bond has a gradual red shift with increase in tellurium contain in the compound as an effect of stronger chalcogen bond between S^{term} and Q_2 of two neighbouring polymers as discussed in Section 3.5.1. The most significant change was observed for the bridging unit. The peaks for bridging unit appear at 527-449 cm^{-1} for P_2S_7, at 380-258 cm^{-1} for P_2S_6Se, at 354-254 for P_2S_5SeTe and at 328-254 for P_2S_6Te. With heavier members in the bridging unit a red shift in the peak position is observe.

Table 3.5.2: Raman shift (cm^{-1}) of similar boning moiety in different compounds

Bond type	**P_2S_7**	**P_2S_6Se**	**P_2S_5SeTe**	**P_2S_6Te**
P-S^{term}	703-690	700-675	665-628	650-638
P_2S_2-Ring	413-391	391	413-391	414-396
Bridging unit	527-449	380-258	354-254	328-254
Deformation region	Below 391	Below 258	Below 254	Below 254

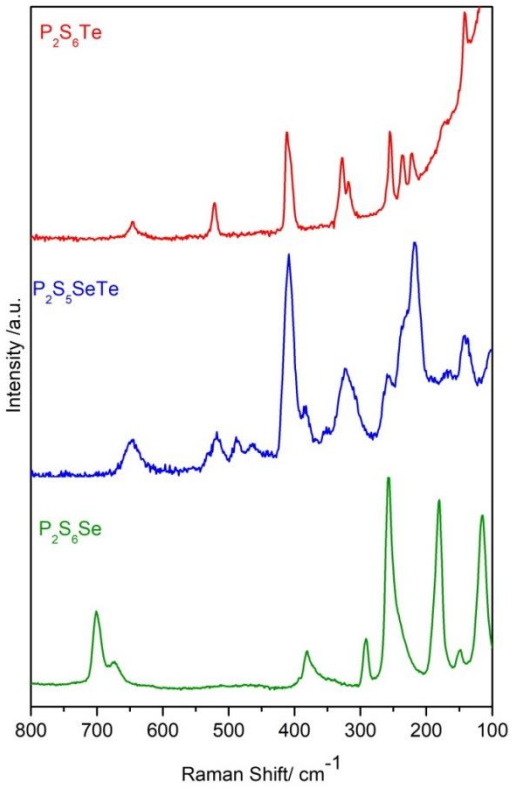

Figure 3.5.3: Comparison between Raman spectra of P_2S_6Se, P_2S_5SeTe and P_2S_6Te

3.6 Another new phosphorus tellurium sulphide, $P_2S_8Te_3$

$P_2S_8Te_3$ was synthesised in a second step reaction starting from P_2S_6Te. While exploring the adduct formation ability of the above mentioned compound with transition metal halide, on reaction with mercuric iodide $P_2S_8Te_3$ was prepared. Though detailed characterisation was beyond scope of thesis because of time restriction but the structure was confirmed by SCXRD, SEM-EDS measurement and Raman spectroscopy. This structure is very unique not only because it is only second compound containing phosphorus, sulphur and tellurium but also this compound has long distance interaction between tellurium atoms.

3.6.1 Synthesis

0.5 gm of P_2S_6Te with catalytic amount of HgI_2 (10 wt% of precursor) and catalytic amount of $FeCl_3 \cdot 6H_2O$ (10 wt% of precursor) were grinded very well in a mortar and filled, evacuated and sealed in a 6 cm long quartz tube. The mixture was heated to 350°C with a heating rate 0.2°C/min and annealed at the same temperature for 10 days. After 10 days the ampoule was cooled at the same rate as heating and few red colour crystals of $P_2S_8Te_3$ along with unreacted precursors were obtained. Starting from elemental precursors of the compound did not work. Also both mineraliser were necessary for the synthesis as without $FeCl_3 \cdot 6H_2O$ no desirable reaction took place and without HgI_2 the resultant product was only starting materials.

3.6.2 Single crystal measurement

The measured crystal at 123 K showed a monoclinic crystal system adopting space group *C2/c* (No. 15) with lattice parameters a = 10.5448(7) Å, b = 7.5851(5) Å, c = 12.1630(7) Å, β = 114.37(1)°. All the crystallographic data is listed below in Table 3.6.1. The crystal structure has very unique Te-Te bond. The basic crystal structure can be derived from P_2S_6Te as shown in Figure 3.6.2. It has PS_4 polyhedron like all the structures mentioned above. But those polyhedrons instead of making edge-sharing unit are connected by tellurium atoms in a plane. Three of the sulphur atoms of the polyhedron are connected by three tellurium atoms and each tellurium in turn is connected to two polyhedrons. This looks like 'A' units of P_2S_6Te are parallelly connected by tellurium atoms (Figure 3.6.1) making a two strand polymeric structure. So in this structure there are two types of bridging or connecting tellurium atoms, Te^{brid1}, connecting PS_4 polyhedrons in unit 'A' and Te^{brid2}, connecting unit 'A' to make double strand polymeric unit. Now these double strand polymers are connected to each other

Table 3.6.1: Crystallographic data and measurement parameters of $P_2S_8Te_3$

Compound name	**$P_2S_8Te_3$**
Empirical formula	$P_2S_8Te_3$
Formula weight, g mol^{-1}	701.23
Crystal colour and shape	Red, block
Crystal system	monoclinic
Space group	*P2$_1$/n* (No.14)
a, Å	12.2157(4)
b, Å	6.0481(2)
c, Å	18.1733(6)
β/^{o}	90.133(3)
V, Å^3; *Z*	1342.67(8), 4
Absorption coefficient , mm^{-1}	16.097
ρ_{calc} , g cm^{-3}	2.5632
Diffractometer	Rigaku Super Nova
Radiation	MoK$_\alpha$, λ = 0.71073 Å
Temperature, K	123
θ-range, ^{o}	3.55-30.58
hkl-range	$-16 \le h \le 16$ $-8 \le k \le 8$ $-25 \le l \le 24$
Absorption correction	numerical (gaussisan)
Number of reflections	14824
Independent reflections	3767
R_{int}	0.046
Structure solution	Charge flipping, Superflip
Structure refinement	*JANA2006*
Completeness to θ_{max}	99.7%
Parameters	118
GooF	1.06
R_1, wR_2 *[I>2σ(I)]*	0.0274, 0.0262
R_1, wR_2 [all reflections]	0.0447, 0.0302
Residual electron density, e Å^{-3}	-1.28/1.18

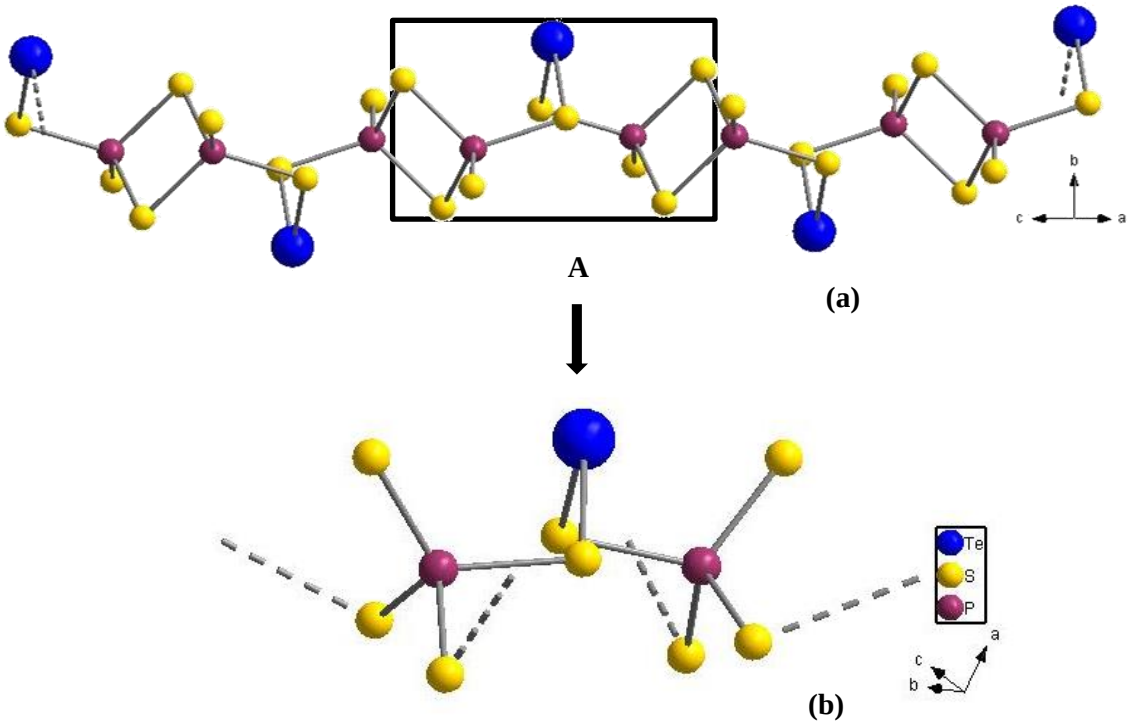

Figure 4.6.1: (a) unit 'A' in P_2S_6Te, (b) similar unit 'A' in $P_2S_8Te_3$

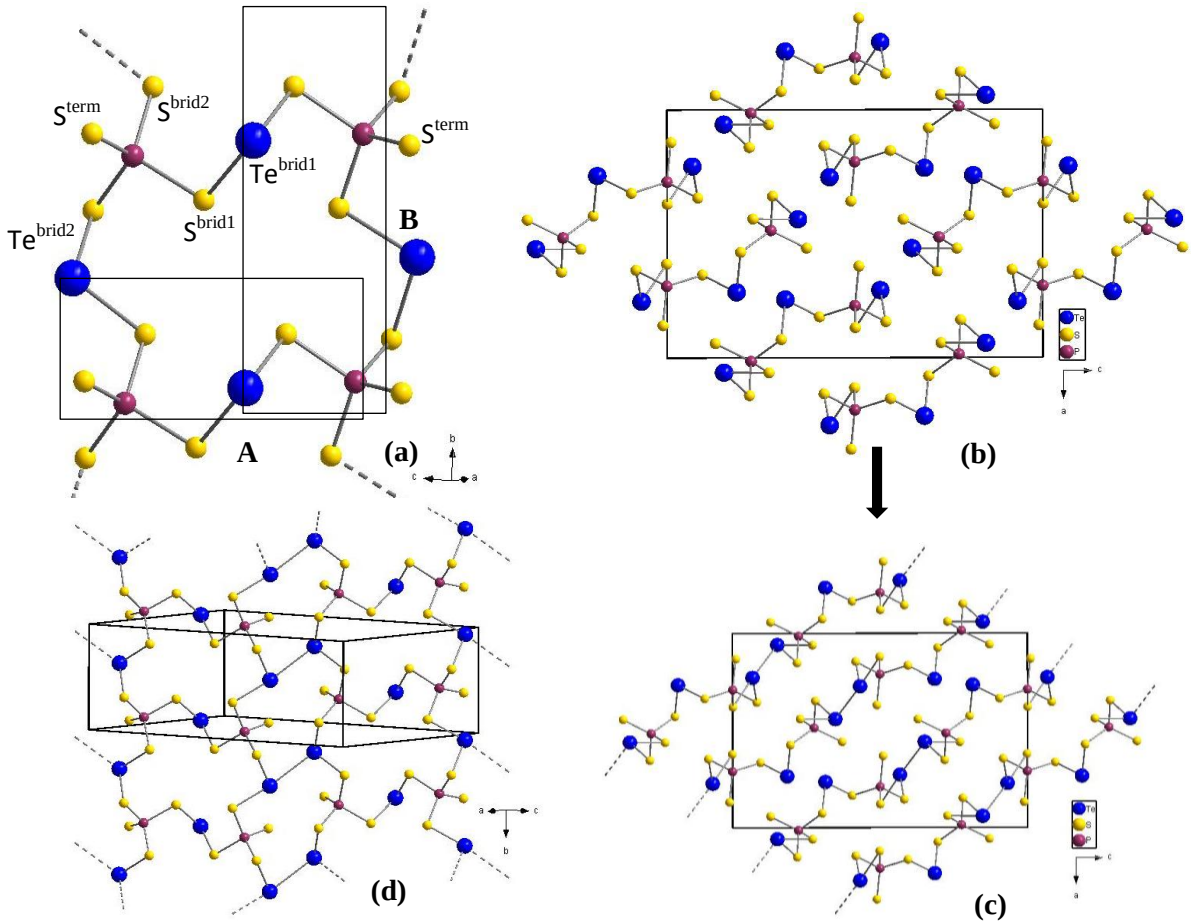

Figure 5.6.2: (a) unit 'A' and 'B' in $P_2S_8Te_3$ connected almost perpendicularly making double strand polymeric unit, (b) arrangement of the polymeric units in the unit cell along 'c'-axis, (c) same unit cell like previous picture but connecting Te^{brid2} atoms with long Te-Te bond of 3.183(1) Å length, (d) one single polymeric sheet in the unit cell

by unique Te-Te bonds between Te^{brid2} atoms in the plane parallel to the polymer making a 2D structure sheet like structure. And this sheet structure is stacked parallel to 101-plane of the unit cell. This kind of layered structure is not so common in phosphorus chalcogen chemistry especially long distance Te-Te bonds. Traditional Te-Te bond distance in solid state compound is 2.74 Å but it can be extended upto 3.6 Å or more, but still less than the van der Waals distance of 4.1 Å[41]. In current compound this distance is 3.183(1) Å so the Te-Te interaction is significantly interesting especially in phosphorus containing compound. Even in room temperature elemental tellurium this near neighbour interaction is observed with a distance of 3.49 Å. This may be due to catenation property of tellurium as even for NaTe compound Te exists as Te_5 zigzag chain resulting resulting into imperial formula $Na_6Te(Te_5)$[41,42]. But here this long distance chalcogen- chalcogen interaction is observed between the double strand polymers of the same plane only. This interaction is not observed between two layers. The minimum distance between two layers is between corresponding tellurium atoms (Te^{brid1}) of the 'A' unit, 3.849(1) Å. Still this distance is lower than the van der Waal distance. Comparison between selected bond distances and bond angles of the common unit of P_2S_6Te and $P_2S_8Te_3$ is listed in Table 3.6.2. The atom coordinates and equivalent isotropic displacement parameters for the final structure solution are listed in Table S3.17. The anisotropic displacement parameters are listed in Table S3.18. There is also an overview of the bond lengths and angles are given in Table S3.19. The 'A' units of double strand polymers are connected along b-axis through Te^{brid2} as mentioned above making structure similar to unit 'A' which can be denoted as unit 'B' but from a crystallographic viewpoint it is very different from unit 'A'. The comparison between two structures is listed in Table 3.6.2. There are three types of S atoms present in the structure. First, the terminal sulphur S^{term}, second bridging sulphur atom of 'A' unit S^{brid1} and lastly bridging sulphur atoms of 'B' unit S^{brid2}. Te-S bond distances [2.450(2) Å- 2.532(2) Å] are longer and ∠S-Te-S bond angle [85.62(2)^o- 87.50(2 ^{o}] are shorter in unit 'B' than in unit 'A'. Te^{brid2}-Te^{brid2} inter-polymeric interaction is responsible for Te^{brid2}-S^{brid2} bond elongation in unit 'B' and because of this interaction electron density on Te^{brid2} is reduced, making ∠S^{brid2}-Te^{brid2}-S^{brid2} bond angle shorter than ∠S^{brid1}-Te^{brid1}-S^{brid1} [96.52(2)^o] where any such long distance bonding interaction is absent. Other bond distances and bond angles are comparable to P_2S_6Te. S^{term} has no long distance interaction with tellurium of neighbouring polymers like P_2S_6Te but it has a distance of only 3.016-3.034(1) Å with one of the Te atom of unit 'B'. So the S^{term} of one strand of the polymeric chain is tilted towards Te^{brid2} and S^{term} of the other strand of the

Table 3.6.2: Comparison between selected bond distances (Å) and bond angles and torsion angle (°) of the common unit of P_2S_6Te and $P_2S_8Te_3$

Bond distances	**$P_2S_8Te_3$**	**P_2S_6Te**
P-S^{term}	1.969(1)-1.991(1)	1.949(2)
P-S^{brid}	2.092(1)-2.097(1)/P- S^{brid1} for unit 'A' 2.090(1)-2.058(1)/ P- S^{brid2} for unit 'B'	2.078(1)
Te-S^{brid}	2.386(1)-2.392(1) /Te-S^{brid1} for unit 'A' 2.450(1)-2.532(1)/Te-S^{brid2} for unit 'B'	2.439(2)
Inter-polymeric distance	3.183(1)	3.100(1)
Bond angles(°)		
∠S-Te-S	96.50(1) for unit 'A' 85.62(1) for unit 'B'	100.82(2)
∠P-S-Te	98.91(1)-101.75(1) for unit 'A' 93.11(3)-97.35(1) for unit 'B'	105.66(3)
Torsion angle(°)		
P-S-Te-S	87.84(2)-89.01(1) for unit 'A' 102.93(1)-171.27(1) for unit 'B'	80.14(3)

same polymer is tilted on the opposite direction as shown in Figure 3.6.2(a). The minimum distance between two layers or two sheets is 3.591(1) Å between Te^{brid1} and S^{brid1} atoms of corresponding sheets but distance between Te^{brid1} atoms of corresponding sheets is 3.849(7) Å. This distance is also lower than van der Waal distance between tellurium atoms. So the inter-layer interaction is also significant enough.

3.6.3 SEM-EDS measurement

The SEM-EDS experiment is done for the crystal which is used for single crystal XRD measurement. The data is listed in Table 3.6.3. The experimental data supported the calculated formula of $P_2S_8Te_3$ but a little bit of iodine was also measured (1.23 wt%). This iodine can be found as impurity on the surface as significant amount of HgI_2 was used for the corresponding experiment.

Table 3.6.3: Atomic percentage of P_2S_5SeTe from SEM-EDS measurement and theoretical value calculated from SCXRD

Elements (atom %)	P	S	Te
Calculated (SCXRD)	15.38	61.53	23.07
Measured (EDS)	16.19	59.66	22.92

3.6.4 Raman Spectroscopy

The spectrum of $P_2S_8Te_3$ is very similar to P_2S_6Te. But assignment of the peaks for interaction between atoms is bit difficult because building units ('A' and 'B') with similar composition and connections has very different crystallographic geometry. It also shows peak for P-S^{term} bond at 635 cm^{-1} even though Te- S^{term} inter-polymer interaction is absent but Te-S^{term} intra-polymer interaction is present. The P-S^{brid} interaction is observed in 508-396 cm^{-1} region. And from 315-207 cm^{-1} region is assigned to bridging unit of S-Te-S. By comparing with literature data[43,44] it was seen that in glass form and exfoliated Tellurium a signature peak can be observed around 130 cm^{-1}. For our measurement also a peak at 128 cm^{-1} was observed which can be assigned to Te-Te inter-polymer interaction. And the very strong peak at 90 cm^{-1} came from the machine error. The measured data and table for the assigned peak can be found in Figure 3.6.3 and Table 3.6.4 respectively.

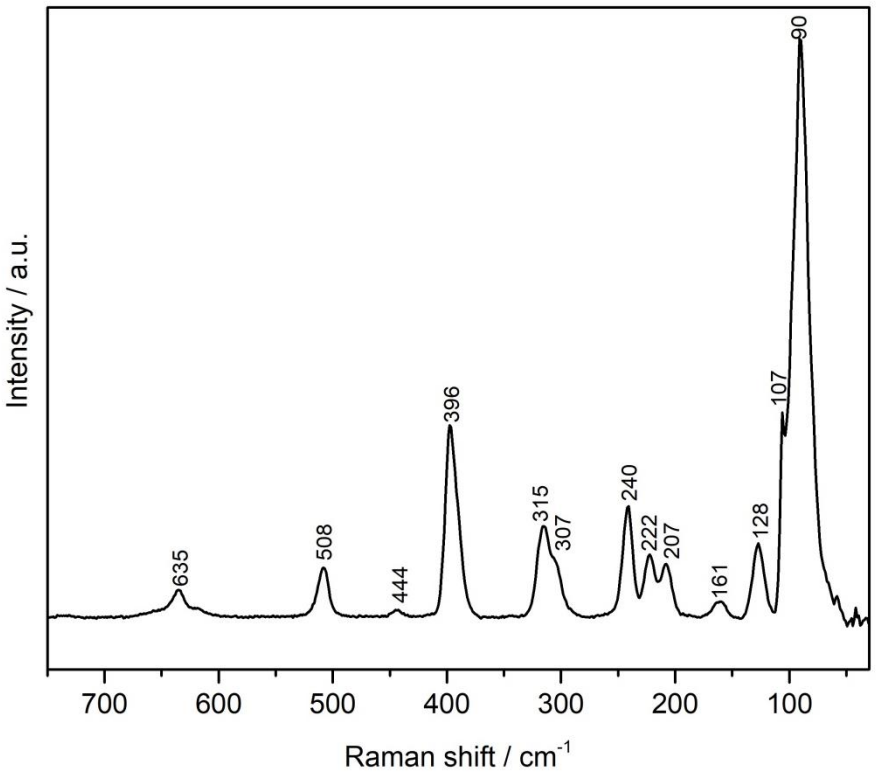

Figure 3.6.3: Raman spectrum of mixture $P_2S_8Te_3$

Table 3.6.4: List of peaks of Raman spectrum of mixture of $P_2S_8Te_3$

Wavenumbers (cm^{-1})	**Intensity**	**$P_2S_8Te_3$**
635	w	ν(P-S^{term})
508	w	ν(P-S^{brid})
444	vw	ν(P-S^{brid})
396	s	ν(P-S^{brid})
315	ms	ν(S-Te-S bridging unit)
307	sh	ν(S-Te-S bridging unit)
240	ms	ν(S-Te-S bridging unit)
222	ms	ν(S-Te-S bridging unit)
207	ms	ν(S-Te-S bridging unit)
161	w	δ
128	ms	δ
107	s	ν (Te-Te)

ms= medium strong, s= strong, w= weak, vw=very weak, sh= shoulder

3.7 References

[1] Cowley, A. H., *J. Chem. Educ.*, (1964) **41**, 530.

[2] Schnering, H. G. von; Hoenle, W., *Chem. Rev.*, (1988) **88**, 243.

[3] Rödl, T.; Weihrich, R.; Wack, J.; Senker, J.; Pfitzner, A., *Angew. Chem. Int. Ed.*, (2011) **50**, 10996.

[4] Donohue, P. C.; Bierstedt, P. E., *Inorg. Chem.*, (1969) **8**, 2690.

[5] Bingham, E.; Cohrssen, B.; Powell, C. H., *Patty's toxicology*, (2001), New York, Wiley.

[6] Malczewska-Toth, B., *Phosphorus, Selenium, Tellurium, and Sulfur*, (2012), New York, Wiley.

[7] Li; Yu; Ohno; Gu; Czajka; Kasuya; Nishina; Kawazoe, *Phys. Rev. B*, (1995) **52**, 1524.

[8] Itthibenchapong, V.; Kokenyesi, R. S.; Ritenour, A. J.; Zakharov, L. N.; Boettcher, S. W.; Wager, J. F.; Keszler, D. A., *J. Mater. Chem. C*, (2013) **1**, 657.

[9] Houska, J.; Alberti, M.; Havel, J., *Rapid Commun. Mass Spectrom.*, (2008) **22**, 417.

[10] Blachnik, R.; Wickel, U., *Z. Naturforsch. B*, (1982) **37**, 1507.

[11] Pfitzner, A., *Chem. Eur. J.*, (2000) **6**, 1891

[12] Feldmann, K.-O.; Wiegand, T.; Ren, J.; Eckert, H.; Breternitz, J.; Groh, M. F.; Müller, U.; Ruck, M.; Maryasin, B.; Ochsenfeld, C.; Schön, O.; Karaghiosoff, K.; Weigand, J. J., *Chem. Eur. J.*, (2015) **21**, 9697.

[13] Rothenberger, A.; Wang, H.-H.; Chung, D.; Kanatzidis, M. G., *Inorg. Chem.*, (2010) **49**, 1144.

[14] Rothenberger, A.; Morris, C.; Wang, H.-H.; Chung, D. Y.; Kanatzidis, M. G., *Inorg. Chem.*, (2009) **48**, 9036.

[15] Groh, M. F.; Isaeva, A.; Müller, U.; Gebauer, P.; Knies, M.; Ruck, M., *Eur. J. Inorg. Chem.*, (2016) **2016**, 880.

[16] Schäfer, H., *Angew. Chem. Int. Ed.*, (1961) **73**, 11.

[17] Gruehn, R.; Glaum, R., *Angew. Chem. Int. Ed.*, (2000) **39**, 692.

[18] Lange, S.; Bawohl, M.; Weihrich, R.; Nilges, T., *Angew. Chem. Int. Ed.*, (2008) **120**, 5736.

[19] Haynes, W. M., *Handbook of Chemistry and Physics*, (2011), Hoboken, CRC Press.

[20] Bawohl, M.; Nilges, T., *Z. anorg. allg. Chem.*, (2015) **641**, 304.

[21] Stein, A.; Keller, S. W.; Mallouk, T. E., *Science*, (1993) **259**, 1558.

[22] Laitinen, R.; Niinistö, L.; Steudel, R., *Acta Chem. Scand.*, (1979) **33a**, 737.

[23] Bondi, A., *J. Phys. Chem.*, (1964) **68**, 441.

[24] Ibers, J., *Nat. Chem*, (2009) **1**, 508.

[25] Jones, R. O.; Seifert, G., *J. Chem. Phys*, (1992) **96**, 2942.

[26] Baldus, H. P.; Blachnik, R., *Z. Naturforsch.*, (1990) **45b,** 1606.

[27] Jörgens, S.; Johrendt, D.; Mewis, A., *Chem. Eur. J*, (2003) **9**, 2405.

[28] Chung, I.; Song, J.-H.; Kim, M. G.; Malliakas, C. D.; Karst, A. L.; Freeman, A. J.; Weliky, D. P.; Kanatzidis, M. G., *J. Am. Chem. Soc*, (2009) **131**, 16303.

[29] Sun, F.; Zhang, B.; Tang, H.; Yue, Z.; Li, X.; Yin, C.; Zhou, L., *J. Mater. Chem. A*, (2018) **6**, 10104.

[30] He, J.; Chen, Y.; Lv, W.; Wen, K.; Wang, Z.; Zhang, W.; Li, Y.; Qin, W.; He, W., *ACS nano*, (2016) **10**, 8837.

[31] Pfitzner, A.; Zimmerer, S., *Z. anorg. allg. Chem.*, (1996) **622**, 853.

[32] Gillespie, R. J.; Luk, W.; Maharajh. E.; Slim, D. R., *J.C.S. Chem. Comm.*, (1976) **19,** 791.

[33] Bondi, A., *J. Phys. Chem.*, (1964), **68**, 441.

[34] Laitinen, R. S.; Pekonen, P.; Suontamo, R. J., *Coord. Chem.*, (1994) **130**, 1.

[35] Nilges, T.; Reiser, S.; Hong, J. H.; Gaudin, E.; Pfitzner, A., *Phys. Chem. Chem. Phys.*, (2002) **4**, 5888.

[36] Pfitzner, A., *Inorg. Chem.*, (1998) **37**, 5164.

[37] Brockner, W.; Becker, R.; Eisenmann, B.; Schäfer, H., *Z. anorg. allg. Chem.*, (1985) **520**, 51.

[38] Haiduc, I.; King, R. B.; Newton, M. G., *Chem. Rev.*, (1994) **94**, 301.

[39] Thomas Rödl, *Dissertation*, (2012), University of Regensburg.

[40] Bagayoko, D., *AIP Advances*, (2014) **4**, 127104.

[41] Tattershall, B. W.; Blachnik, R.; Baldus, H. P., *J. Chem. Soc., Dalton Trans.*, (1989) **5**, 977.

[42] P.BöttcherR.Keller, *Journal of the Less Common Metals*, (1985) **109**, 311.

[43] Tverjanovich, A.; Cuisset, A.; Fontanari, D.; Bychkov, E., *J. Am. Ceram. Soc.*, (2018) **101**, 5188.

[44] Churchill, H. O. H.; Salamo, G. J.; Yu, S.-Q.; Hironaka, T.; Hu, X.; Stacy, J.; Shih, I., *Nanoscale Res. Lett.*, (2017) **12**, 488.

4. Boracite-type host-guest and adduct compounds

Adduct compounds of pnictogen chalcogenides with copper halides is a well explored part of co-ordination chemistry[1–7]. Interestingly Pfitzner and co-workers showed that copper halides can also be used as 'preparative tool' for the synthesis of new polymeric and oligomeric main group compounds[8–12]. All these examples established the extensive diversity and versatility of copper halide compounds. Host-guest interaction between discrete moieties is observed in organic, inorganic as well as metalorganic compounds like MOFs or metal organic frame works[13] which are extensively used in catalysis[14], gas storage[15], biological sensing[16] and imaging[17] and even as superconductors[18,19]. Other than that, clathrates[20,21], supramolecular assemblies[22,23], inclusion compounds[24] are prominent examples of such host-guest interactions. Usually the 'guest' atoms or molecules or ions are trapped or enclosed or caged inside the 'host' framework by non-covalent interactions like hydrogen bonding[25], dipole-dipole interaction[26], van der Waals interaction[27], hydrophobic interactions[28] etc.. Boracite[29–32] (e.g., $Mg_3B_7O_{13}Cl$) is one of such compounds where halides or hydroxyl ions are caged inside a metal borate frame work. In previous work Jung[33] and Braü[34] have shown Zn and Cd halides host-guest compounds with pnictogen chalcogenide cage molecules, $(ZnI_2)_6(ZnS)(P_4S_x)$ and $(CdI_2)_6(CdS)(As_4S_x)$ respectively, having similar crystal structure as boracite. Vitzthumecker[35] in his thesis has extended this series with host network using copper iodide and mercury iodide as the backbone of the structure. $(ZnI_2)_6(ZnS)(P_4S_x)$ was synthesised by one-step or two-step reaction of stoichiometric amounts of ZnI_2, P_n, elemental Zn and varying amounts of chalcogen depending on the composition in evacuated silica ampoules and characterised by Jung[33]. The basic structures of such compounds consist of monomeric α-Pn_4Q_x cage molecules which are separated by a cubic host lattice of metal chalcogen halide (or metal halide)-metal chalcogenide network. This chapter involves not only the extended series of such compounds but also the actual composition, and physical state of the guest molecule is elucidated here. This research work is supported by single crystal X-ray diffraction, Raman spectroscopy, and NMR spectroscopy. And it can be concluded that the formula of the above mentioned compound can be better described as $(P_4S_3)@Zn_7SI_{12}$, and all the other isostructural compounds are addressed with similar formula in this chapter.

4.1 $(P_4S_3)@Zn_7SI_{12}$

4.1.1 Synthesis

This compound was synthesised as described by Jung[33]: 0.8223 g white ZnI_2 (6 eqiv.), 0.0281 g metallic Zn (1 eqiv.), 0.0532 g red phosphorus (4 eqiv.) and 0.0551 g sulphur (3 eqiv.) were grinded intensively in glove box and after evacuation sealed into a 7 cm long quartz ampoule (for 1 g starting material). The synthesis time was 10 days at 650 °C with subsequent cooling to room temperature for 17 hours. But after first heating cycle only few crystals of the desired compound was obtained along with the mixture of starting materials, and intermediates. So a recrystallization step was followed by the first heating of the starting materials (as described by Jung). The miscellaneous mixture was again grinded thoroughly and heated in 7 cm long ampoule at 400 ^oC for six months with a heating rate of 0.5 ^oC/min. The cooling rate was 1.5 ^oC/min in order to avoid formation of side product on the crystals. After six months almost transparent pure crystals were formed.

4.1.2 Single crystal measurement

Almost transparent crystals of $(P_4S_3)@Zn_7SI_{12}$ were obtained from the ampoule. Crystal of $(P_4S_3)@Zn_7SI_{12}$ was measured at 293 K to cubic space group $F\bar{4}3c$ with cell parameter a= 19.405(2) Å. The refinement for all data for $(P_4S_3)@Zn_7SI_{12}$ converged at GooF value of 1.07 with R_1 value of 2.54% and wR_2 value of 4.63%. The same crystal was also measure at 123 K for comparison. Table 4.1.1 provides an overview of the crystallographic data and the measurement parameters of the clathrate compound at 293K and 123K. The atom coordinates and equivalent isotropic displacement parameters for the final structure solution are listed in table Table S4.1. The anisotropic displacement parameters are listed in Table S4.2. There is also an overview of the bond lengths and angles are given in Table S4.3 in the Supporting information section. All crystallographic data in the Supporting information section are derived from the refinement in the $F\bar{4}3c$ space group at 293 K. For structure determination and refinement of the cage molecule, the phosphorus and sulphur atoms of the cage were added according to symmetry requirement of the P_4S_3 molecule, i.e. the residual electron density with 3-fold symmetry is assigned to apical P atom where residual electron density with site symmetry order 1 is assigned to S and basal P atoms consecutively. Then distant restrain was applied according to crystallographic data of α- P_4S_3 cage[36].

Table 4.2.1: Crystallographic data of $(P_4S_3)@Zn_7SI_{12}$ at 293 K and 123 K

Compound	**$(P_4S_3)@Zn_7SI_{12}$**	
Empirical formula	$Zn_7\ I_{12}\ P_4\ S_4$	
Formula weight, g mol^{-1}	2232.7	
Crystal colour and shape	Colourless, Block	
Crystal system	Cubic	
Space group	$F\bar{4}3c$ (No. 219)	
Temperature, K	293	123
a, Å	19.4050(16)	19.2983(16)
V, Å^3; *Z*	7307.0(10), 8	7187.2(10), 8
Absorption coefficient , mm^{-1}	15.059	15.31
ρ_{calc} , g cm^{-3}	4.059	4.127
Diffractometer	Rigaku Super Nova	
Radiation	MoK_α, λ = 0.71073 Å	
θ-range, ^{O}	3.64 – 32.31	4.21 – 32.08
hkl-range	$-19 \le h \le 16$ $-24 \le k \le 10$ $-7 \le l \le 28$	$-28 \le h \le 20$ $-25 \le k \le 25$ $-28 \le l \le 20$
Absorption correction	numerical (Gaussian)	
Number of reflections	2937	1037
Independent reflections	964	927
R_{int}	0.0229	0.0266
Completeness	99.5%	99.2%
Twin matrix	-1 0 0, 0 -1 0, 0 0 -1	
Twin fraction	0.34(2)	0.48(9)
Structure solution	Charge flipping, Superflip	
Structure refinement	*JANA2006*	
Parameters	43	40
GooF	1.07	1.06
R_1, wR_2 $[I>2\sigma(I)]$	0.0193, 0.0437	0.0152, 0.0345
R_1, wR_2 [all reflections]	0.0254, 0.0463	0.0187, 0.0360
Residual electron density, e Å^{-3}	1.56/ -0.94	3.28/ -0.85

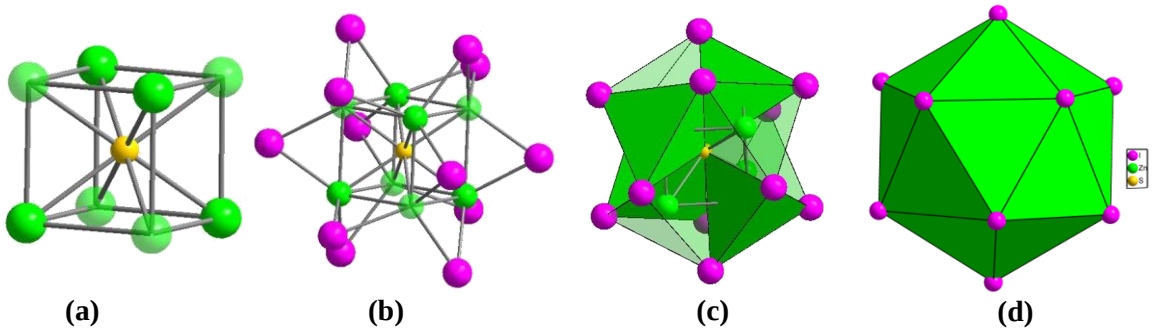

Figure 4.1.1: (a) $S(Zn_{1/2})_8$ cubic base unit in the zinc halide matrix, but feasible co-ordination no. of S is four so half of the S atoms are shown with light green colour; (b) cubic base unit is capped by 12 iodine atoms along 12 edges of the cubic structure; (c) 8 ZnI_3S tetrahedron formed with Zn atom as central atom and 3 iodine and one sulphur as the co-ordinating atoms, alternative tetrahedron are shown with transparent green colour, as either of them is possible; (d) I_{12} icosahedron

Then the occupancy factors a_i of the S and both types of phosphorus was refined. With further refinement with numerical absorption correction the refinement converges to R_1 0.0229 and wR_2 0.0643 and the residual electron density is much lower than in previous works[33,35]. After free refinement of the occupancy factors of the zinc atoms, total 7 zinc

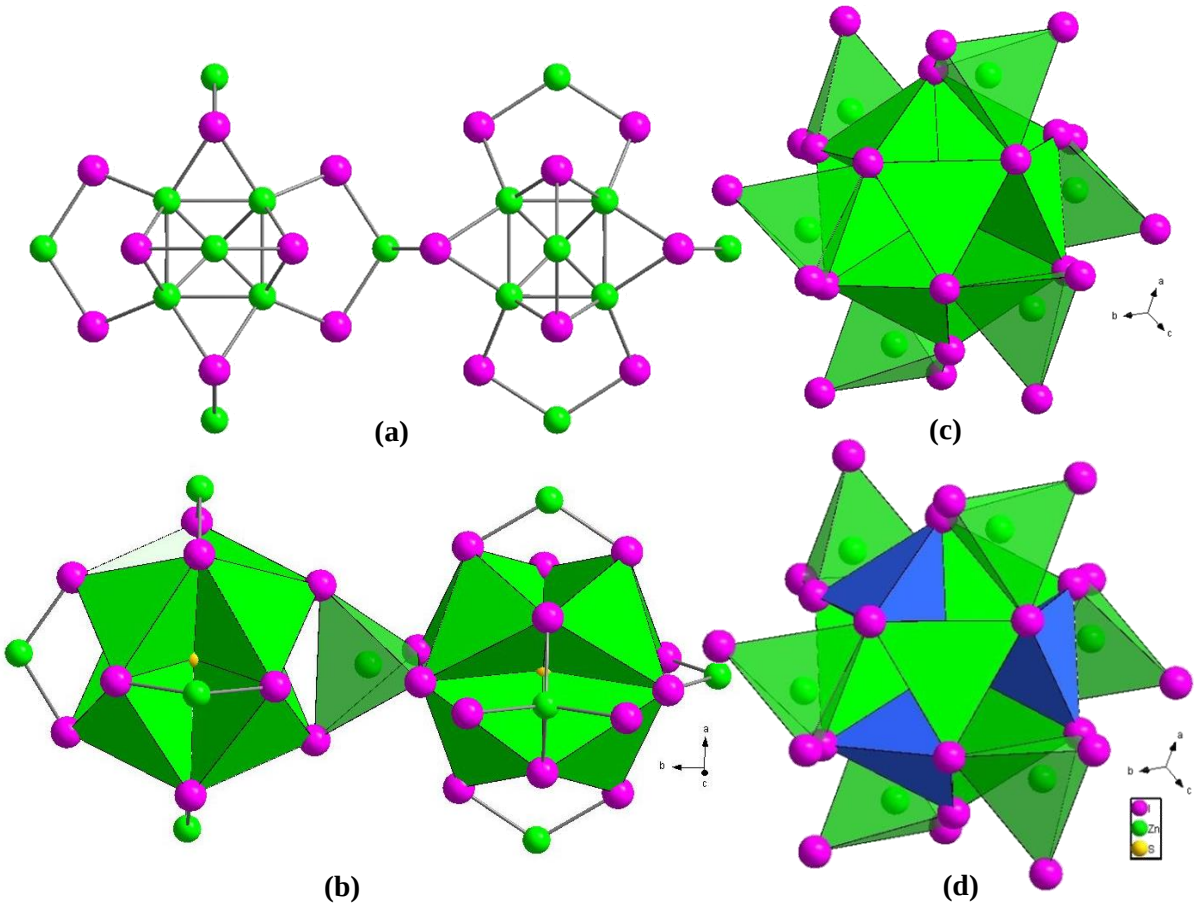

Figure 4.1.2: (a) and (b) Connection pattern of two basic construction units made of zinc, sulphur and iodine $S@Zn_4@I_{12}$ via ZnI_4 tetrahedra; (c) Basic unit $S@Zn_4@I_{12}$ with all six connecting ZnI_4 tetrahedra and (d) showing sae unit as 'c' but the blue tetrahedra designate alternative $ZnSI_3$ units considering tetrahedral co-ordination of sulphur

atoms per formula unit was calculated. As the compound crystallises in space group $F\bar{4}3c$, with inversion twin so it can be concluded that only 50% of the occupancy of copper in SCu_8 cubic unit is feasible (shown in figure 4.1.1). Either of the two intercalated disordered SZn_4 units serves as the basic construction unit of the matrix. The zinc atoms are themselves surrounded by icosahedron of iodine atoms, I_{12} and make 8 $ZnSI_3$ tetrahedrons. This basic unit is shown in Figure 4.1.1(b) and (c). Due to the disorder, 8 of the 20 possible tetrahedrons are inside an icosahedron. The $ZnSI_3$ tetrahedrons shares single sulphur atom and are connected with each other by sharing three corners containing iodine atoms.

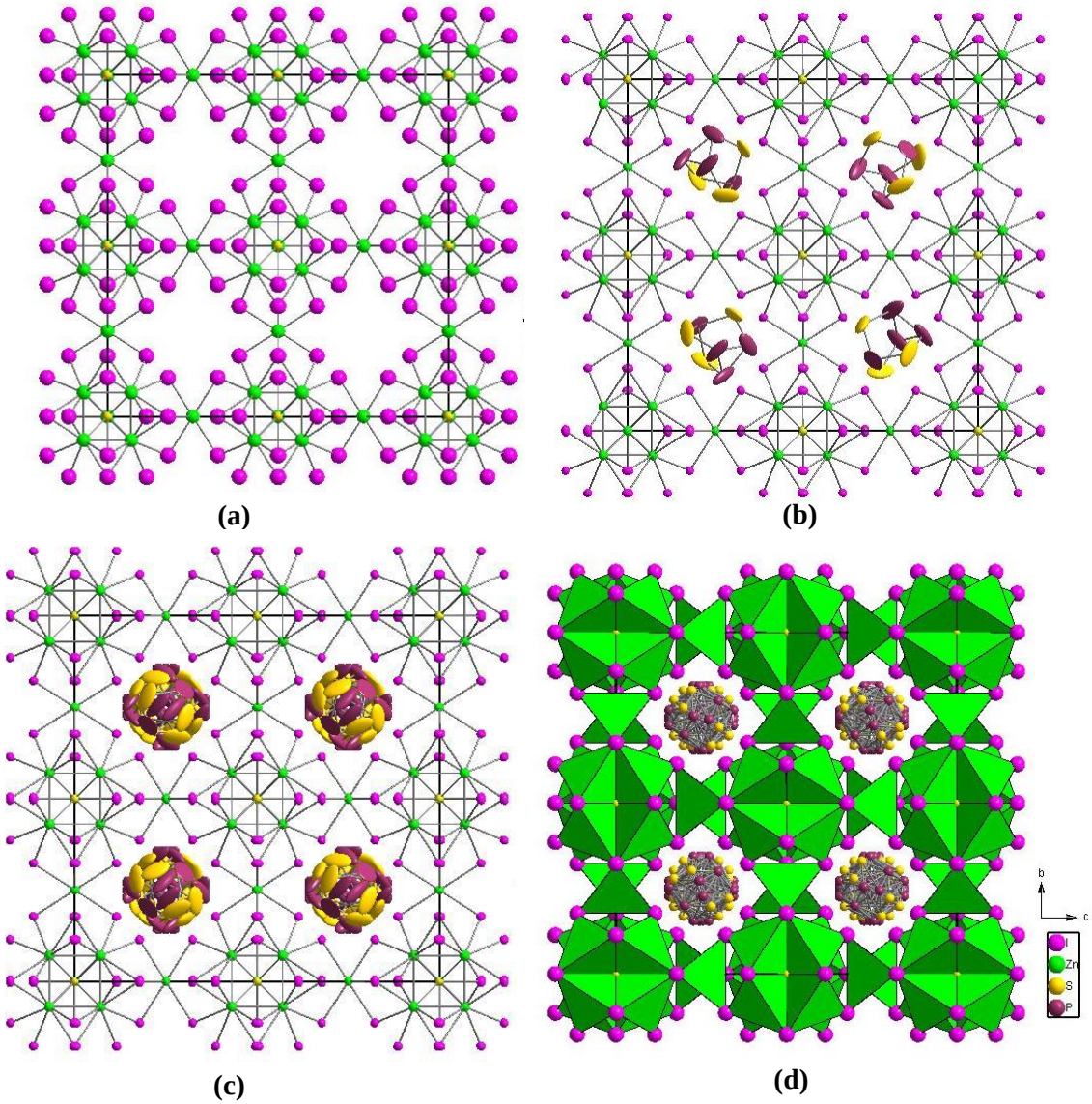

Figure 4.1.3: (a) Zn-I-S unit connected by ZnI_4 tetrahedra with cavities in the structure; (b) Four different cage orientations in four cavities in the Zn-I-S framework and (c) rotating P_4S_3 cage with all possible orientations with anisotropic atoms which visibly show high displacement of electron density of P and S of the cage; (d) Zn-I-S framework with $ZnSI_3$ and ZnI_4 tetrahedra and rotating P_4S_3 cage in the unit cell

Two corner shared tetrahedrons are bridged to neighbouring similar pair by Zn atom (designated as Zn1) so there are total 6 zinc atoms bridging 12 iodine atoms, In this second layer of zinc atoms, Zn1 is tetrahedrally co-ordinated, connecting two $S@Zn_4@I_{12}$ units through ZnI_4 tetrahedron. Each Zn1 is connecting two icosahedrons (Figure 4.1.2). So each icosahedron is connected to 6 other icosahedrons through ZnI_4 tetrahedron to form a three dimensional network as shown in Figure 4.1.2. A similar iodo-centered icosahedron of iodine and copper can be found in $(DabcoH_x)_4(Cu_yI_{16})$ (DabcoH = 1-Azonium-4-azabicyclo[2.2.2]octan) in which 14 of the possible tetrahedron gaps in I_{12} icosahedron is partially occupied by copper layers. So the 4 out of total 7 zinc atoms of the formula unit belong to icosahedral structure and 3 zinc atoms distributed in 6 connecting tetrahedrons. So the icosahedrons of Zn, I and S form a rigid structure by three dimensional linkages with each other through ZnI_4 tetrahedrons. And this whole network has cubic symmetry. Between the linked icosahedrons there are large cavities, see Figure 4.1.3. P_4S_3 cages are stored in these cavities. Table 4.1.2 gives an overview of P_4S_3 cage molecule and its point group.

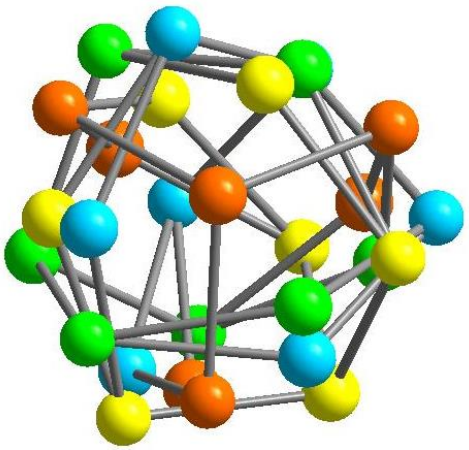

Figure 4.1.4: Four different orientations of one cage with four different 3- fold axis inside the cavity of framework- four orientations designated in four colours orange, yellow, blue and green.

Table 4.3.2: Details of the P_4S_3 cage inside the cavity of Zn-I-S framework

Bond distances (Å)		
	Measured	Literature[20]
P1-S1	2.100(12)	1.996-2.130
S1-S1	3.180(18)	3.207-3.222
P2-S1	2.099(18)	2.095-2.103
P2-P2	2.223(14)	2.223-2.239
P1-P2	3.280(10)	3.208-3.258
Bond angel (°)		
P1 S1 P2	102.71(4)	102.98
S1 P1 S1	98.41(5)	98.74-102.40
P1 S1 S1	40.79(2)	40.51
S1 S1 S1	60.00(2)	60.30
P2 P2 P2	60.00(3)	60.1
S1 P2 P2	107.64(3)	103.54
P2 S1 S1	72.3-79.9(3)	76.69

In cubic symmetry there are four three-fold rotational axes along the diagonals and P_4S_3 cage, having C_{3v} symmetry also contains three-fold rotational axis and one P_4S_3 molecule can be oriented in two opposite directions along its rotational axis. So there should be 8 possible orientations of the P_4S_3 molecule in the cavity of the cubic matrix. To avoid the complexity and easier understanding only 4 orientations along 4 diagonals are considered for crystal structure solution. Despite of the discrepancy between the overall symmetries of the matrix and cage symmetry, we were able to fit P and S of the cage molecule inside the Zn-I-S

network according to three fold rotational symmetry of P_4S_3. The similar problem was not solved previously[33–35]. According to symmetry restriction 4 cages were constructed inside one cavity which can be designated by 4 different orientations of the same cage. Even though t The other 4 orientation And after applying distance restrain from literature[36] for P^{apical}-P^{basal}, P^{apical}-S, P^{basal}-S, P^{basal}-P^{basal}, S-S distances, the displacement parameters of 3 types of atoms of the cage, were refined with ¼ a_i of that suggested by *JANA* as same cage is oriented along 4 different diagonals of the cubic symmetry according to rotation theory. And this results into better goodness of fit value. No third order anharmonic oscillation tensors were needed to use for this refinement. So basically inside one cavity there are 4 P_4S_3 intercalated molecule which is physically impossible but it depicts that the P_4S_3 cage is rotating inside the Zn-I-S matrix. This free rotation of P_4S_3 molecule is also supported by NMR data which is discussed later. The free rotation of the guest molecule is also justified by Zn-P or Zn-S^{cage} distances. The shortest diagonal distance of the cavity occupied by the guest molecule in the matrix is d (Zn-Zn) = 12.117(6) Å. The longest distance in the cage (P^{basal}-S) molecule is 3.48 Å and if all 4 orientations of the cage are being considered still the maximum distance is 3.53 Å between two different orientations. The discrepancy of the diameters of the gaps of the matrices with the diameters of the cage is probably the reason for free rotating cage inside the cavity. NMR study also supported no Cu-P or Cu-S interaction. So it is finally clarified that free rotating P_4S_3 is embedded in Zn-I S matrix and we are also able to assign the residual electron density of the cage as 4 different orientation of the same molecule with reasonable refinement values of single crystal data.

4.1.3 Powder-XRD

The PXRD was measured with re-crystallised sample. Pure sample from recrystallized product was grinded as finely as possible in an agate mortar and filled into a capillary and was measured. The data obtained from measurement is showed in Figure 4.1.5. The data fits almost perfectly with the theoretical pattern and after indexing and refinement of the raw data, 75 reflections were found and all of them were indexed with FOM value 259. Details of the refinement can be found in Table S4.4. The unit cell measured by PXRD is 19.377(1) Å where 19.405(1) Å by SCXRD measurement even though both the measurements were done at 293 K. From thesis of Jung, cell parameters also calculated as 19.38 Å[33].

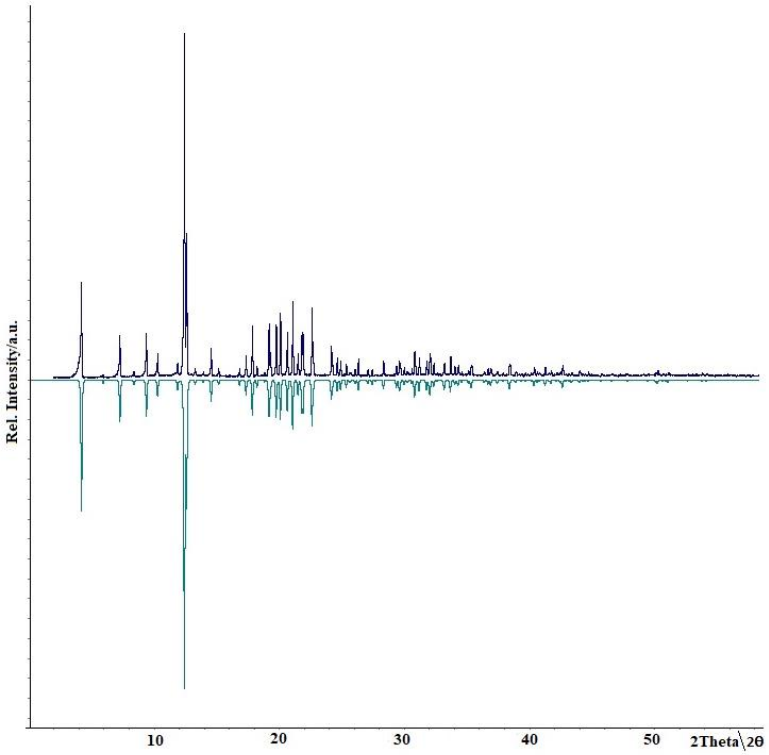

Figure 4.1.5: Measured powder diffractogram of mixture of $(P_4S_3)@Zn_7SI_{12}$ (positive intensity); and purple diffractogram for theoretical pattern of $(P_4S_3)@Zn_7SI_{12}$ derived from SCXRD data (negative intensity)

4.1.4 Raman spectroscopy

Crystals of $(P_4S_3)@Zn_7SI_{12}$ grinded and then packed in a capillary for Raman spectroscopy measurement at room temperature. The area below 200 cm^{-1} is assigned to Zn-I-S framework vibration by comparing with literature[37] and deformation region of P_4S_3 cage. But the higher wave-number vibrations are quite prominent and fit perfectly with Raman data of P_4S_3 from literature[38]. In Table 4.1.3 the peaks from measured Raman spectra of $(P_4S_3)@Zn_7SI_{12}$ and P_4S_3 from literature are listed. In Figure 4.1.6 the spectra of those two compounds are shown. It can be observed that the position and intensities of the peaks in 200-500 cm^{-1} region perfectly matches for both data. So the guest cage molecule is P_4S_3, it can be confirmed. No shift in that region of the peaks in measured compound might be an indication of no P_4S_3-framework interaction i.e. the P-Zn interaction or S^{cage}-Zn interaction is too weak to be detected which ultimately supports the findings from single crystal data.

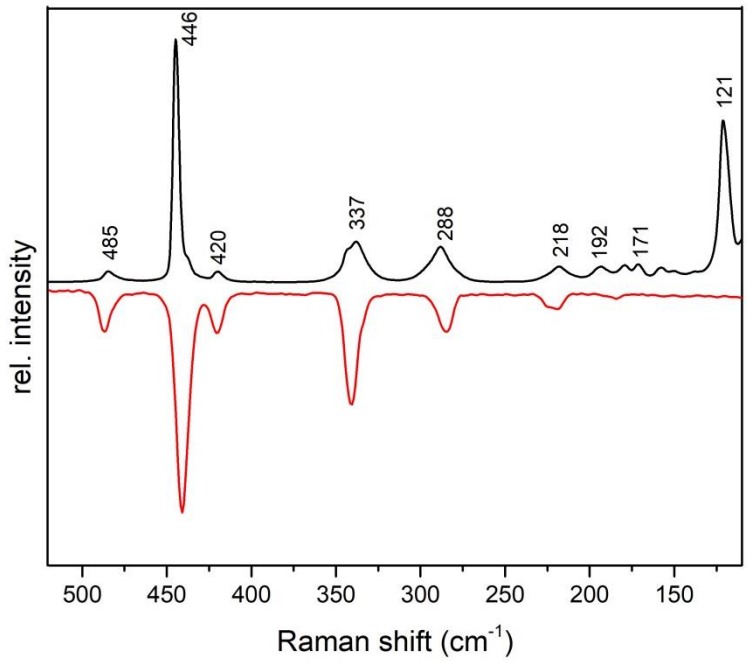

Figure 4.1.6: Raman spectrum of mixture $(P_4S_3)@Zn_7SI_{12}$ (positive intensities) in comparison with Raman spectra of P_4S_3 (negative intensities)

Table 4.1.3: Assignment of experimental peaks to the unit $(P_4S_3)@Zn_7SI_{12}$. The assignments for Zn-I-S framework are not very accurate as the peaks below 100 cm^{-1} are not so prominent or they are in the same position with P_4S_3 unit.

Wavenumbers (cm^{-1})	**Intensity**	**$(P_4S_3)@Zn_7SI_{12}$**
485	w	P_4S_3
446	s	P_4S_3
420	w	P_4S_3
337	ms	P_4S_3
288	ms	P_4S_3
218	w	P_4S_3
192	vw	deformation region of P_4S_3
179	vw	deformation region of P_4S_3
171	vw	deformation region of P_4S_3
158	vw	Zn-I
150	vw	deformation region of P_4S_3
121	s	Zn-I

vw= very weak, w= weak, ms= medium strong, s= stong

4.1.5 NMR Spectroscopy

In cooperation with the chair of Prof. Dr. Jörn Schmedt auf der Günne of the University of Siegen, solid-state NMR investigations were carried out on the compound $(P_4S_3)@Zn_7SI_{12}$. In the following ^{31}P NMR experiments were conducted to elucidate the motional degrees of freedom which are activated on the NMR time scale. For the isolated P_4S_3 molecule by molecular symmetry two different motional degrees are possible. Fast statistical rotation of the molecule around the C_3 axis would leave the chemical shift tensor of the apical untouched; while the chemical shift tensors of the basal P atoms would be reduced in chemical shift anisotropy δ_{ansio} and show an asymmetry parameter η of 0. The second motional degree implies the free rotation of the molecule in 3D. A fast rotation of this kind would reduce the chemical shift anisotropy of both the apical and the basal P atoms to zero.

In the ^{31}P MAS NMR spectra (Figure 4.1.7a), two sharp signals with a peak area ratio of 2.9:1 can be observed, as expected for the presence of P_4S_3 units. Compared to crystalline P_4S_3[39], the isotropic chemical shift values δ_{iso} are shifted to higher ppm values due to a different chemical environment of the ^{31}P spins in the ZnI_2 matrix, whereas the absence of spinning sidebands indicates smaller chemical shift anisotropy.

The possible rotation axes for the molecular motion in 3D are illustrated with red lines in Figure a.

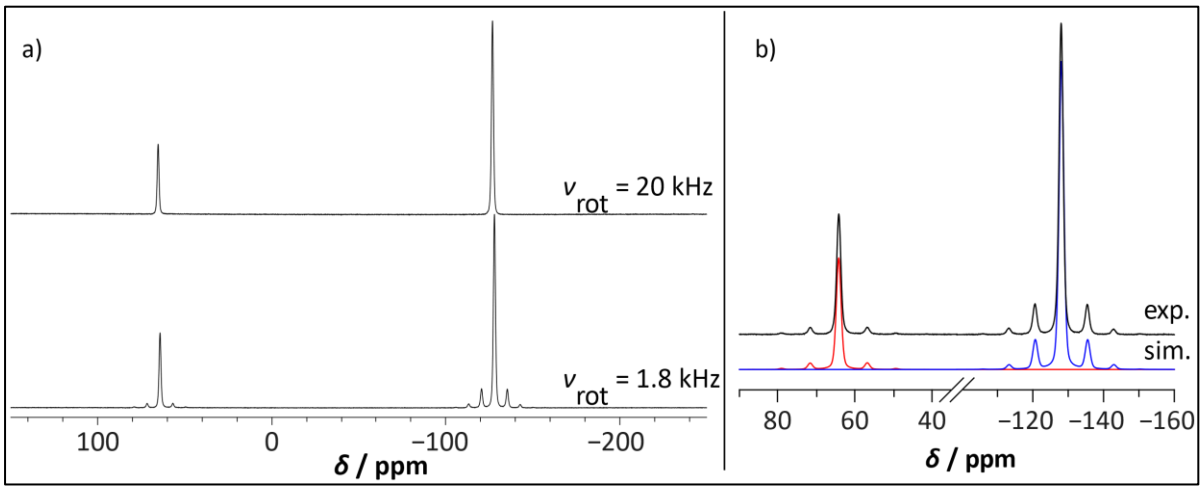

Figure 4.1.7: a) experimental ^{31}P MAS NMR spectra of $(P_4S_3)@Zn_7SI_{12}$ at different spinning frequencies ν_{rot} = 20 kHz and ν_{rot} = 1.8 kHz. b) Experimental ^{31}P MAS NMR spectra of $(ZnI_2)_6(ZnS)(P_4S_3)$ at ν_{rot} = 1.8 kHz and simulated spectra at the same spinning speed for the apical P atoms (red) and the basal P atoms (blue)

Table 4.1.4: Chemical shift anisotropy parameters and eigenvalues of the ^{31}P chemical shift tensors for P_4S_3[40,41]

	$\mathbf{P_{apical}}$		$\mathbf{P_{basal}}$	
	$\mathbf{(P_4S_3)@Zn_7SI_{12}}$	$\boldsymbol{\alpha}$**-$\mathbf{P_4S_3}$**[39][4]	$\mathbf{(P_4S_3)@Zn_7SI_{12}}$	$\boldsymbol{\alpha}$**-$\mathbf{P_4S_3}$**[39]
δ_{iso} / ppm	64.2 ± 0.1	84.8 ± 0.1	–128.0 ± 0.1	–87.4 ± 0.5
δ_{aniso} / ppm	5.9 ± 0.2	225 ± 3	–7.4 ± 0.2	–470 ± 10
η	0.88 ± 0.06	0.1 ± 0.1	0.99 ± 0.05	0.18 ± 0.1
δ_{11} / ppm	70.2 ± 0.2	3 ± 7	–120.7 ± 0.2	98 ± 20
δ_{22} / ppm	63.9 ± 0.2	18 ± 8	–128.0 ± 0.2	40 ± 20
δ_{33} / ppm	58.7 ± 0.2	235 ± 2	–135.4 ± 0.2	401 ± 4
M_2 / kHz^2	0.517 ± 0.029	600 ± 16	0.857 ± 0.048	2636 ± 116

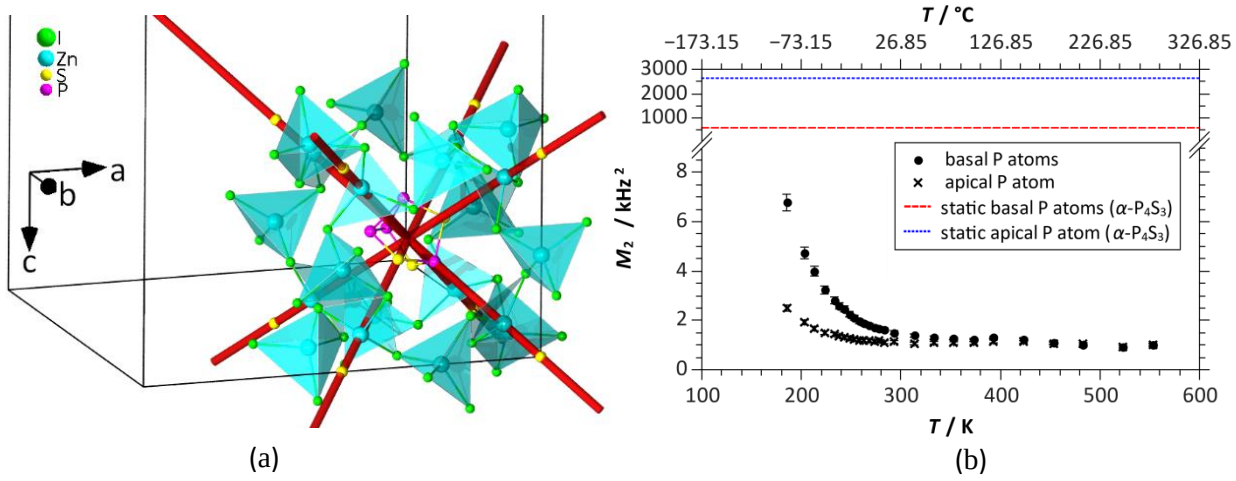

(a) (b)

Figure 4.1.8: a) Detailed view of one P_4S_3 molecule and its chemical environment with all possible rotation axes (red). b) Second moments M_2 of the static ^{31}P NMR line shape of the signals of the basal P atoms and the apical P atoms at different temperatures in comparison to the second moments for static P atoms of α-P_4S_3 calculated from the chemical shift anisotropy.

In order to investigate, if activation energies can be determined for the rotational dynamics of the P_4S_3 units, the line shapes of both phosphorus signals as well as the spin-lattice relaxation times were probed by static VT ^{31}P NMR (Figure b). The decrease of the second moments M_2 for both signals is indicative for motional narrowing and hence for motional averaging of the anisotropic terms of the chemical shift tensor. Since the second moments of both signals decrease, rotations around more than one axis are expected. Although cooling to 185 K, an onset for this motional process could not be observed, which hints for a low activation energy of the motional processes. The ^{31}P NMR experiments helped to investigate a thermal

activated rotation of the P_4S_3 cages around several axes in the ZnI_2 matrix from chemical shift anisotropy analysis and moment analysis.

The characterization of $(P_4S_3)@Zn_7SI_{12}$ by ^{31}P MAS NMR confirmed the presence of two phosphorus sides with a ratio of approx. 3:1, which fits to the expected P_4S_3 units. The low chemical shift anisotropy and the second moments of these signals indicated thermal activated rotations of the molecular P_4S_3 units around several axes. These dynamics were also investigated and confirmed by static VT ^{31}P NMR line shape analysis and spin-lattice relaxometry. The activation barriers for these motional processes are quite low, which made it difficult to investigate in the low temperature regime by line shape analysis and by relaxometry in the high temperature regime.

4.2 $(Pn_4Q_3)@Cu_7M_3I_{13}$ [M= Zn, Cd; *Pn* = P, As; Q= S, Se]

Even though there are series of compounds available in the literature for metal halide adduct compounds[1,5,42–45] with pnictogen chalcogenides but compound, containing more than one metal in the framework is still rare. Vitzthumecker[35] synthesised such compound, $(Pn_4S_x)@Cu_7Hg_3I_{13}$ which is iso-structural to previously discussed $(P_4S_3)@Zn_7SI_{12}$. Here in this section that series is extended by four compounds. Those compounds are designated with short names for easier execution of writing as follows, $(P_4S_3)@Cu_7Zn_3I_{13}$-CZPS, $(P_4S_3)@Cu_7Cd_3I_{13}$-CCPS, $(P_4Se_3)@Cu_7Cd_3I_{13}$-CCPSe and $(As_4S_3)@Cu_7Cd_3I_{13}$-CCAS.

4.2.1 Synthesis

For synthesis the starting materials were copper iodide, the other corresponding metal in elemental state, elemental pnictogen and elemental chalcogen were grinded thoroughly in a mortar in stoichiometric amount in a glove box. The detailed synthesis is listed in Table4.2.1. The mixtures in sealed evacuated ampoules, then annealed at 500 °C with a heating rate 0.5°C/min. After 7 days the ampoules were cooled in faster rate, 1.5 °C/min in order to avoid formation of side product on desired compound. Still the final product contained desired compound along with mixture of precursors and intermediate products. CZPS, CCPS and CCPSe crystals are dark red in colour where arsenic containing compound CCAS, is yellow coloured crystal. Recrystallization was not performed for these compounds. Further characterisations were performed by separating block like crystals of the product from rest of the mixture manually.

Table 4.2.1: Weighing amount of synthesised compounds

Compound	Mass eqv.	$(P_4S_3)@Cu_7Zn_3I_{13}$	$(P_4S_3)@Cu_7Cd_3I_{13}$	$(P_4Se_3)@Cu_7Cd_3I_{13}$	$(As_4S_3)@Cu_7Cd_3I_{13}$
CuI	7	0.5309 g	0.5027 g	0.476 g	0.5116 g
MI_2 (Zn/Cd)	3	0.3814 g	0.4143 g	0.52 g	0.3886 g
Pn (P/As)	4	0.0493 g	0.0467 g	0.023 g	0.1060 g
Q (S/Se)	3	0.0383 g	0.0363 g	0.042 g	0.0940 g

4.2.2 Single crystal measurement

All crystals were separated from the ampoule manually and measured at 123 K except CCAS. CCAS was measured at 223 K. All compounds were crystallised in cubic space group $F\bar{4}3c$ with cell parameters a = 19.4338(4) Å for CZPS, a = 19.6954(10) Å for CCPS, a = 19.6505(10) Å for CCPSe and a = 19.653(2) Å for CCAS. The discrepancy in cell parameter is explained later. Refinement values for these crystals are not as good as the previous compound because of stronger metal halide framework-cage interaction. All the crystallographic data are listed in Table 4.2.2. The atom coordinates and equivalent isotropic displacement parameters for the final structure solution are listed in table Table S4.5, S4.8, S4.12 and S4.15 for CZPS, CCPS, CCPSe and CCAS respectively. The anisotropic displacement parameters are listed in Table S4.6, S4.9, S4.13 and S4.16 for CZPS, CCPS, CCPSe and CCAS respectively. There is also an overview of the bond lengths and angles are given in Table S4.7, S4.10, S4.14 and S4.17 for CZPS, CCPS, CCPSe and CCAS respectively. The refinement for all data for CZPS converged at a goof of 1.71 with R_1 = 2.54% and wR_2 = 5.67 %, for CCPS goof is 1.23 with R_1 = 4.68% and wR_2 = 5.20 %, for CCPSe goof is 1.64 with R_1 = 2.54% and wR_2 = 5.67 % and for CCAS goof is 1.79 with R_1 = 7.77% and wR_2 = 9.22 %. The occupancy factors a_i for all metal and iodine atoms freely refined. The structure determination and refinement of the cage molecule was done in similar way was done for $(P_4S_3)@Zn_7SI_{12}$. The refinement of atoms of the cage is better for As_4S_3 than P_4S_3 because of larger electron density difference between arsenic and sulphur than

between phosphorus and sulphur. After free refinement of the occupancy factors of the metal atoms, total 7 copper and 3 zinc/cadmium atoms per formula unit were calculated. Since all four compounds are isostructural, CZPS with matrix made up of copper, zinc and iodine is described for basic structural investigation of metal halide framework. Basic structure is shown similar to $(P_4S_3)@Zn_7SI_{12}$ as described in section 4.1.2. The basic unit of the matrix of all compounds is a disordered ICu_4 tetrahedron, instead of SZn_4 in $(P_4S_3)@Zn_7SI_{12}$, which in turn is surrounded by an icosahedron of iodine atoms. Again I_{12} icosahedrons are capped by eight partially occupied copper atoms which are placed over eight CuI_4 tetrahedrons or eight triangular faces of the icosahedron. Twelve other triangular surfaces share a common edge and so there are total 6 edges. Two iodine atoms at the end of this edge in connected to the Zn atom which actually forms a ZnI_4 tetrahedron by connecting with two other similar edge-sharing iodine atoms of the neighbouring icosahedron. This base unit and connecting unit are shown in Figure 4.2.1 and Figure 4.2.2 step by step for CZPS and CCAS respectively. So each icosahedron is connected to six other icosahedrons via ZnI_4 tetrahedra. This three dimensional metal halide network with cubic symmetry can be refined easily. For CCPS, CCPSe and CCAS the connecting polyhedron is CdI_4 instead of ZnI_4. Between the linked icosahedrons there are large cavities where cage molecules are stored. It was assumed that these cages are Pn_4Q_3 with C_{3v} point group. And after refining the framework one pnictogen and two types of chalcogen atoms of the cage molecule are added according to symmetry requirement. Apical pnictogen atom has site symmetry order three where chalcogen and basal pnictogen atoms have site symmetry order one as described previously. The pnictogen and chalcogen atoms are refined after specifying distance restrain from literature[36,40]. And as expected 4 cages with 1/4th occupancy than the original structure are constructed. But the refinement is not as good as $(P_4S_3)@Zn_7SI_{12}$. This can be rationalised by smaller cavity size and stronger metal-cage interaction in copper containing compounds.

Table 4.2.2: Crystallographic data of the compounds

	CZPS	**CCPS**	**CCPSe**	**CCAS**
Empirical formula	$Cu_7Zn_3I_{13}P_4S_3$	$Cu_7Cd_3I_{13}P_4S_3$	$Cu_7Cd_3I_{13}P_{4.8}Se_3$	$Cu_7Cd_3I_{13}As_4S_3$
Formula weight, g mol^{-1}	2510.22	2651.89	2820.28	2827.68
Crystal colour and shape	Red, Block-like	Orange, Block-like	Red, Block-like	Orange, Block-like
Crystal system	Cubic			
Space group	$F\bar{4}3c$ (No. 219)			
a, Å	19.4338(4)	19.6954(10)	19.6505(10)	19.653(2)
V, Å^3; Z	7339.6(3), 8	7640.0(7), 8	7587.9(7)	7590.4(15), 8
Absorption coefficient , mm^{-1}	17.174	16.285	19.15	19.684
ρ_{calc} , g cm^{-3}	4.5434	4.6111	4.9375	4.9488
Diffractometer, radiation	Rigaku Super Nova, MoK_α, λ = 0.71073 Å			
Temperature, K	123	123	123	223
Θ-range, ^{O}	3.46- 28.85	3.56- 29.04	3.59- 30.42	4.15- 28.74
hkl-range	$-26 \le h \le 25$	$-22 \le h \le 25$	$-26 \le h \le 13$	$-7 \le h \le 24$
	$-25 \le k \le 26$	$-25 \le k \le 24$	$-22 \le k \le 16$	$-21 \le k \le 3$
	$-26 \le l \le 26$	$-24 \le l \le 26$	$-24 \le l \le 26$	$-15 \le l \le 15$
Absorption correction	numerical (Gaussian)			
Number of reflections	33591	14708	4619	2169
independent reflections	824	835	914	732
R_{int}	0.0323	0.0657	0.0192	0.0375
Completeness (%)	99.7	99.3	99.4	98.9
Twin matrix	-1 0 0, 0 -1 0, 0 0 -1			
Twin fraction	0.49(9)	0.49(5)	0.23(9)	0.33(9)
Structure solution; refinement	Charge flipping, Superflip; *JANA2006*			
Parameters	46	46	47	46
GooF	1.64	1.17	1.64	1.75
R_1, wR_2 $[I>2\sigma(I)]$	0.0240, 0.0537	0.0335, 0.0480	0.0332, 0.0585	0.0615, 0.0853
R_1, wR_2 [all reflections]	0.0253, 0.0545	0.0468, 0.0520	0.0367, 0.0607	0.0777, 0.0922
Residual electron density, e Å^{-3}	1.00/-1.35	1.59/-1.20	2.24/-1.68	2.96/-2.54

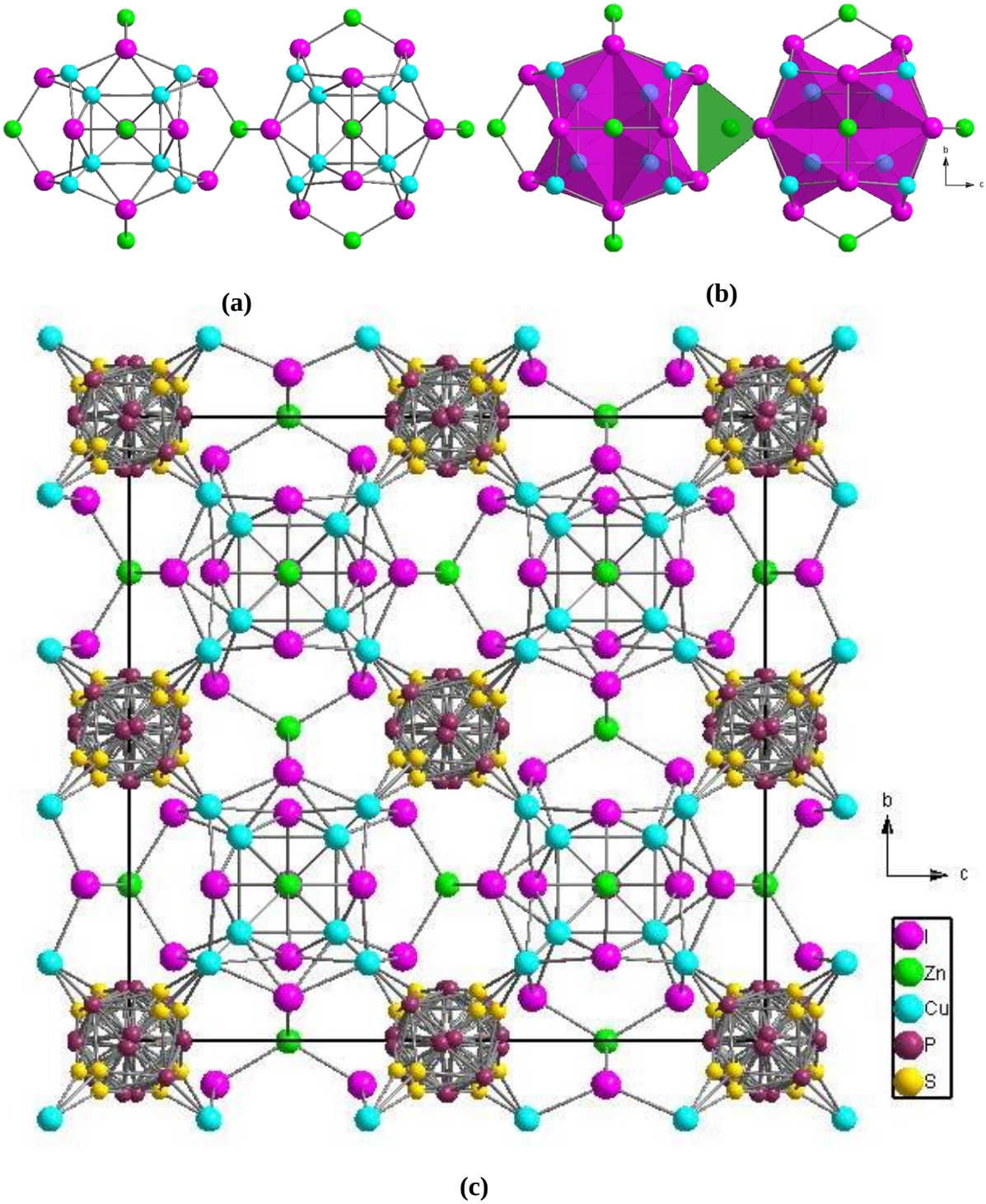

Figure 4.2.1: (a) and (b) Connection pattern of two basic construction units ($I@Cu_7@I_{12}$) connected via ZnI_4 tetrahedra; (c) metal halide framework with rotating P_4S_3 cage with four different orientations in CZPS compound

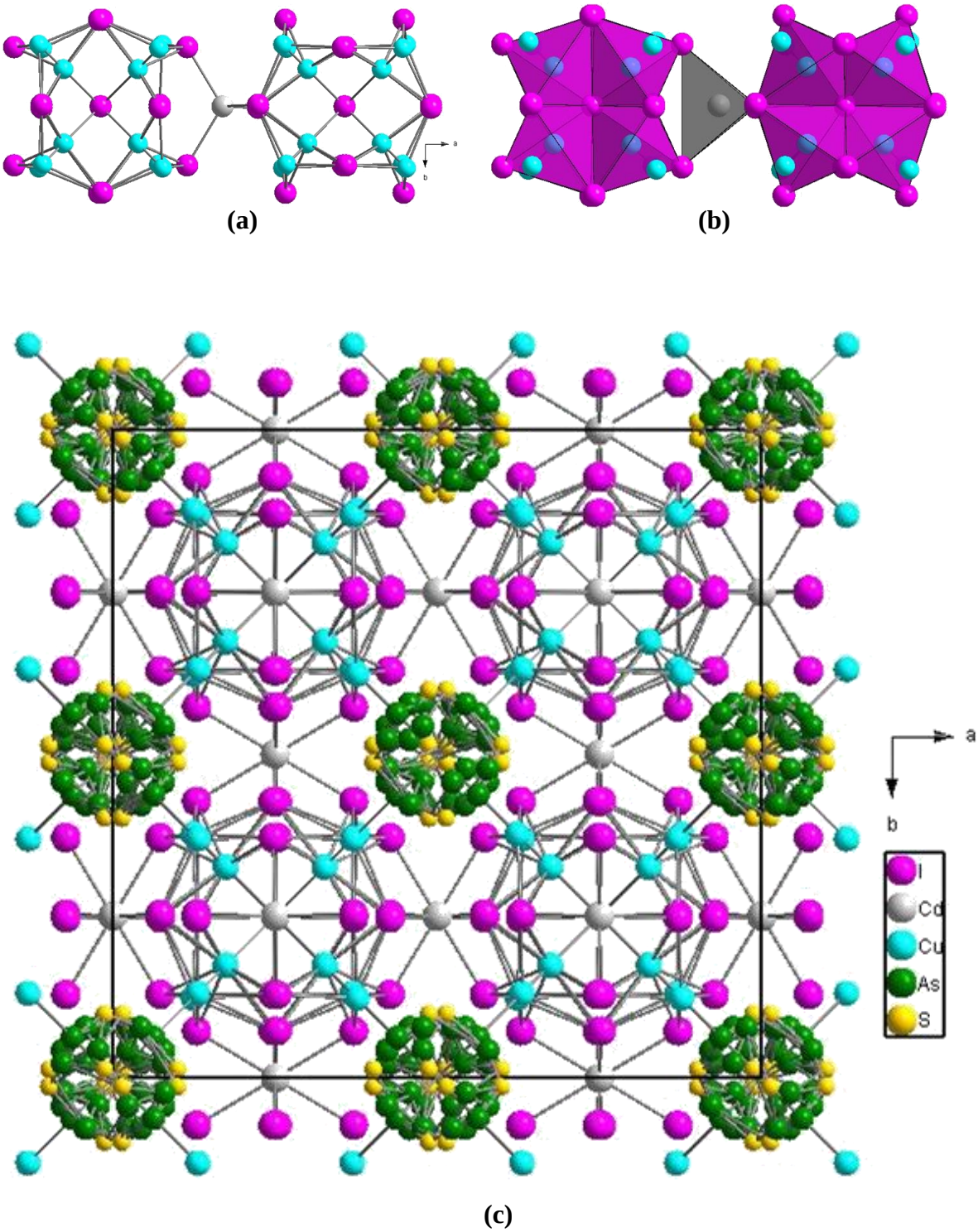

(a) **(b)**

(c)

Figure 4.2.2: (a) and (b) Connection pattern of two basic construction units ($I@Cu_7@I_{12}$) connected via CdI_4 tetrahedra; (c) metal halide framework with rotating As_4S_3 cage with four different orientations in CCAS compound

In $(P_4S_3)@Zn_7SI_{12}$, the cavity size is d_{cavity}= 10.31 Å where in CZPS d_{cavity} is 8.416(1) Å; in CCPS, d_{cavity} is 8.460(1) Å; in CCPSe, d_{cavity} is 8.502(2) Å and in CCAS, d_{cavity} is 8.658(1) Å. So with increase in size of cage molecule the cavity size increased in Cd-containing compounds. In $(P_4S_3)@Zn_7SI_{12}$, the distance of the cage molecule is almost in equal distance from each of the eight icosahedrons (4.405-4.303 Å) in the cubic unit cell. In CZPS, CCPS and CCPS these distances are also almost similar e.g. 2.268-2.276 Å, 2.296-2.365 Å and 2.228-2.340 Å respectively. These show that the distances are almost half than in $(P_4S_3)@Zn_7SI_{12}$ i.e. the cavity size is almost in half than the previous compound. So the cage molecules have significant interaction with Cu atoms of the frameworks. The Cu-P or Cu-As or Cu- S or Cu-Se distance as showed in Table 4.2.3 is comparable with literature. So the cage molecules in the bi-metal containing compounds cannot rotate freely like in $(P_4S_3)@Zn_7SI_{12}$. And that is why the cages are more distorted and refinement values are higher than for $(P_4S_3)@Zn_7SI_{12}$. But in CCAS, because of the heavier cage molecule and occupation of arsenic in apical and basal positions of the cage it has stronger effect on the structure. The cage is not placed not in equal distance from the two opposite Cu-atoms but the apical As-atoms are near to the corresponding copper atom than the basal As-atoms. So the corresponding distances (Cu-As) are 3.402 Å and 2.325 Å, with significant differences unlike previous compounds.

Table 4.2.3: Comparison between distances of metal and cage molecules in five compounds

Distances (Å)	**$(P_4S_3)@Zn_7SI_{12}$**	**CZPS**	**CCPS**	**CCPSe**	**CCAS**
Cavity size (b/w two opposite metal atoms)	10.31	8.416(1)	8.460(1)	8.502(2)	8.658(1)
Zn/Cu-Pn/ Literature value	4.405/2.342[46]	2.267/2.271-2.316[47]	2.296/2.271-2.316[47]	2.227/2.271-2.316[47]	2.325/2.429[48]
Zn/Cu-Q/ Literature value	4.303/2.379[49]	2.275/2.360[50]	2.365/2.360[50]	2.340/2.506[51]	3.487/2.360[50]

4.2.3 Powder-XRD

With the separated crystals of CZPS and CCPS PXRD was measured. Crystals were grinded thoroughly and sealed in a 0.3 mm diameter capillary for the measurement. The diffractograms obtained are shown in Figure 4.2.3 and Figure 4.2.4 for CZPS and CCPS

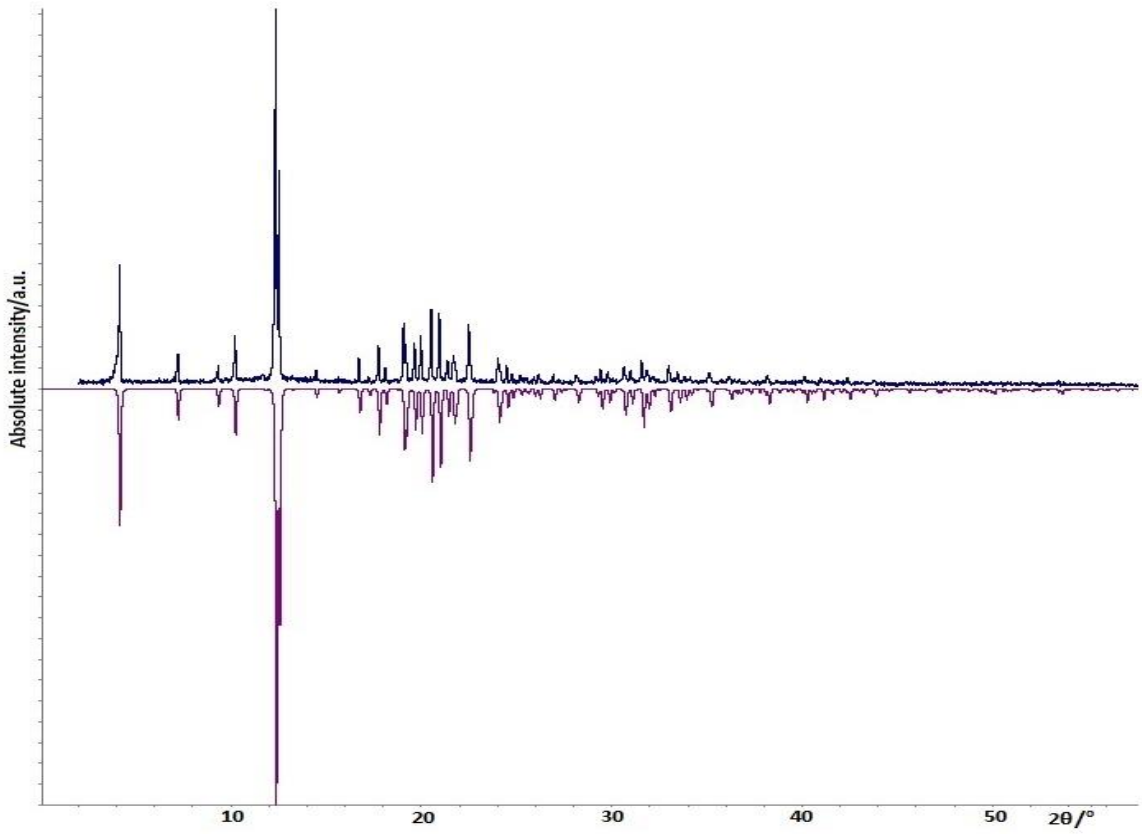

Figure 4.2.3: Powder diffractogram of CZPS.

respectively. The measured and theoretical diffraction pattern calculated from single crystal data are in good agreement for CZPS. The shown diffractogram (Figure 4.2.3) was refined by 45 reflexes and all of them were indexed. The calculated cell parameter from PXRD is 19.511(4) Å with a Figure of Merit (F30) value of 85.6 where from SCXRD the measured cell parameter is 19.434(4) Å (details of refinement is shown in Table S4.7). This discrepancy in cell parameter can be justified by temperature of measurement. As SCXRD sample was measured at 123 K and PXRD sample was measured at room temperature so elongated cell parameter for PXRD sample can be expected.

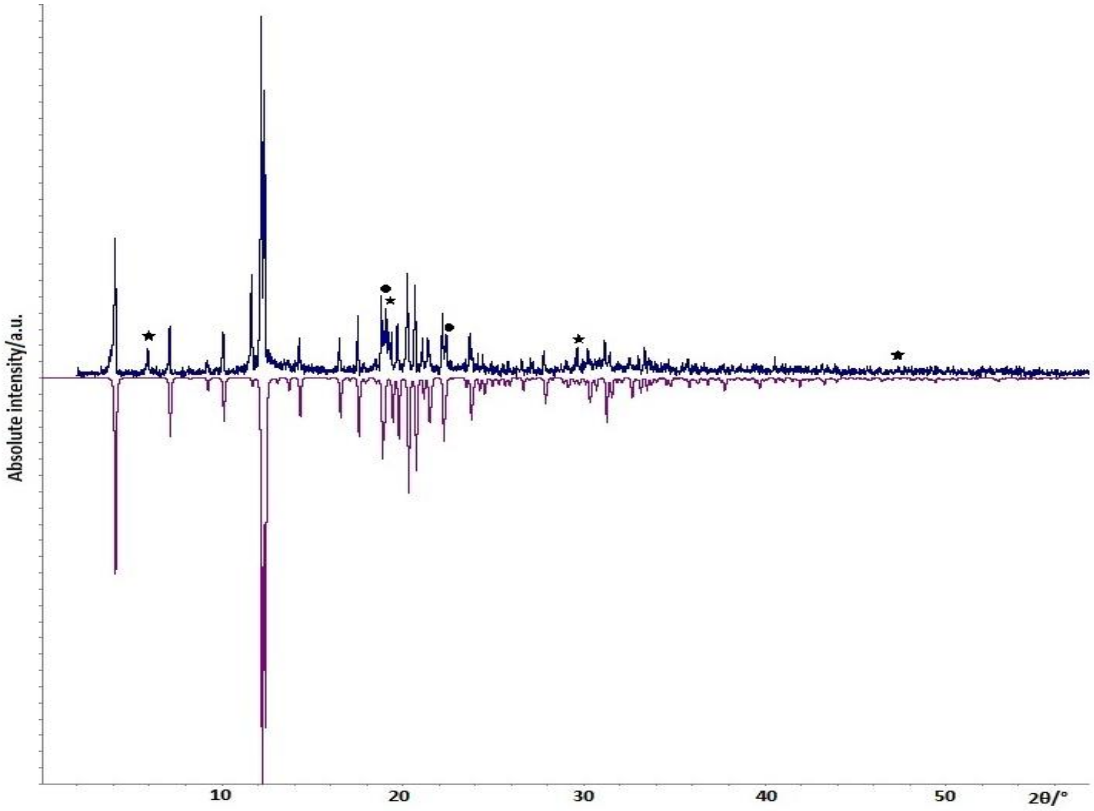

Figure 4.2.4: Powder diffractogram of CCPS. Total 6 peaks cannot be indexed after the refinement. By comparing with literature data in Match programme, it was found that, those reflexes belong to cadmium iodide and copper iodide. The reflexes marked by asterisks are for cadmium iodide and those marked with circles belong to copper iodide.

For CCPS after refining the PXRD data and comparing with literature data, it was evident that starting material CuI and intermediate CdI_2 is present in the sample as six reflexes could not be indexed(Showed in Figure 4.2.4). Finally the powder data was converged with a Figure of Merit (F30) value 94 to cell parameter 19.765(3) Å (details of refinement is shown in Table S4.8).

4.2.4 SEM-EDS measurement

The elemental analysis by EDX was done for CZPS, CCPS and CCAS. For CZPS the theoretical calculation of chemical composition from single crystal XRD matched almost perfectly with measured composition by elemental analysis of EDX. For CCPS and CCAS the measured compositions deviated from calculated one. In last two cases the standard deviation is more than ±5%[52]. This may be caused be caused by lack of standardisation of EDX measurement. The comparison between measured and calculated data is shown in Table

4.2.4. The SEM images of block like crystal of CZPS and CCPS are shown in Figure S4.3 and Figure S4.4 respectively in Supporting information section.

Table 4.2.4: Comparison between the chemical composition calculated from single crystal refinement and measured by SEM-EDX of CZPS, CCPS and CCAS

Compounds	Elements	Calculated (atom %)	Measured (atom %)
CZPS	Cu	23.33	23.04
	Zn	10	10.85
	I	43.33	41.50
	P	13	13.49
	S	10	11.11
CCPS	Cu	23.33	29.04
	Cd	10	4.60
	I	43.33	37.86
	P	13	16.77
	S	10	11.01
CCAS	Cu	23.33	24.61
	Cd	10	8.35
	I	43.33	43.70
	As	13	11.52
	S	10	11.13

4.2.5 Raman Spectroscopy

Sample for Raman measurement was prepared in the same way as $(P_4S_3)@Zn_7SI_{12}$. In the Figure 4.2.5 and Figure 4.2.6, the resultant spectra of CZPS and CCPS are shown respectively. The Raman bands are not very clear or prominent like $(P_4S_3)@Zn_7SI_{12}$ but a similar problem is known from the Raman spectrum of $(P_4S_x)@Cu_7Hg_3I_{13}$[35]. The Raman bands are assigned by comparing a spectrum of P_4S_3 and literature data[34,35,38]. The area below 200 cm^{-1} framework vibrations must belong to deformation region of matrix of metal halides. The oscillations above 200 cm^{-1} are very complex and relatively badly resolved. Therefore, a clear assignment of the bands above 200 cm^{-1} is not done specifically. One possible assignment of the Raman bands of CZPS is demonstrated in Table 4.2.5. Raman spectra of CCPS are more complex and disordered. So assignment of the Raman bands is not feasible. From the Raman spectrum, it is obvious that the intercalated cage is mainly P_4S_3. A

final conclusion on the shape and composition of the stored P_4S_3 cage is also supported by Raman spectroscopy.

Table 4.2.5: Assignment of experimental peaks to the unit of $(P_4S_3)@Cu_7Zn_3I_{13}$. The assignments for Cu-I-Zn framework are not very accurate as the peaks below 100 cm^{-1} are not so prominent or they are in the same position with P_4S_3 unit.

Wavenumbers (cm^{-1})	**Intensity**	**$(P_4S_3)@Cu_7Zn_3I_{13}$**
497	vw	P_4S_3
475	w	P_4S_3
462	w	P_4S_3
454	w	P_4S_3
423	vw	P_4S_3
407	w	Cu-P
389	sh	deformation region of P_4S_3
358	w	deformation region of P_4S_3
337	vw	deformation region of P_4S_3
323	w	Cu-P
297	vw	Cu-P
285	vw	
277	w	deformation region of P_4S_3
265	vw	
250	sh	Cu-P
238	w	Cu-P
230	w	deformation region of P_4S_3
213	w	deformation region of P_4S_3

vw= very weak, w= weak, sh= shoulder

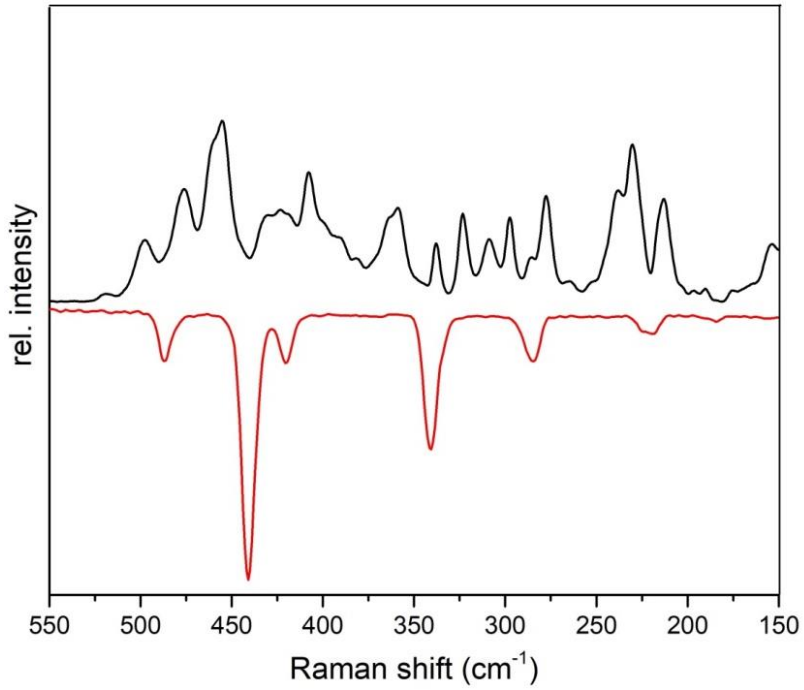

Figure 4.2.5: Raman spectra of CZPS (with positive intensity) comparing with pure P_4S_3(with negative intensity)

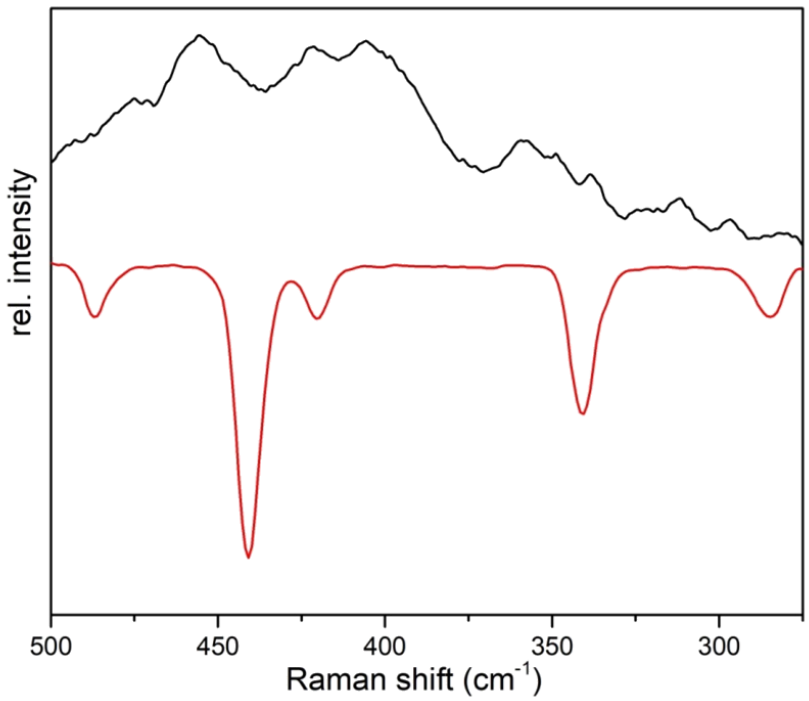

Figure 4.2.6: Raman spectra of CCPS (with positive intensity) comparing with pure P_4S_3(with negative intensity)

4.3 References

[1] Biegerl, A.; Gröger, C.; Kalbitzer, H. R.; Pfitzner, A.; Wachter, J.; Weihrich, R.; Zabel, M., *J. Solid State Chem.*, (2011) **184**, 1719.

[2] Nilges, S.; Nilges, T.; Haeuseler, H.; Pfitzner, A., *J. of Mol. Struc.*, (2004) **706**, 89.

[3] Pfitzner, A.; Reiser, S.; Nilges, T., *Angew. Chem. Int. Ed.*, (2000) **39**, 4160.

[4] Reiser, S.; Brunklaus, G.; Hong, J. H.; Chan, J. C. C.; Eckert, H.; Pfitzner, A., *Chem. Eur. J.*, (2002) **8**, 4228.

[5] Biegerl, A.; Brunner, E.; Gröger, C.; Scheer, M.; Wachter, J.; Zabel, M., *Chem. Eur. J.*, (2007) **13**, 9270.

[6] Biegerl, A.; Gröger, C.; Kalbitzer, H. R.; Wachter, J.; Zabel, M., *Z. anorg. allg. Chem.*, (2010) **636**, 770.

[7] Biegerl, A.; Piryazev, D.; Scheer, M.; Wachter, J.; Virovets, A.; Zabel, M., *Eur. J. Inorg. Chem.*, (2011) **2011**, 4248.

[8] Pfitzner, A., *Chem. Eur. J.*, (2000) **6**, 1891.

[9] Pfitzner, A.; Freudenthaler, E., *Z. Naturforsch., B: Chem. Sci.*, (1997) **52**, 199.

[10] Freudenthaler, E., *Dissertation*, (1997), Universität Siegen.

[11] Pfitzner, A.; Freudenthaler, E., *Z. Kristallogr. Cryst. Mater.*, (1995) **210**, 59.

[12] Freudenthaler, E.; Pfitzner, A., *Z. Kristallogr. Cryst. Mater.*, (1997) **212**, 384.

[13] Long, J. R.; Yaghi, O. M., *Chem. Soc. Rev.*, (2009) **38**, 1213.

[14] Lee, J.; Farha, O. K.; Roberts, J.; Scheidt, K. A.; Nguyen, S. T.; Hupp, J. T., *Chem. Soc. Rev.*, (2009) **38**, 1450.

[15] Getman, R. B.; Bae, Y.-S.; Wilmer, C. E.; Snurr, R. Q., *Chem. Rev.*, (2012) **112**, 703.

[16] Zhang, J.-W.; Zhang, H.-T.; Du, Z.-Y.; Wang, X.; Yu, S.-H.; Jiang, H.-L., *Chem. comm.*, (2014) **50**, 1092.

[17] Turner, S.; Lebedev, O. I.; Schröder, F.; Esken, D.; Fischer, R. A.; van Tendeloo, G., *Chem. Mater.*, (2008) **20**, 5622.

[18] Luo, H.; Xie, W.; Tao, J.; Pletikosic, I.; Valla, T.; Sahasrabudhe, G. S.; Osterhoudt, G.; Sutton, E.; Burch, K. S.; Seibel, E. M.; Krizan, J. W.; Zhu, Y.; Cava, R. J., *Chem. Mater.*, (2016) **28**, 1927.

[19] Riess, J., *Phys. Rev. B*, (1976) **13**, 3862.

[20] Mandelcorn, L., *Chem. Rev.*, (1959) **59**, 827.

[21] Chatti, I.; Delahaye, A.; Fournaison, L.; Petitet, J.-P., *Energy Convers. Manag.*, (2005) **46**, 1333.

[22] Brown, C. J.; Toste, F. D.; Bergman, R. G.; Raymond, K. N., *Chem. Rev.*, (2015) **115**, 3012.

[23] Pitt, M. A.; Johnson, D. W., *Chem. Soc. Rev.*, (2007) **36**, 1441.

[24] Cramer, F.; Saenger, W.; Spatz, H.-C., *J. Am. Chem. Soc.*, (1967) **89**, 14.

[25] Cooke, G.; Rotello, V. M., *Chem. Soc. Rev.*, (2002) **31**, 275.

[26] Tayi, A. S.; Kaeser, A.; Matsumoto, M.; Aida, T.; Stupp, S. I., *Nat. Chem.*, (2015) **7**, 281.

[27] Teyssandier, J.; Feyter, S. de; Mali, K. S., *Chem. Comm.*, (2016) **52**, 11465.

[28] Watfa, N.; Melgar, D.; Haouas, M.; Taulelle, F.; Hijazi, A.; Naoufal, D.; Avalos, J. B.; Floquet, S.; Bo, C.; Cadot, E., *J. Am. Chem. Soc.*, (2015) **137**, 5845.

[29] O.Crottaz, F.Kubel, H.Schmid, *J. Solid State Chem.*, (1995) **120**, 60.

[30] Kubel, F., *Ferroelectrics*, (1994) **160**, 61.

[31] Berset, G.; Depmeier, W.; Boutellier, R.; Schmid, H., *Acta Crystallogr. C Cryst. Struct. Commun.*, (1985) **41**, 1694.

[32] Nelmes, R. J.; Thornley, F. R., *J. Phys. C: Solid State Phys.*, (1974) **7**, 3855.

[33] J. H. Hong, *Dissertation*, (2004), Universität Regensburg.

[34] M. Bräu, *Dissertation*, (2007), Universität Regensburg.

[35] Christoph Vitzthumecker, *Dissertation*, (2017), Universität Regensburg.

[36] Raabe, I.; Antonijevic, S.; Krossing, I., *Chem. Eur. J.*, (2007) **13**, 7510.

[37] Takamuku, T.; Yamaguchi, T.; Wakita, H., *J. Phys. Chem*, (1991) **95**, 10098.

[38] Burns, G. R.; Rollo, J. R., *J. Raman Spectrosc.*, (1988), 345.

[39] Bjorholm, T.; Jakobsen, H. J., *J. Magn. Reson.*, (1989) **84**, 204.

[40] Mehring, M., *Principles of High Resolution NMR in Solids*, (1983), Springer Berlin Heidelberg.

[41] Haeberlen, U., *High Resolution NMR in Solids Selective Averaging: Supplement 1 Advances in Magnetic Resonance*, (2014), Saint Louis, Elsevier Science.

[42] Pfitzner, A.; Reiser, S.; Deiseroth, H., *Z. anorg. allg. Chem.*, (1999) **625**, 2196.

[43] Adolf, A.; Gonsior, M.; Krossing, I., *J. Am. Chem. Soc.*, (2002) **124**, 7111.

[44] P. Schwarz, *Dissertation*, (2010), Universität Regensburg.

[45] Weis, P.; Hettich, C.; Kratzert, D.; Krossing, I., *Eur. J. Inorg. Chem.*, (2019) **2019**, 1657.

[46] Elrod, U.; Lux-Steiner, M.; Bucher, E.; Hönigschmid, J.; Bickmann, K.; Gain, L., *J. Cryst. Growth*, (1984) **67**, 195.

[47] Lange, S.; Bawohl, M.; Weihrich, R.; Nilges, T., *Angew. Chem. Int. Ed.*, (2008) **47**, 5654.

[48] Liebisch, W.; Schubert, K., *Journal of the Less Common Metals*, (1971) **23**, 231.

[49] Liu, Z.; Wang, X.; Zhu, H., *Phys. Chem. Chem. Phys.*, (2015) **17**, 13117.

[50] Lukashev, P.; Lambrecht, W. R. L.; Kotani, T.; van Schilfgaarde, M., *Phys. Rev. B*, (2007) **76**, 195202.

[51] Yamamoto, K.; Kashida, S., *J. Solid State Chem.*, (1991) **93**, 202.

[52] Miler, M.; Mirtič, B., *Geologija*, (2013) **56**, 5.

5. New phases of phosphorus sulphide, P_4S_9 and phosphorus sulphide iodide, $P_4S_3I_2$

As discussed in Chapter 1, there is a range of binary phosphorus sulphide compounds with cage like structures. In order to explore the effects of mineraliser/s on traditional solid state reactions between elemental phosphorus, elemental sulphur, and cage-like phosphorus sulphides, two compounds, i.e., tetraphosphorus nonasulphide P_4S_9 and phosphorus sulphide iodide $P_4S_3I_2$ were synthesised each consisting with a new phase.

5.1 Tetraphosphorus nonasulphide, P_4S_9

Two crystal structures of P_4S_9 (i.e., cubic P_4S_9-II[1] and monoclinic P_4S_9-III[2] were synthesised by Willmer in 1969 and Wolf and co-worker in 1990, respectively. Meisel and Grunze in 1969 first reported P_4S_9 as P_4S_9-I[3] consisting of 25% trivalent sulphur atoms and 75% penta-valent phosphorus atoms by hydrolysis tests with quantitative paper chromatographic phosphorus determination, however no crystallographic data is available. P_4S_9 has two conformational isomers α-P_4S_9 with three exocyclic and six bridging sulphur atoms, and β-P_4S_9, with four exocyclic and five bridging sulphur atoms. The cubic phase was synthesised by reaction of red P or P_4S_3 or P_4S_7 with sulphur or reducing sulphur from P_4S_{10}. The monoclinic one was prepared from CS_2 by reaction of P_4S_{10} and isopropanol. Here we report a new triclinic phase of P_4S_9 with α-isomers (i.e., with lower number of exocyclic sulphur atoms) which was synthesised by using iodine as a transport agent for the reaction between P_4S_3 and S_8. Though the effect of I_2 catalysis on the reaction between P_4S_3 and S, in CS_2 was reported by Beeli[4] in 1935 to produce P_4S_5 but by using excess amount of I_2, a new modification of P_4S_9 was found.

P_4S_{10} was compared with P_4S_9 in many literature specially for vibration and Raman spectra analysis[5,6]. But only triclinic modification of P_4S_{10} was found until the present. But for P_4S_9 only cubic and monoclinic modifications are known but triclinic. The new synthesised compound has triclinic symmetry with same space group as P_4S_{10} with cell volume similar to monoclinic modification. So a new compound is introduced to Table 1.1 as discussed in Section 1.

5.1.1 Synthesis

The P_4S_9 with triclinic phase was synthesised by standard high-temperature reaction in a quartz ampule. The starting materials P_4S_3, S, and I_2 were taken in a 1.15:1:1.15 ratio for a total of 0.5 g in a quartz tube. The quartz tube was then sealed to a 5 cm ampule with oxy-hydrogen flame after evacuating the tube under reduced 3.5×10^{-2} mbar pressure. Then the ampule was annealed at 350° C for 10 days. White crystals of P_4S_9 with excess I_2 was obtained. These crystals are stable initially, but after 2–3 days it dissociated to P_4S_7 and P_4S_{10}.

5.1.2 Single crystal measurement

The adamantane-type cage-molecules crystallise in triclinic space group $P\bar{1}$, with non-merohedral twinning[7]. 77% of the total reflections are indexed by one domain and 9% by another domain. The later basically has same cell parameters with the former but with different orientation with 38% overlap. These two domains can be transformed to each other by the Twin law:

$$\begin{pmatrix} -1 & 0.008 & -0.004 \\ 0 & 0.005 & -0.503 \\ 0 & -1.989 & -0.005 \end{pmatrix}$$

The triclinic cell parameters are a=8.5740(5) Å, b=8.8938(5) Å, c=17.7014(10) Å, α= 85.305(4)°, β=77.600(5)°, γ=77.202(5)°, V=1284.76(13) Å^3, Z=4. The volume for triclinic modification is comparable with the monoclinic modification. The crystal structure was refined to R=0.052 and wR_2= 0.0541 with GOF= 1.41. The reason for moderate refinement value is the twinning. The crystal was measured at 123 K but for the density comparison with the monoclinic and cubic modifications the crystal was measured again at 293 K. All the crystallographic data are listed in Table 5.1.1. Atom coordinates and equivalent isotropic parameters for two non-equivalent P_4S_9 molecules are listed in Table S5.1. The anisotropic displacement parameters are listed in Table S5.2. Like the other phosphorus sulphides, the molecular structure can be derived from the P4 tetrahedron of the white phosphorus, with additional six bridging and three terminal sulphur atoms (see Figure 5.1.1). In the unit cell there are two same molecules which are not related by any symmetry.

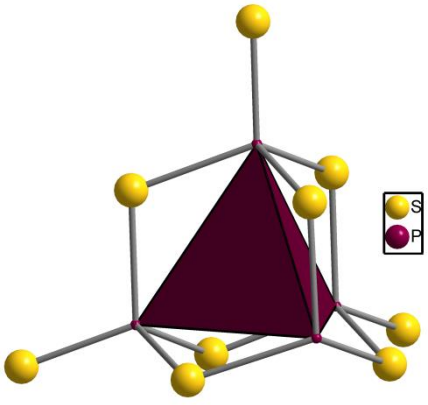

Figure 5.1.1: Tetrahedron connecting four phosphorus atoms

Table 5.4.1: Crystallographic data of triclinic modification of P_4S_9

Compound name	**P_4S_9-aP52**
Empirical formula	P_4S_9
Formula weight, g mol^{-1}	412.40
Crystal colour and shape	White, block
Crystal system	triclinic
Space group	$P\bar{1}$(No. 2)
a, Å	8.5740(5)
b, Å	8.8938(5)
c, Å	17.7014(3)
α, ^{o}	85.305(4)
β, ^{o}	77.600(5)
γ, ^{o}	77.202(5)
V, Å^3; *Z*	1284.76(13), 4
Absorption coefficient (MoK$_\alpha$), mm^{-1}	2.001
ρ_{calc} , g cm^{-3}	2.132
Diffractometer	Rigaku Super Nova
Radiation	MoK$_\alpha$, λ = 0.71073 Å
Temperature, K	123
θ-*range*, ^{o}	3.74– 26.37
hkl-range	$-10 \le h \le 10$ $-11 \le k \le 11$ $-22 \le l \le 22$
Absorption correction	numerical (gaussisan)
Number of reflections	16752
Independent reflections	4159
R_{int}	0.029
Structure solution	Charge flipping, Superflip
Structure refinement	*JANA2006*
Completeness to θ_{max}	99.81%
Twin matrix	-1 0 0, 0.008 0.005 -1.989, -0.004 -0.503 -0.005
Twin fraction	0.12 (7)
Parameters	238
GooF	1.41
R_1, wR_2 $[I>2\sigma(I)]$	0.04, 0.050
R_1, wR_2 [all reflections]	0.052, 0.054
Residual electron density, e Å^{-3}	-0.74/1.37

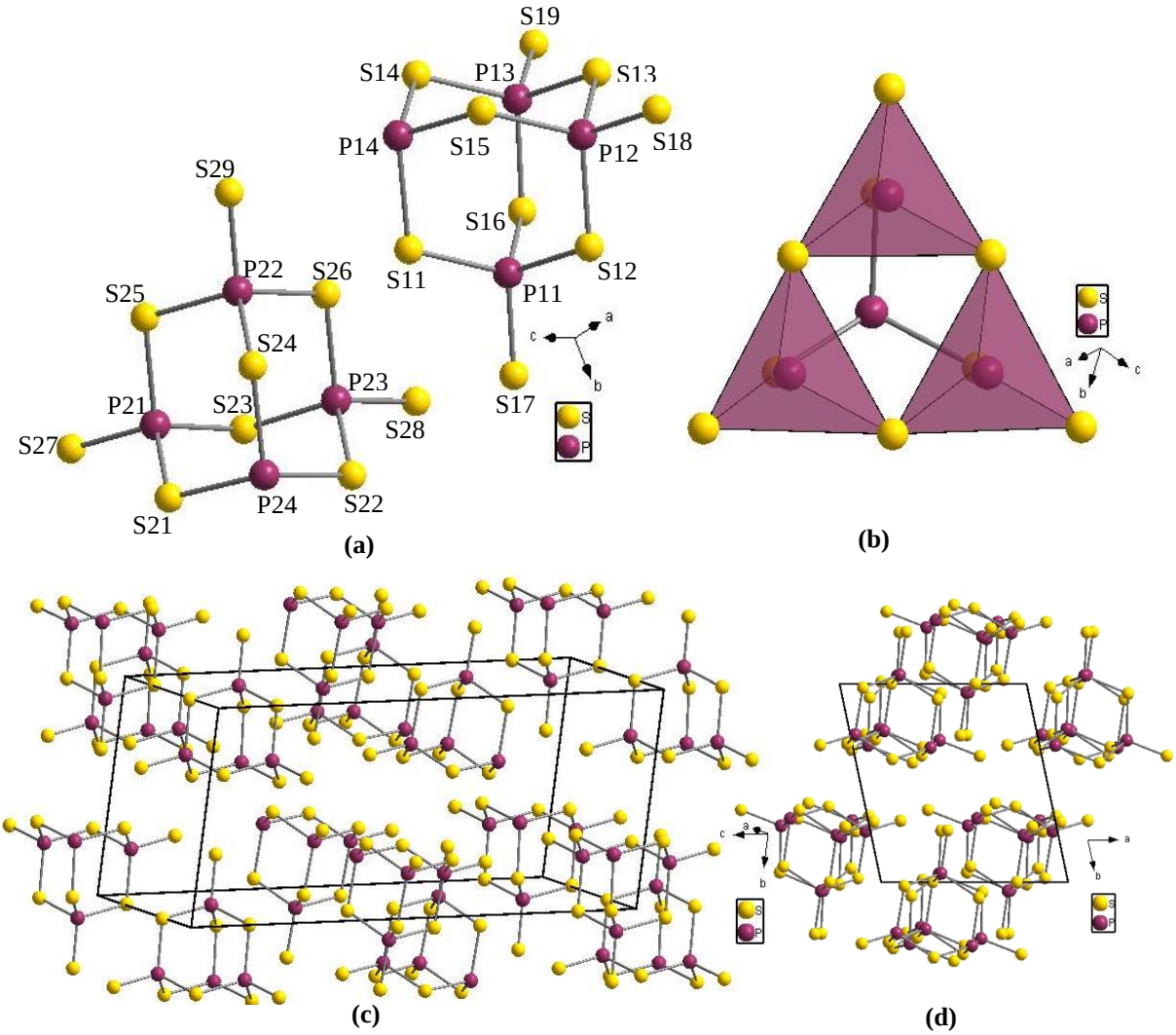

Figure 5.1.2: (a) two independent molecules of P_4S_9, (b) three corner-shared irregular PS_4 tetrahedrons in one molecule, (c) arrangement of the molecules in the unit cell along a-axis, (d) arrangement of the molecules in the unit cell along c-axis fabricating hexagonal closed packed structure

They cannot be converted to each other by any symmetry operations, i.e., they are independent molecules and they are designated as 1 and 2. This is why there are 8 independent P atoms and 18 independent S atoms instead of 4 and 9 respectively. This triclinic phase consists of thermodynamically stable α-modification having three exocyclic sulphur atoms. This phase like the other two phases has adamantine-like cage structure where all three PS_4 tetrahedra connected to each other via vertices and connected to the remaining PS_3 unit [Figure 5.1.2(b)]. These PS_4 tetrahedrons are a bit irregular because of relatively smaller bond length between the P and terminal S (S^{term}) (1.916-1.926 Å) than with the bridging S (S^{brid}) (2.078-2.127 Å). The four P atoms form relatively regular tetrahedron as all the edges of P_4 tetrahedron is around 3.459-3.48 Å (Figure 5.1.1). The minimum distance between two same cage-molecules is 3.452 Å for cage1 (P14-S19) and 3.464 Å for cage2

(P24-S28) and for two symmetrically different units the minimum distance is 3.611 Å (S11-S24). The bond lengths and bond angle are similar to the monoclinic phase[1] and a detailed data is listed in Table S5.3. The arrangement of the 1 and 2 cage molecules are in layered manner (shown in Figure 5.1.2). Along c-axis on the ab-plane type 1 and type 2 cages are bedded one above another making hexagonal closed packed structure. The layers are not situated exactly one below another as shown in Figure 5.1.2(d).

5.1.3 Raman spectroscopy

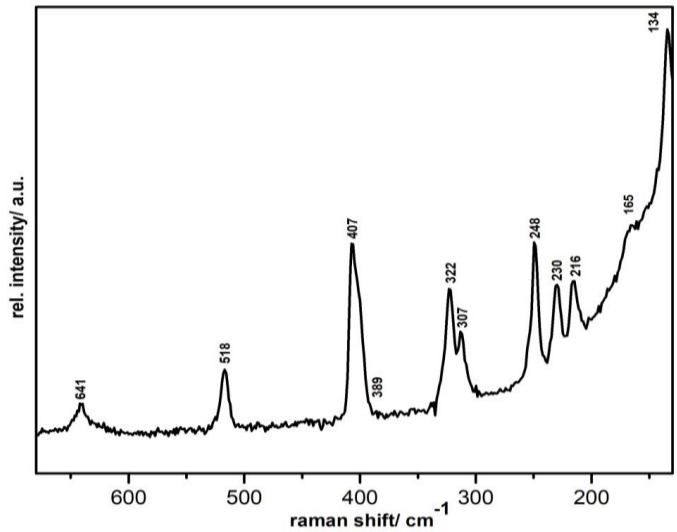

Figure 5.1.3: Raman spectrum of P_4S_9

Table 5.1.2: List of peaks of measured Raman spectrum of P_4S_9

Assignments	Intensity	Wavenumbers (cm^{-1})	
		P_4S_9 (measured)	P_4S_{10} [6][8]
ν(P-S^{term})	w	650-633	717, 691
ν (P-S^{brid}-P)	ms	518	535
δ(P-S^{brid}-P)	s	407	–
δ(P-S^{brid}-P)	sh	389	398
ν (P-S^{brid}-P)	s	322	354
ν (P-S^{brid}-P)	ms	307	–
δ(P-S^{brid}-P)	s	248	272
ν (P-S^{brid}-P)	ms	230	261
δ(P-S^{term})	ms	216	–
δ(P-S^{term})	ms	207	208
δ(P-S^{brid}-P)	sh, w	165	190
δ(P-S^{brid}-P)	m	134	168

w= weak, ms= medium strong, s= strong, vs=very strong, sh=shoulder

Raman spectra were recorded from P_4S_9 crystals as shown in Figure 5.1.3. Note that the proper Raman spectra of P_4S_9 (both for cubic and monoclinic) are not available in the literature. However, the Raman spectra of the triclinic phase of P_4S_{10} are reported in the literature. Therefore the obtained Raman spectra is compared with the Raman spectra reported for triclinic P_4S_{10}[8][6]. The measured frequencies are listed in Table 5.1.2.

5.1.4 SEM-EDS measurement

Energy dispersive X-ray spectrometric (EDS, associated with SEM) measurements were performed in order to confirm the presence of only sulphur and phosphorus in the P_4S_9 crystals and no traces of iodine as the excess iodine was used during the synthesis. EDS study shows no impurity, and the observed chemical composition was in good agreement with the refined and theoretical data from Single Crystal-XRD measurements. The calculated and observed atomic percentages are listed In Table 5.1.3. Note that the standard deviation is ±5% due to the irregular surface of the crystals.

Table 5.1.3: Comparison between the chemical composition calculated from single crystal refinement and measured by SEM-EDX

Elements (atom %)	**P**	**S**
Calculated (SCXRD)	30.77	69.23
Measured (EDS)	30	70

5.1.5 Comparison between 3 modifications

The single crystal X-ray diffraction patterns of three different phases are compared in Figure 5.1.4. As can be seen the triclinic phase has more peaks than other two phases. The volumes and the densities of all 3 phases at 293 K are reported in Table.5.1.4. As can be seen the cubic phase has the least density, and the monoclinic phase has the highest density, and the reported triclinic phase has slightly lower density than the monoclinic phase. It is interesting to notice that the densities of monoclinic[2] (2.106 $g.cm^{-3}$) and triclinic (2.1042 $g.cm^{-3}$) phases are almost 5% higher than that of cubic phase[1] (2.009 $g.cm^{-3}$), even though they are comparable with P_4S_{10}[5] (2.09 $g.cm^{-3}$).

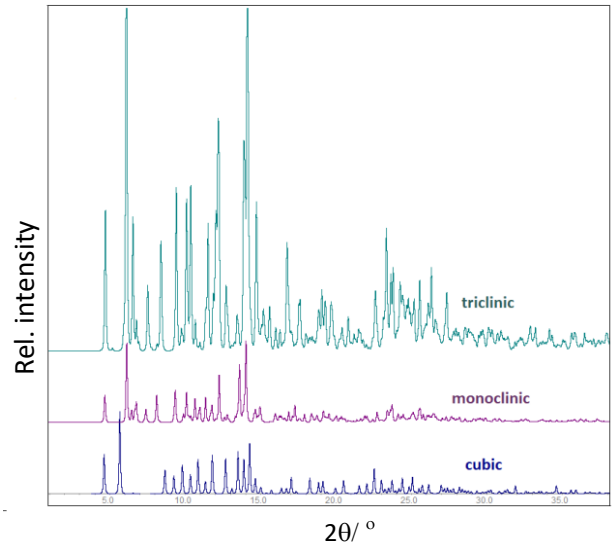

Figure 5.1.4: Calculated powder data of all 3 phases

Table 5.1.4: Comparison between 3 phases of P_4S_9 at room temperature

P_4S_9 phase	**Cubic[1]**	**Monoclinic[2]**	**Triclinic**
Space group	$Ia\bar{3}$	$P2_1/n$	$P\bar{1}$
Volume ($Å^3$)	5451.78	1300.78	1301.88
Z	16	4	4
Cell parameters	a=17.60(53) Å	a=8.555(2) Å b=12.637(5) Å c=12.453(4) Å β=104.94(2)°	a=8.5740(5) Å b=8.8938(5) Å c=17.7014(3) Å α=85.305(4)° β=77.600(5)° γ=77.202(5)°
Density, $g.cm^{-3}$	2.0099	2.1060	2.1042

5.2 Phosphorus sulphide iodide $P_4S_3I_2$

There are three phosphorus sulphide iodides to be found in literature, $P_4S_3I_2$, PSI and P_2SI_4 with several methods of preparation by Ouvrard[9,10]. In an attempt to reproduce the above mentioned compounds by Topsom and co-workers[11], they were able to synthesise only $P_4S_3I_2$. The existence of other two compounds is still in doubt. Molecular configuration was predicted to be closely related to phosphorus sulphides like P_4S_7[12] and P_4S_{10}[5] and relative orientation of phosphorus and sulphur is a bit difficult to differentiate. So different structures with different configuration were predicted but no solid evidence was given. Wright and co-workers[13] first confirmed the structure by X-ray crystallographic analysis in 1959. They found triclinic modification with $P\bar{1}$ space group, α-$P_4S_3I_2$. Later in 1970, Cordes and co-workers[14] synthesised and confirmed β-$P_4S_3I_2$ with orthorhombic space group *Pnma*. α-$P_4S_3I_2$, more stable form was synthesised by mixing white phosphorus, sulphur and iodine in carbon disulphide and controlled evaporation of the solvent from as solution of CS_2 and precursors at room temperature where β-$P_4S_3I_2$ was prepared by direct reaction between equimolar amount of P_4S_3 and I_2 in dry benzene under nitrogen atmosphere at room temperature. Both structures crystallise in different space group and the relative arrangements of phosphorus and sulphur atoms and position of the iodine atoms are different i.e. they are linkage isomers as shown in Figure 5.2.1.

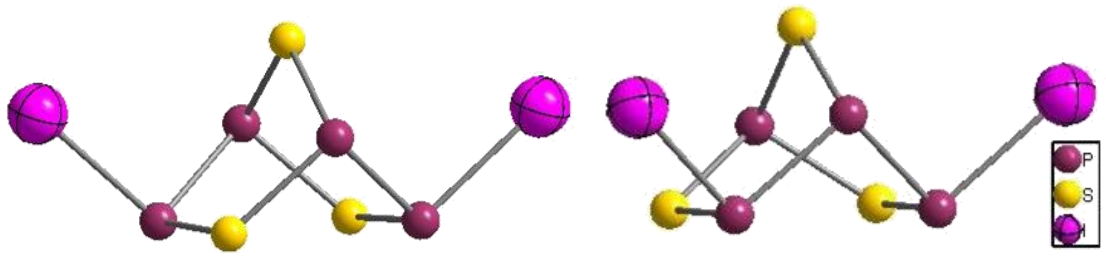

Figure 5.2.1: Molecule of α-$P_4S_3I_2$ with iodine atoms in shown in left and molecule of β-$P_4S_3I_2$ is shown in right

In 1984, Blachnik and coworkers[15] reported another phase of α-$P_4S_3I_2$, α'-$P_4S_3I_2$. α'-$P_4S_3I_2$ was synthesised by heating mixtures of P_4S_3 and I_2 in an evacuated ampoule at 440 K. The crystal structure for only selenium compound α'-$P_4Se_3I_2$ was found in the crystallographic database. No α'-$P_4S_3I_2$ compound with proper crystal structure was available. They suggested that more stable α-$P_4S_3I_2$ forms in a high iodine concentration condition where iodine vigorously attack P_4S_3 destroying the cage structure completely and rearranging the elements in thermodynamically stable form. Formation of β modification takes place in relatively

diluted iodine concentration where iodine reacts with P_4S_3 only by diffusing in the structure. In current chapter a new phase of $P_4S_3I_2$ is discussed. The cage-molecules have same structure as α-$P_4S_3I_2$ but crystallise in tetragonal space group $P4_3$. The compound can be denoted as α'-$P_4S_3I_2$.

5.2.1 Synthesis

α'-$P_4S_3I_2$ was obtained during our exploration for the mineraliser property of iodine. P_4S_3 (0.09 g, 1 equiv.), I_2 (0.104 g, 1 equiv.), and tellurium pieces (0.3 g, 6 equiv.) were mixed, grinded, and sealed in an evacuated quartz ampoule. The sample was then heated and annealed at 623 K for 7 days, resulting in the formation of yellow coloured block-shaped crystals. Note that tellurium does not have any effect in the reaction or participated in the reaction (c.f, Blachnik's theory as discussed in the introduction).

5.2.2 Single crystal measurement

Single crystal of the new phase of $P_4S_3I_2$ was measured by using Mo-radiation of the single crystal XRD. Block like crystal was measured to have tetragonal symmetry similar to α'-$P_4S_3I_2$ but different space group $P4_3$. But unlike α'-$P_4S_3I_2$ no β modification was found. The measured cell parameters are a =7.2842(1) Å, c = 39.0275(3) Å, V = 2070.78(4) Å^3 and Z=4. All the crystallographic data is listed in Table 5.2.1. The atom coordinates and equivalent isotropic displacement parameters for the final structure are listed in Table S5.4. The anisotropic displacement parameters are listed in Table S5.5. In Table 5.2.2, a comparative study of three phases, i.e., α-$P_4S_3I_2$, β-$P_4S_3I_2$, α'-$P_4S_3I_2$ are listed. Note that α'-$P_4S_3I_2$ cannot be included because of the unavailability of the crystallographic data. For current than the *'a'* parameter.

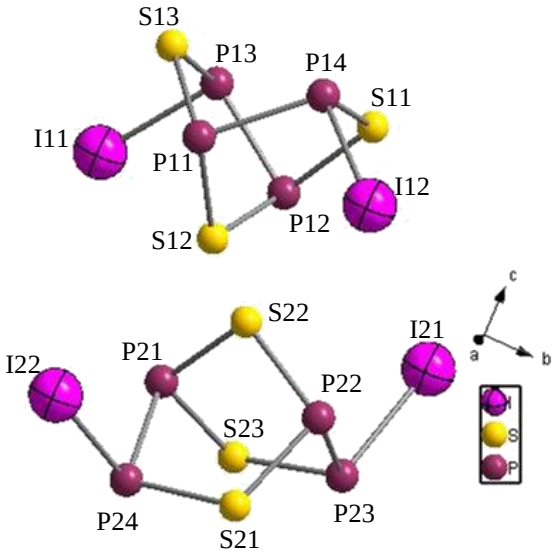

Figure 5.2.2: (a) two independent molecules of α''-$P_4S_3I_2$ with C_2 symmetry

Table 5.2.1: Crystallographic data and measurement parameters of tetragonal modification of $P_4S_3I_2$

Compound name	**$P_4S_3I_2$-t72**
Empirical formula	$P_4S_3I_2$
Formula weight, g mol^{-1}	473.9
Crystal colour and shape	Yellowish, block
Crystal system	tetragonal
Space group	$P4_3$ (No.78)
a, Å	7.2842(10)
c, Å	39.0275(3)
V, Å^3; Z	2070.78(4),8
Absorption coefficient , mm^{-1}	7.223
ρ_{calc} , g cm^{-3}	3.04
Diffractometer	Rigaku Super Nova
Radiation	MoK_α, λ = 0.71073 Å
Temperature, K	123
Θ-range, ^{o}	3.81-29.61
hkl-range	$-10 \leq h \leq 9$ $-9 \leq k \leq 9$ $-53 \leq l \leq 54$
Absorption correction	numerical (gaussisan)
Number of reflections	20965
Independent reflections	5742
R_{int}	0.038
Structure solution	Charge flipping, Superflip
Structure refinement	*JANA2006*
Completeness to θ_{max}	99.9%
Parameters	163
GooF	1.26
R_1, wR_2 $[I>2\sigma(I)]$	0.0354, 0.0432
R_1, wR_2 [all reflections]	0.0423, 0.0450
Residual electron density, e Å^{-3}	-0.66/1.00

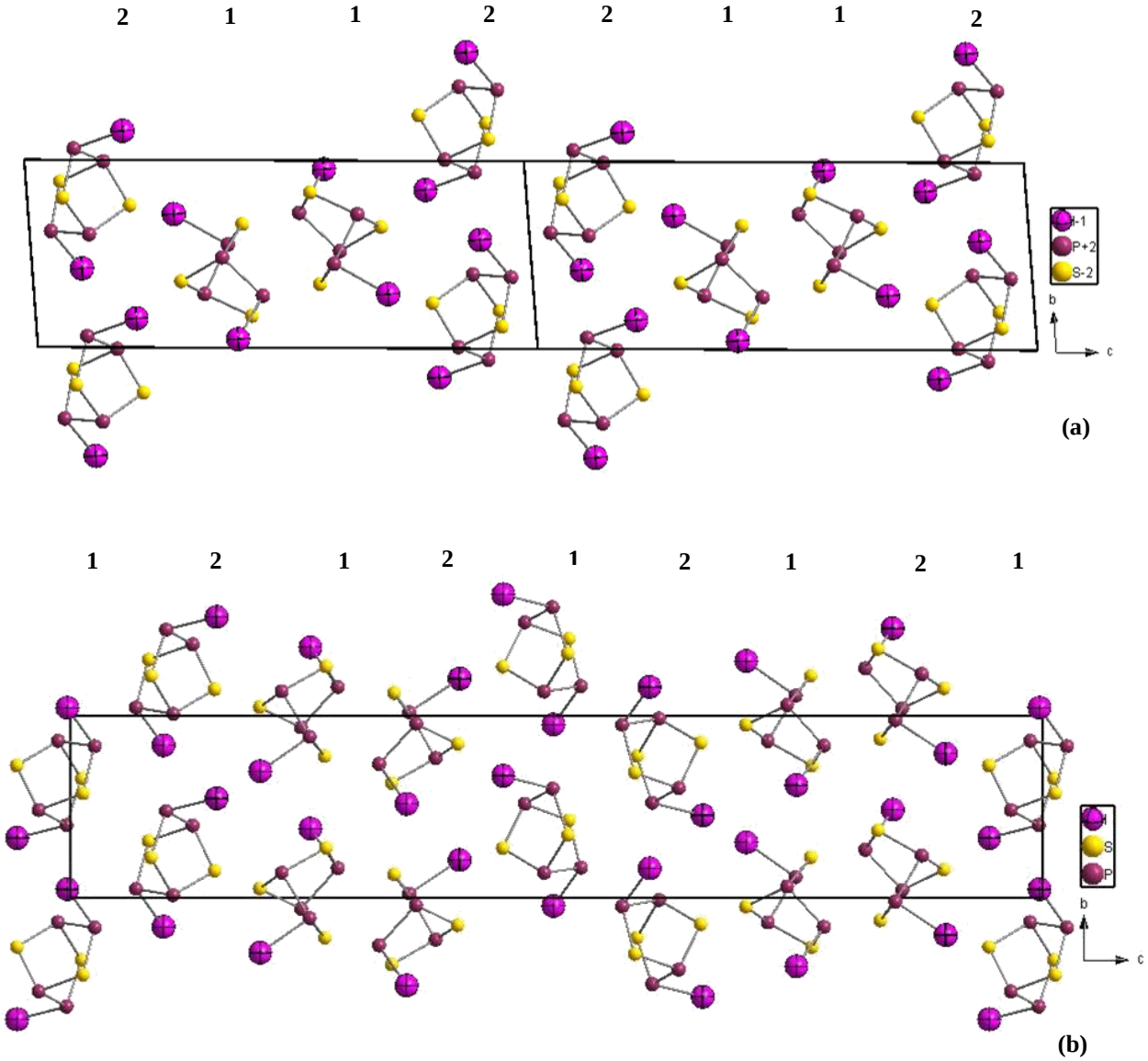

Figure 5.2.3: Arrangement of two types of molecules in (a) α-$P_4S_3I_2$ and in (b) α'-$P_4S_3I_2$

As expected the structure adopts thermodynamically stable modification positioning two exocyclic iodine atoms in opposite positions of the cage. The bond lengths and bond angle are listed in Table S5.6 I Supporting information section. Similar to α-modification, the α'-modification has also two types of independent cage molecules in the asymmetric unit with C_2 point group (shown in Figure 5.2.2). But because of different relative arrangement of the independent molecules than the earlier modifications, the unit cell elongated along c-axis. Two independent molecules are named as '1' and '2'. In earlier α-modifications layers of '1' and '2' are arranged along c-axis in '1-1-2-2-1-1-2-2' manner (Figure 5.2.3). In the α'-modification, '1' and '2' are also present in layers but their positioning in the unit cell is not similar as the molecules are present in layer like '1-2-1-2-1-2' as can be seen in Figure 5.2.3.

Each molecule consists of two types of P atoms, one connected to iodine atoms $P^{I\text{-}conn}$ (P11, P12, P21 and P22) and other are connected to only sulphur atoms, $P^{S\text{-}conn}$ (P13, P14, P23, P24); and two types of sulphur atoms, connecting iodo-linked P atoms, S^{brid1} (S11, S13, S21, S23) and connecting non-iodo-linked P atoms, S^{brid2} (S12 and S22). The 'book angles' between two five membered rings showed the greatest difference in two molecules i.e. ∠P13-P12-S11 is 92.93(1)^o and ∠P14-P11-S13 is 91.97^o for molecule '1' and corresponding angles are 94.07(1)^o and 93.33(7)^o for molecule '2'. Each molecule has two five membered rings, i.e. P11-S12-P12-S11-P14 and P11-S12-P12-S13-P13 for molecule '1'. Those book angles are controlled by distance between corresponding phosphorus and sulphur of two five-membered rings, i.e. distance between P13-S11 is 3.156(1) Å and P14-S13 is 3.124 Å (which is 3.178 Å and 3.165(4) Å respectively for the other molecule). This distance between phosphorus and sulphur (which is lower than their van-der Waal distances[16], 3.60 Å) and distance between iodine and non-iodo-linked phosphorus bridging sulphur (i.e. I-S12 or I-S22) govern the book angle. A detailed overview of the bond distances and angles are listed in Table S5.6.

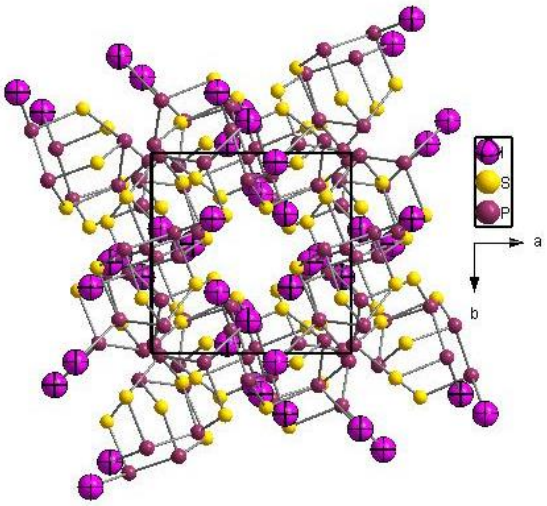

Figure 5.2.4: Arrangement of the molecules along 'c'-axis

Table 5.2.2: Structural comparison between different modifications of $P_4S_3I_2$

Parameters	**α'-$P_4S_3I_2$**	**α-$P_4S_3I_2$[17]**	**β-$P_4S_3I_2$[18]**
Symmetry	tetragonal	triclinic	orthorhombic
Space group	$P4_3$	$P\bar{1}$	*Pnma*
a, Å	7.284(1)	7.268(4)	9.399(2)
b, Å	7.284(1)	7.342(4)	16.343(4)
c, Å	39.027(3)	19.553(11)	6.657(9)
V, Å^3; *Z*	2070.78(4), *8*	1040.11(100), *4*	1028.58(240), *4*
Book angle(^{o})	91.97-94.07(1) (P-P-S)	92.52(12)-92.90(11) (P-P-S)	95.11(64)-104.09(56) (P-P-P) (S-P-S)

Apart from different arrangement of the molecules in the unit cell for α- and α''-modifications, the minimum distance between two independent molecules is also different. In α-$P_4S_3I_2$, this minimum distance is between S^{brid2} atoms of the corresponding molecules, 3.672(3) Å. But the minimum distance between '1' and '2' is 3.617(1) Å (between S^{brid2} and $P^{S\text{-}conn}$ of the corresponding molecules) where distance between S^{brid2} atoms of two molecules is 3.659(1) Å. So the inter-molecular distance in α''-$P_4S_3I_2$ is lower than the α-modification.

5.2.3 SEM-EDS measurement

Block like crystals were measured by EDS for quantitative analysis[19]. The measured data is in agreement (with less than 1% differences) with the calculated value from SCXRD measurement.

Table 5.2.4: Comparison between the chemical composition calculated from single crystal refinement and measured by SEM-EDX

Elements (atom %)	P	S	I
Calculated (SCXRD)	44.44	33.33	22.22
Measured (EDS)	44.32	33.56	22.11

5.3 References

[1] Hilmer, W., *Acta Crystallogr. Sect. B*, (1969) **25**, 1229.

[2] Wallis, B.; Wolf, G. U.; Leibnitz, P., *Z. Anorg. Allg. Chem.*, (1990) **588**, 139.

[3] Meisel, W.; Grunze, H., *Z. Anorg. Allg. Chem.*, (1969) **366**, 152.

[4] Treadwell, W.; Beeli, C., *Helv.Chim.Acta.*, (1935) **18**, 1161.

[5] Vos, A.; Wiebenga, E. H., *Acta Cryst*, (1955) **8**, 217.

[6] Wood, P. T., *Dissertation, Imperial College*, (1988).

[7] Parsons, S., *Acta Cryst*, (2003) **D59**, 1995.

[8] Jensen, J. O.; Zeroka, D., *J. Mol. Struct.*, (1999) **487**, 267.

[9] Ouvrard, L., *C. Acad. Sci. Paris*, (1892) **115**, 1301.

[10] Ouvrard, L., *Ann. Chim. Phys.*, (1894) **7**, 221.

[11] Topsom, R. D.; Wilkins, C. J., *J. Inorg. Nucl. Chem.*, (1957) **3**, 293.

[12] Dixon, D. T.; Einstein, F. W. B.; Penfold, B. R., *Acta Cryst*,. (1965) **18**, 221.

[13] Wright, D. A.; Penfold, B. R., *Acta Cryst.*, (1959) **12**, 455.

[14] Cordes, A. W.; Hunt, G. W., *Inorg. Chem.*, (1971) **10**, 1935.

[15] Blachnik, R.; Kurz, G.; Wickel, U., *Z. Naturforsch.*, (1984) **39b**, 778.

[16] Batsanov, S. S., *Inorg. Mater.*, (2001) **37**, 871.

[17] Tattershall, B. W.; Kendall, N. L.; McCamley, A.; Clegg, W., *Acta Cryst. C Cryst Struct Comm.*, (1993) **49**, 571.

[18] Penney, G. J.; Sheldrick, G. M., *J. Chem. Soc., A*, (1971) **0**, 1100.

[19] Newbury, D. E.; Ritchie, N. W. M., *Scanning*, (2013) **35**, 141.

6. Conclusion

This thesis deals with the synthesis and structural characterization of new inorganic materials. A range of polymeric compounds containing phosphorus and group 16 elements were synthesised. First, inorganic phosphorus chalcogenide compounds containing tellurium and all three non-radioactive chalcogens except oxygen were synthesised. Total six different phosphorus chalcogenides containing sulphur and selenium and/or tellurium are reported; α-P_2S_6Se, β-P_2S_6Se, P_2S_6Te, $P_2S_{6.35}Se_{0.64}$, P_2S_5SeTe and $P_2S_8Te_3$. For only P_2S_6Se, more than one modification was found. Except for $P_2S_8Te_3$, all five other compounds have four-membered P_4S_4 rings which are connected via quite rare, chalcogen-chalcogen bonds. For P_2S_6Te, S-Te bond is ordered. The repeated formation of two types of binary chemical bonds, i.e., $(P\text{-}Q_1)–(Q_2)–(Q_1\text{-}P)$ (Q_1, Q_2, occupancy by one or more chalcogens), allow formation of parallel-stacked polymeric chains in which the four-membered P-S units are connected via $Q_1–Q_2–Q_1$ bridges instead of otherwise known polysulfide bridges (c.f., the crystal structure of P_2S_7). The packing of the polymeric strands changed drastically on going from lower to higher chalcogens. Stronger long distance non-covalent chalcogen bond between Te and S^{term} of two parallel polymers cause perfect tetrahedral packing in compounds containing tellurium. This chalcogen bond is much stronger in P_2S_6Te than other compounds, and thus the packing is completely different. Composition of P_2S_6Te was confirmed by ^{31}P-NMR. For most of the reported structures, Raman spectra were measured to obtain some insight into bonds between the components, especially the chalcogen bond. It gave a logical analogy of the effect of chalcogen bond on $P\text{-}S^{term}$ bond in P_2S_6Te and this can be co-related nicely with other compounds where chalcogen bond is not so strong. $P_2S_8Te_3$ was synthesised starting from P_2S_6Te, and the unique P_4S_4 ring is not present here. Instead of strand like polymeric structure, $P_2S_8Te_3$ contains layered sheet-like structure formed by long distance Te-Te bond.

All six phosphorus chalcogenides were achieved by using hexa-hydrated $FeCl_3$ as a mineraliser. P_2S_6Te can be synthesised starting from corresponding elements.

In this thesis, a range of inclusion compounds were discussed with host-guest as well as adduct interactions. $(P_4S_3)@Zn_7SI_{12}$ was synthesised before but the composition of the guest cage molecule was not clarified. Here, the guest molecule was proven to be P_4S_3 by single crystal XRD, Raman spectroscopy, and EDS measurement. A family of compounds isostructural with $(P_4S_3)@Zn_7SI_{12}$ with sum formula $(Pn_4Q_3)@Cu_7M_3I_{13}$ [M= Zn, Cd; Pn= P, As; Q= S, Se] were synthesised in order to understand the interaction between the transition

metal halide and the cage molecules (Pn_4Q_3). Even though both the compound types have similar metal halide framework $(SZn_4)@I_{12}$ and $(ICu_4)@I_{12}$ and connected via MI_2 tetrahedrons with Pn_4Q_3 type cage molecule embedded in that framework, but metal-cage interaction is completely different. In $(P_4S_3)@Zn_7SI_{12}$, there is a non-bonding host-guest interaction between metal (Zn) and the cage molecule. The guest molecules are simply trapped inside the framework and rotate almost freely with significantly lower activation energy. The rotation was confirmed by ^{31}P-NMR spectroscopy, and was also resolved by crystallography. Even though $(Pn_4Q_3)@Cu_7M_3I_{13}$ is isostructural with the previous compound, metal (Cu)-cage (P) interaction is Lewis acid-Lewis base interaction like most of the adduct molecules. Cage molecules possess restricted rotation because of stronger interaction with the framework. For detailed information NMR study is needed, which cannot be done because of the time limitation.

On the quest of new phosphorus chalcogenides new phases of phosphorus nonasulphide, P_4S_9 and phosphorus sulphide iodide, $P_4S_3I_2$ were found. The structural analysis of a non-merohedrally twinned single crystal of phosphorus nonasulphide shows that like all other cage structured phosphorus sulphides, it is composed of neutral molecules, which can be derived from P_4-tetrahedron of the white phosphorus. While the structure reported before has cubic and monoclinic symmetry, this one has triclinic symmetry with almost same density as monoclinic modification. The unit cell consists of two types of non-symmetry related molecules. They differ slightly in bond length and in bond angles. The new modification of phosphorus sulphide iodide consists of similar cage molecules like α-$P_4S_3I_2$, but crystallised in tetragonal symmetry.

Supporting information of Chapter 3

Table S3.1: Atomic co-ordinates, equivalent isotropic displacement parameters and occupation factors a_i in α-P_2S_6Se at 125 K

Atom	*Wyckoff*	a_i	*x*	*y*	*z*	U_{iso}/Å^2
P1	4e	1	0.25997(10)	0.81125(7)	-0.08221(5)	0.01118(19)
P2	4e	1	0.63041(9)	0.80930(7)	0.34724(5)	0.01112(19)
S1/ Se1’	4e	0.80(1)/0.20	0.69887(7)	0.79175(5)	0.18584(4)	0.01518(15)
Se1/ S1’	4e	0.78(4)/0.22	0.45227(4)	0.65751(3)	0.13126(2)	0.01376(9)
S2/ Se2’	4e	0.83(1)/0.17	0.19728(6)	0.78517(4)	0.07925(3)	0.01473(12)
S3	4e	1	0.57144(9)	0.87201(6)	-0.08877(5)	0.01193(18)
S4	4e	1	0.31759(9)	0.86808(6)	0.35033(5)	0.01177(18)
S5	4e	1	0.83918(9)	0.91428(7)	0.41736(5)	0.01534(19)
S6	4e	1	0.04987(9)	0.91877(7)	-0.14647(5)	0.0165(2)

Table S3.2: Anisotropic Displacement Values (Å^2) for α-P_2S_6Se at 125K

Atom	U_{11}	U_{22}	U_{33}	U_{12}	U_{13}	U_{23}
P1	0.0086(3)	0.0137(4)	0.0114(3)	0.0001(2)	0.0017(2)	-0.0001(3)
P2	0.0082(3)	0.0144(4)	0.0108(3)	-0.0005(2)	0.0007(2)	0.0004(3)
S1/Se1’	0.0117(2)	0.0216(3)	0.0123(3)	-0.00252(19)	0.00122(18)	-0.0006(2)
Se1/S1’	0.01388(15)	0.01640(17)	0.01098(15)	-0.00084(12)	0.00049(10)	-0.00033(12)
S2/Se2’	0.01218(18)	0.0204(2)	0.01177(19)	0.00055(15)	0.00161(13)	-0.00083(16)
S3	0.0085(3)	0.0150(4)	0.0125(3)	-0.0006(2)	0.0027(2)	-0.0020(2)
S4	0.0095(3)	0.0141(3)	0.0118(3)	0.0004(2)	0.0014(2)	0.0010(2)
S5	0.0100(3)	0.0165(4)	0.0191(3)	-0.0009(2)	-0.0018(2)	-0.0022(3)
S6	0.0099(3)	0.0163(4)	0.0234(4)	0.0013(2)	0.0008(2)	0.0036(3)

Table S3.3: Selected interatomic distances and angle for α-P_2S_6Se at 125 K

Interatomic distances (Å)		Bond angles (^{o})	
Se1 - S1	2.217(6)	S1 - Se1 - S2	102.38(2)
Se1 - S2	2.204(5)	Se - S1 - P2	99.75(3)
S1 - P2	2.135(9)	Se1- S2 - P1	100.67(3)
S2 - P1	2.136(8)	P1 - S3 - P2[5]	86.29(3)
S3 - P1	2.123(9)	P1 - S4 - P2	86.39(3)
S3[2] - P2	2.127(10)	S2 - P1 - S3	108.26(3)

S4 - P1[3]	2.124(10)	S2 - P1 - S4[6]	108.76(4)
S4 - P2	2.122(9)	S2 - P1 - S6	108.37(4)
S5 - P2	1.926(9)	S3 - P1 - S4[7]	93.66(4)
S6 - P1	1.918(9)	S3 - P1 - S6	117.07(4)
Se1 - S5[1]	3.228(8)	S4 - P1 - S6	119.64(4)
S1 - S2	3.445(7)	S1 - P2 - S3[8]	110.02(4)
P1[4] - P2	2.906(10)	S1 - P2 - S4	107.30(3)
		S1 - P2 - S5	108.34(4)
		S3 - P2 - S4	93.63(3)
		S3 - P2 - S5	118.66(4)
		S4 - P2 - S5	117.83(4)

Symmetry code: [1]-x+1,y-1/2,-z+1/2; x, [2]-y+3/2,z-1/2; [3]x,-y+3/2,z+1/2; [4]x,-y+3/2,z+1/2; [5]x,-y+3/2,z-1/2; [6]x,-y+3/2,z-1/2; [7]x,-y+3/2,z-1/2; [8]x,-y+3/2,z+1/2

Table S3.4: Atomic co-ordinates, equivalent isotropic displacement parameters and occupation factors a_i in β-P_2S_6Se at 125 K

Atom	*Wyckoff*	a_i	*x*	*y*	*z*	U_{iso}/Å^2
P1	2i	1	0.6296(2)	0.30208(19)	0.49479(12)	0.0187(4)
P2	2i	1	1.0536(2)	0.67049(19)	0.06348(12)	0.0181(4)
S1/ Se1’	2i	0.79(1)/0.21	0.85261(17)	0.73934(15)	0.21310(9)	0.0251(3)
Se1/ S1’	2i	0.72(2)/0.28	0.60900(10)	0.50699(9)	0.20964(6)	0.0223(2)
S2/ Se2’	2i	0.86(1)/0.14	0.76137(18)	0.23875(16)	0.32635(10)	0.0241(3)
S3	2i	1	0.2874(2)	0.39669(18)	0.47555(12)	0.0203(4)
S4	2i	1	1.1504(2)	0.34634(18)	0.08536(12)	0.0204(4)
S5	2i	1	0.7262(2)	0.07372(19)	0.61075(13)	0.0288(5)
S6	2i	1	1.2844(2)	0.85748(19)	0.04680(13)	0.0252(4)

Table S3.5: Anisotropic Displacement Values (Å^2) for β-P_2S_6Se at 125 K

Atom	U_{11}	U_{22}	U_{33}	U_{12}	U_{13}	U_{23}
P1	0.0176(6)	0.0141(6)	0.0249(8)	-0.0019(5)	0.0021(6)	-0.0044(5)
P2	0.0188(6)	0.0145(6)	0.0214(7)	-0.0021(5)	0.0007(5)	-0.0036(5)
S1/Se1’	0.0310(6)	0.0202(5)	0.0256(6)	-0.0053(4)	0.0059(5)	-0.0073(4)
Se1/S1’	0.0199(3)	0.0245(3)	0.0225(4)	-0.0032(3)	0.0020(3)	-0.0021(3)
S2/Se2’	0.0272(6)	0.0182(5)	0.0269(6)	0.0006(4)	0.0062(5)	-0.0051(5)
S3	0.0162(6)	0.0159(6)	0.0300(8)	-0.0034(5)	0.0013(5)	-0.0067(5)
S4	0.0224(6)	0.0154(6)	0.0239(7)	-0.0006(5)	-0.0016(5)	-0.0046(5)
S5	0.0353(8)	0.0175(7)	0.0330(9)	-0.0005(6)	-0.0084(6)	-0.0003(6)
S6	0.0221(7)	0.0169(6)	0.0370(9)	-0.0062(5)	-0.0013(6)	-0.0017(6)

Table S3.6: Selected interatomic distances and angle for β-P_2S_6Se at 125 K

Interatomic distances (Å)		Bond angles (°)	
Se1 - S1	2.200(1)	S1 - Se1 - S2	102.58(5)
Se1 - S2	2.196(1)	Se1 - S1 - P2	100.26(5)
S1 - P2	2.134(1)	Se1 - S2 - P1	100.94(6)
S2 - P1	2.120(1)	P1 - S3 - P1^1	86.45(7)
S3 - P1	2.118(1)	P2 - S4 - P2^2	86.13(6)
S3 - P1^1	2.120(2)	S2 - P1 - S3	108.97(7)
S4 - P2	2.117(2)	S2 - P1 - S3^4	107.78(7)
S4 - P2^2	2.114(1)	S2 - P1 - S5	108.13(8)
S6 - P2	1.921(1)	S3 - P1 - S3^5	93.55(7)
S5 - P1	1.912(1)	S3 - P1 - S5	119.82(8)
S6 - Se1^3	3.277(15)	S4 - P1 - S5	117.47(8)
		S1 - P2 - S4	107.82(6)
		S1 - P2 - S4^7	109.60(7)
		S1 - P2 - S6	108.42(8)
		S4 - P2 - S4^6	93.87(7)
		S4 - P2 - S6	117.46(8)
		S4 - P2 - S6	118.66(7)

Symmetry code: ^{1}-x+1,-y+1,-z+1; ^{2}-x+2,-y+1,-z; ^{3}x+1,y,z; ^{4}-x+1,-y+1,-z+1; ^{5}-x+1,-y+1,-z+1; ^{6}-x+2,-y+1,-z; ^{7}-x+2,-y+1,-z

Table S3.7: Atomic co-ordinates, equivalent isotropic displacement parameters and occupation factors a_i in $P_2S_{6.36}Se_{0.64}$ at 123 K

Atom	*Wyckoff*	a_i	*x*	*y*	*z*	U_{iso}/Å^2
P1	4e	1	0.24008(10)	0.68876(6)	0.58258(5)	0.01246(18)
P2	4e	1	-0.12986(11)	0.69034(6)	0.15357(5)	0.01263(19)
S1/ Se1’	4e	0.95(3)/0.05	0.29755(10)	0.71513(5)	0.42128(5)	0.01591(18)
Se1/ S1’	4e	0.53(3)/0.47	0.04774(6)	0.83987(3)	0.36913(3)	0.01497(11)
S2/ Se2’	4e	0.94(4)/0.06	-0.19356(10)	0.70894(5))	0.31450(5)	0.01628(19)
S3	4e	1	0.45112(10)	0.58122(6)	0.64716(6)	0.0177(2)
S4	4e	1	0.18225(10)	0.63104(5)	0.14984(5)	0.01357(18)
S5	4e	1	-0.07067(10)	0.62786(6)	0.58949(5)	0.01416(18)
S6	4e	1	-0.34007(10)	0.58549(6)	0.08329(5)	0.01674(19)

Table S3.8: Anisotropic Displacement Values (Å^2) for $P_2S_{6.36}Se_{0.64}$ at 123 K

Atom	U_{11}	U_{22}	U_{33}	U_{12}	U_{13}	U_{23}
P1	0.0114(3)	0.0134(3)	0.0126(3)	0.0002(2)	0.0003(3)	-0.0006(2)
P2	0.0115(3)	0.0137(3)	0.0124(3)	-0.0004(3)	-0.0009(3)	0.0001(2)
S1/Se1’	0.0154(3)	0.0194(3)	0.0130(3)	0.0000(2)	0.0007(2)	-0.0012(2)
Se1/S1’	0.0157(2)	0.01650(17)	0.01245(18)	-0.00071(14)	-0.00143(14)	-0.00051(14)
S2/Se2’	0.0145(3)	0.0202(3)	0.0140(3)	-0.0026(2)	0.0004(2)	0.0002(2)
S3	0.0130(3)	0.0156(3)	0.0241(4)	0.0011(3)	-0.0010(3)	0.0034(3)
S4	0.0123(3)	0.0139(3)	0.0144(3)	0.0005(2)	-0.0001(3)	0.0013(2)
S5	0.0123(3)	0.0143(3)	0.0159(3)	-0.0011(2)	0.0007(3)	-0.0019(2)
S6	0.0125(3)	0.0168(3)	0.0205(4)	-0.0010(3)	-0.0029(3)	-0.0026(2)

Table S3.9 Selected interatomic distances and angle for $P_2S_{6.36}Se_{0.64}$ at 123 K

Interatomic distances (Å)		Bond angles (°)	
Se1 - S1	2.151(7)	S1 - Se1 - S2	102.79(3)
Se1 - S2	2.160 (7)	Se1 - S1 - P1	101.53(3)
S1 - P1	2.103(9)	Se1 - S2 - P2	100.64(3)
S2 - P2	2.099(9)	P1 - S5 - P2[4]	86.38(3)
S3 - P1	1.913(9)	P1 - S4 - P2	86.41(3)
S5 - P2[3]	2.119 (9)	S1 - P1 - S3	108.85(4)
S4 - P2	2.114(10)	S3 - P1 - S4[4]	119.91(4)
S4 - P1[2]	2.118(9)	S4 - P1 - S5	93.59(4)
S6 - P2	1.921(9)	S1 - P1 - S5	107.76(4)
S5 - P1	2.115(10)	S1 - P1 - S4[4]	108.26(4)
S6 - Se1[1]	3.234(8)	S3 - P1 - S5	117.19(4)
		S2 - P2 - S4	107.08(4)
		S2 - P2 - S5[2]	109.47(4)
		S2 - P2 - S6	108.73(4)
		S4 - P2 - S5[2]	93.59(3)
		S4 - P2 - S6	117.93(4)
		S5 - P2 - S6	118.84(4)

Symmetry code: [1]-x,y+1/2,-z+1/2; [2]x,-y+3/2,z-1/2; [3]x,-y+3/2,z-1/2; [4]x,-y+3/2,z+1/2

Table S3.10: Atomic co-ordinates, equivalent isotropic displacement parameters and occupation factors a_i in P_2S_6Te at 123 K

Atom	*Wyckoff*	a_i	*x*	*y*	*z*	U_{iso}/Å^2
P1	8f	1	-0.14063(6)	-0.00727(7)	-0.00911(5)	0.00708(19)
S1	8f	1	-0.30707(6)	-0.10176(7)	-0.13896(5)	0.00982(19)
S2	8f	1	-0.03004(6)	0.18419(7)	-0.06028(5)	0.00877(19)
S3	8f	1	-0.18539(6)	0.07468(7)	0.13405(5)	0.00892(19)
Te1	4e	1	0	0.27964(3)	0.25	0.00929(9)

Table S3.11: Anisotropic Displacement Values (Å^2) for P_2S_6Te at 123 K

Atom	U_{11}	U_{22}	U_{33}	U_{12}	U_{13}	U_{23}
P1	0.0073(3)	0.0087(3)	0.0058(3)	0.0001(2)	0.0033(2)	0.00032(19)
S1	0.0089(3)	0.0109(3)	0.0082(3)	-0.0015(2)	0.0020(2)	-0.0004(2)
S2	0.0084(3)	0.0101(2)	0.0091(3)	0.0013(2)	0.0049(2)	0.00231(19)
S3	0.0089(3)	0.0112(2)	0.0083(3)	-0.0010(2)	0.0052(2)	-0.00169(19)
Te1	0.00999(13)	0.01125(13)	0.00646(13)	0	0.00323(9)	0

Table S3.12 Selected interatomic distances and angle for P_2S_6Te at 123 K

Interatomic distances (Å)		Bond angles (°)	
Te1 - S3[1]	2.439(6)	S3 - Te1 - S3[1]	100.83(2)
S1 - P1	1.949(8)	Te1 - S1 - P1	105.78(3)
S2 - P1[2]	2.121(8)	P1 - S2 - P1[4]	85.91(3)
S2 - P1	2.110(9)	Te1 - S3 - P1	105.67(3)
S3 - P1	2.078(10)	S1 - P1 - S2	115.87(4)
Te1 - S1[3]	3.108(7)	S1 - P1 - S2[5]	114.97(3)
		S1 - P1 - S3	110.42(4)
		S2 - P1 - S3	112.67(3)
		S2 - P1 - S3	107.74(3)

Symmetry code: [1]-x,y,-z+1/2; [2]-x,-y,-z; [3]-x-1/2,-y+1/2,-z; [4]-x,-y,-z; [5]-x,-y,-z;

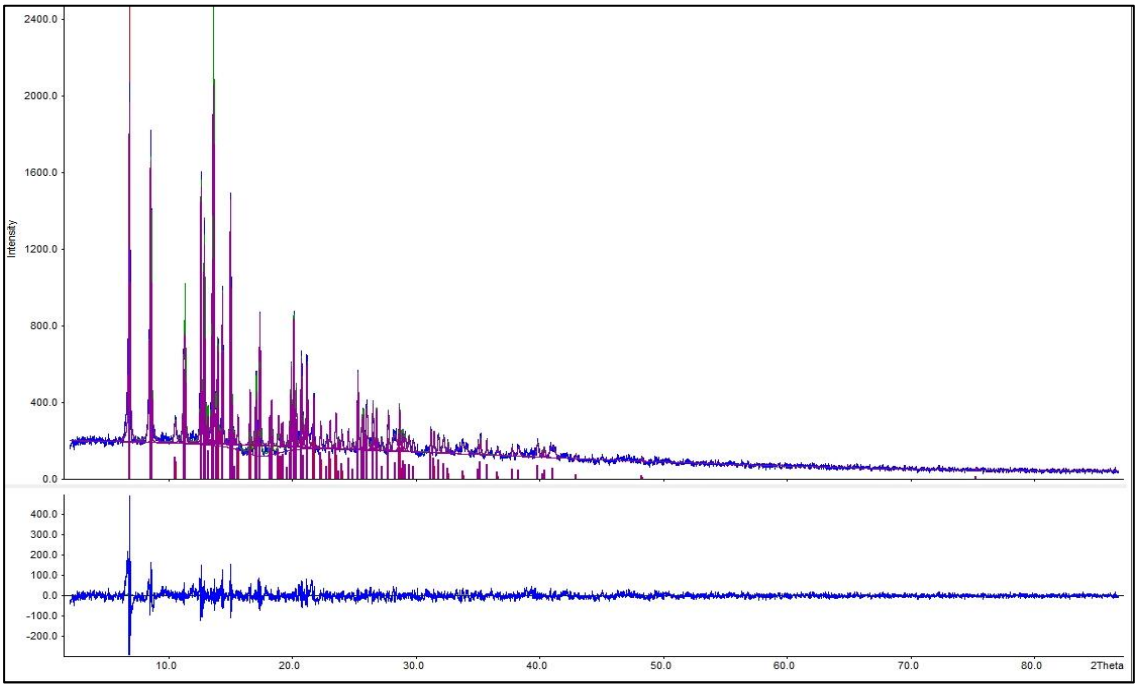

Figure S6: Indexing the powder diffractogram of P_2S_6Te upto 75°

Table S3.13: List of refinement of the powder diffraction of P_2S_6Te upto 75°

Wavelength : 0.709300

Number of accepted peaks : 81

2Theta window : 0.050

2Theta zeropoint : 0.0010 (refineable)

Symmetry : Monoclinic_B C
Spacegroup : C 2/c (No. 15)

Initial cell parameters :
Cell_A : 12.2250

Cell_B : 7.6460
Cell_C : 10.5500
Cell_Beta : 114.510

Refined cell parameters :
Cell_A : 12.227(9)
Cell_B : 7.648(4)
Cell_C : 10.550(5)
Cell_Beta : 114.50(3)
Cell_Volume: 897.7(13)

Number of single indexed lines : 36
Number of unindexed lines : 9

2Theta zeropoint : 0.001(9)

Final 2Theta window : 0.0500

N	2Th[obs]	H	K	L	2Th[calc]	obs-calc	Int.	d[obs]	d[calc]
1	6.830	-1	1	1	6.836	-0.0061	100.0	5.9539	5.9486
2	8.514	0	0	2	8.474	0.0406	59.0	4.7774	4.8003
		1	1	1	8.512	0.0024			4.7788
3	8.599	-2	0	2	8.596	0.0030	53.7	4.7306	4.7323
4	10.551	--- not indexed ---					3.9	3.8573	
5	11.215	--- not indexed ---					16.2	3.6295	
6	11.321	-3	1	1	11.322	-0.0007	30.3	3.5956	3.5953
7	12.602	-2	2	1	12.619	-0.0165	62.2	3.2314	3.2272
8	12.850	-1	1	3	12.848	0.0018	55.2	3.1694	3.1698
9	12.930	2	2	0	12.924	0.0060	37.0	3.1498	3.1513
10	13.167	--- not indexed ---					6.3	3.0932	
11	13.528	-4	0	2	13.543	-0.0158	19.5	3.0112	3.0077
12	13.628	0	2	2	13.620	0.0088	90.3	2.9891	2.9910
13	13.789	--- not indexed ---					5.9	2.9544	
14	13.967	-3	1	3	13.969	-0.0024	19.8	2.9170	2.9165
15	14.351	3	1	1	14.345	0.0053	31.8	2.8394	2.8404
16	15.007	--- not indexed ---					54.8	2.7158	
17	15.135	--- not indexed ---					9.3	2.6930	
18	15.319	--- not indexed ---					2.8	2.6609	
19	15.593	1	1	3	15.583	0.0103	6.4	2.6144	2.6161
20	16.586	-1	3	1	16.567	0.0189	10.6	2.4588	2.4616
		0	2	3	16.618	-0.0316			2.4542
21	16.987	0	0	4	16.995	-0.0071	5.7	2.4011	2.4001
22	17.083	2	2	2	17.072	0.0113	15.1	2.3878	2.3894
23	17.343	3	1	2	17.298	0.0450	2.8	2.3523	2.3584
	?	1	3	1	17.335	0.0078			2.3534
24	17.378 ?	1	3	1	17.335	0.0434	22.5	2.3475	2.3534
25	18.150	4	2	0	18.143	0.0069	6.5	2.2485	2.2494
26	18.319	-4	2	3	18.349	-0.0301	7.5	2.2280	2.2243
27	18.885	-3	3	1	18.891	-0.0066	5.0	2.1618	2.1610
28	19.102	5	1	0	19.110	-0.0078	4.2	2.1374	2.1366
29	19.205	1	3	2	19.189	0.0164	4.4	2.1260	2.1278
30	19.582	1	1	4	19.578	0.0038	2.2	2.0855	2.0859
31	19.784	4	0	2	19.790	-0.0057	4.4	2.0644	2.0638
32	19.893	-1	3	3	19.854	0.0384	14.7	2.0532	2.0572

		-5	1	4	19.900	-0.0068		2.0525
33	20.100	-6	0	2	20.055	0.0448	24.5 2.0323	2.0368
		0	2	4	20.094	0.0062		2.0329
34	20.191	-3	1	5	20.203	-0.0117	9.4 2.0232	2.0221
		2	2	3	20.218	-0.0267		2.0206
35	20.300	-4	2	4	20.304	-0.0039	10.6 2.0125	2.0121
36	20.726	3	1	3	20.729	-0.0031	16.1 1.9716	1.9713
		-1	1	5	20.739	-0.0135		1.9703
37	20.870	3	3	1	20.866	0.0041	3.5 1.9581	1.9585
38	21.186	2	0	4	21.160	0.0261	11.4 1.9292	1.9316
		5	1	1	21.188	-0.0024		1.9290
39	21.727	1	3	3	21.745	-0.0185	8.7 1.8817	1.8802
40	22.291	-5	1	5	22.257	0.0340	4.3 1.8347	1.8375
41	22.768	-6	2	2	22.756	0.0117	2.5 1.7968	1.7977
42	23.045	3	3	2	23.020	0.0254	4.4 1.7754	1.7773
		0	4	2	23.034	0.0116		1.7763
		-6	2	3	23.040	0.0055		1.7758
		-2	4	2	23.080	-0.0347		1.7728
43	23.523	-2	0	6	23.500	0.0226	5.3 1.7399	1.7415
44	23.745	1	1	5	23.699	0.0458	1.6 1.7238	1.7271
		2	2	4	23.741	0.0037		1.7241
		-5	3	3	23.762	-0.0178		1.7226
45	24.008	--- not indexed ---					2.0 1.7052	
46	24.543	6	2	0	24.545	-0.0014	3.2 1.6686	1.6685
47	24.888	-7	1	4	24.887	0.0014	1.9 1.6458	1.6459
		-1	1	6	24.888	0.0003		1.6458
		-7	1	1	24.897	-0.0094		1.6452
48	25.302	2	4	2	25.267	0.0350	10.7 1.6193	1.6216
		-3	3	5	25.301	0.0002		1.6194
		-4	4	1	25.343	-0.0419		1.6167
49	25.606	0	0	6	25.611	-0.0047	5.2 1.6004	1.6001
50	25.739	3	3	3	25.728	0.0107	6.8 1.5923	1.5929
		-1	3	5	25.737	0.0022		1.5924
51	26.015	-4	2	6	25.985	0.0302	5.3 1.5757	1.5774
		-6	0	6	25.986	0.0297		1.5774
		4	4	0	26.016	-0.0002		1.5756
52	26.514	6	2	1	26.467	0.0465	6.2 1.5465	1.5492
		-2	4	4	26.489	0.0248		1.5480
53	26.799	4	0	4	26.803	-0.0032	6.1 1.5304	1.5302
		6	0	2	26.813	-0.0135		1.5296
54	27.189	-1	5	1	27.167	0.0221	1.1 1.5088	1.5100
55	27.753	-3	1	7	27.786	-0.0329	5.9 1.4788	1.4770
56	28.287	--- not indexed ---					2.5 1.4514	
57	28.659	-3	5	1	28.679	-0.0197	6.8 1.4329	1.4320
58	28.830	3	3	4	28.849	-0.0188	1.8 1.4246	1.4237
59	28.913	1	5	2	28.880	0.0330	3.0 1.4206	1.4222
		4	2	4	28.912	0.0014		1.4207
		6	2	2	28.922	-0.0082		1.4202
		-8	2	3	28.949	-0.0358		1.4189
		-3	5	2	28.955	-0.0419		1.4186
60	29.120	-1	1	7	29.119	0.0006	2.4 1.4107	1.4108
61	29.422	-4	2	7	29.397	0.0251	2.3 1.3966	1.3977
		-5	3	6	29.444	-0.0224		1.3955
62	29.778	-2	2	7	29.740	0.0379	1.9 1.3802	1.3820
63	31.187	-9	1	2	31.204	-0.0173	3.8 1.3193	1.3186

		-4	0	8	31.205	-0.0186		1.3186
64	31.452	2	2	6	31.463	-0.0106	3.0	1.3085	1.3080
		8	2	0	31.490	-0.0373			1.3070
65	31.821	6	2	3	31.797	0.0237	2.6	1.2937	1.2946
		-3	1	8	31.830	-0.0088			1.2933
		1	3	6	31.865	-0.0442			1.2919
66	32.231	1	1	7	32.193	0.0382	1.9	1.2777	1.2792
		-9	1	1	32.227	0.0033			1.2778
		-6	0	8	32.229	0.0019			1.2778
		-7	3	6	32.275	-0.0438			1.2760
		3	3	5	32.277	-0.0463			1.2759
67	32.580	4	2	5	32.543	0.0369	1.5	1.2644	1.2657
		0	6	1	32.600	-0.0203			1.2636
68	33.804	-2	2	8	33.773	0.0318	0.9	1.2198	1.2209
		-10	0	4	33.774	0.0306			1.2209
		9	1	0	33.789	0.0151			1.2204
		-7	1	8	33.816	-0.0114			1.2194
		7	1	3	33.846	-0.0414			1.2184
69	35.020	6	2	4	35.006	0.0140	1.4	1.1787	1.1792
70	35.189	-4	6	1	35.140	0.0486	2.4	1.1733	1.1748
		-4	6	2	35.177	0.0113			1.1736
71	35.710	1	5	5	35.663	0.0462	2.0	1.1567	1.1581
		1	3	7	35.722	-0.0126			1.1563
		-5	1	9	35.735	-0.0259			1.1559
		-4	6	3	35.753	-0.0439			1.1553
		-9	3	1	35.754	-0.0444			1.1553
72	36.594	1	1	8	36.547	0.0471	0.8	1.1297	1.1311
		-8	2	8	36.576	0.0182			1.1302
		3	1	7	36.615	-0.0213			1.1290
73	37.776	-1	1	9	37.798	-0.0217	1.3	1.0955	1.0949
74	38.291	9	1	2	38.278	0.0129	1.2	1.0814	1.0817
		-6	6	2	38.322	-0.0308			1.0805
75	39.829	3	3	7	39.803	0.0267	1.8	1.0412	1.0419
		-9	1	9	39.805	0.0247			1.0418
		6	4	4	39.871	-0.0422			1.0401
76	40.198	-3	7	3	40.182	0.0159	1.0	1.0320	1.0324
		8	0	4	40.203	-0.0046			1.0319
		-7	3	9	40.208	-0.0103			1.0318
		7	3	4	40.239	-0.0409			1.0310
77	40.372	3	7	1	40.324	0.0474	1.4	1.0278	1.0289
		-6	6	5	40.325	0.0467			1.0289
		-2	6	6	40.338	0.0336			1.0286
		-10	4	3	40.359	0.0127			1.0281
		2	4	7	40.361	0.0113			1.0280
		4	2	7	40.372	0.0003			1.0278
		0	2	9	40.383	-0.0111			1.0275
78	41.017	1	1	9	40.973	0.0439	1.5	1.0123	1.0133
		-7	5	7	40.985	0.0317			1.0130
		7	5	2	41.006	0.0109			1.0125
		-11	3	5	41.010	0.0063			1.0124
		-9	5	4	41.016	0.0003			1.0123
79	42.920	-12	2	6	42.901	0.0196	0.5	0.9694	0.9698
		-11	3	7	42.941	-0.0204			0.9689
		-3	7	5	42.942	-0.0214			0.9689
80	48.274	4	8	2	48.264	0.0099	0.5	0.8673	0.8675

		-8 6 8	48.283	-0.0094			0.8671
		-11 5 1	48.292	-0.0180			0.8670
		-9 5 9	48.316	-0.0427			0.8666
81	75.287	12 6 7	75.242	0.0445	0.4	0.5807	0.5810
		-20 4 6	75.260	0.0266			0.5809
		4 4 14	75.264	0.0228			0.5808
		-9 9 13	75.266	0.0207			0.5808
		-20 0 2	75.267	0.0199			0.5808
		-15 9 8	75.279	0.0079			0.5807
		-3 3 17	75.293	-0.0063			0.5806
		-5 11 10	75.312	-0.0249			0.5805
		-6 0 18	75.314	-0.0273			0.5805
		5 5 13	75.316	-0.0296			0.5805

Average delta(2Theta) = 0.011
Maximum delta(2Theta) = 0.043 (peak 24) = 3.9 * average

Figure of Merit F(30) = 49.3 (0.009, 65)

Durbin-Watson serial correlation = 2.299 (not significant)

Sqrt[sum(w * delta(q)^2) / (Nobs - Nvar)] = 0.00060054

Table S3.14: Atomic co-ordinates, equivalent isotropic displacement parameters and occupation factors a_i in P_2S_5SeTe at 123 K

Atom	*Wyckoff*	a_i	*x*	*y*	*z*	U_{iso}/Å^2
P1	8f	1	0.85934(8)	-0.00749(11)	-0.01012(7)	0.0141(3)
Te1/ Se1’	4e	0.87(1)/0.13	0	0.27996(4)	0.25	0.01542(12)
S1/ Se2’	8f	0.65(3)/0.35	0.81056(5)	0.07228(7)	0.13810(4)	0.01671(18)
S2/ Se3’	8f	0.96(1)/0.04	0.97081(8)	0.18593(10)	-0.05943(7)	0.0166(3)
S3	8f	1	0.69406(8)	-0.10177(11)	-0.13906(7)	0.0161(3)

Table S3.15: Anisotropic Displacement Values ($Å^2$) for P_2S_5SeTe at 123 K

Atom	U_{11}	U_{22}	U_{33}	U_{12}	U_{13}	U_{23}
P1	0.0141(4)	0.0137(4)	0.0144(4)	0.0002(3)	0.0059(3)	0.0008(3)
Te1/Se1’	0.01481(17)	0.01684(18)	0.01305(16)	0	0.00415(12)	0
S1/ Se2’	0.0168(3)	0.0157(3)	0.0163(3)	0.00056(18)	0.0055(2)	-0.00233(18)
S2/ Se3’	0.0141(4)	0.0192(4)	0.0167(4)	0.0016(3)	0.0065(3)	0.0012(3)
S3	0.0152(4)	0.0148(4)	0.0160(4)	0.0160(4)	0.0041(3)	0.0007(3)

Table S3.16: Selected interatomic distances and angle for P_2S_5SeTe at 123 K

Interatomic distances (Å)		Bond angles (^{o})	
Te1 - S1[1]	2.483(6)	S1 - Te1 - S1[3]	100.83(2)
S2 - P1	2.136(1)	P1 - S2 - P1[4]	85.55(4)
S3 - P1	1.954(1)	S2 - P1 - S2[5]	94.45(5)
P1 - S1	2.172(1)	S2 - P1 - S3	116.34(5)
P1 - S2	2.127(3)	S2 - P1 - S3	114.80(5)
S3 - Te1[2]	3.131(8)	S3 - P1 - S1	109.72(5)
		Te1 - S1 - P1	102.94(3)

Symmetry code: [1] x-1,y,z; [2] -x+1/2,-y+1/2,-z; [3] -x+1,y,-z+1/2; [4] -x+2,-y,-z; [5] -x+2,-y,-z

Table S3.17: Atomic co-ordinates, equivalent isotropic displacement parameters and occupation factors a_i in $P_2S_8Te_3$ at 123 K

Atom	*Wyckoff*	a_i	*x*	*y*	*z*	U_{iso}/Å^2
Te1	4e	1	0.73536(3)	0.39195(6)	0.18517(8)	0.01828(10)
Te2	4e	1	0.44132(3)	0.83690(5)	0.34835(17)	0.01088(9)
Te3	4e	1	0.77235(3)	0.97369(5)	-0.06763(7)	0.01164(9)
S1	4e	1	0.44014(10)	0.63693(18)	0.22890(6)	0.0120(3)
S2	4e	1	0.64536(10)	0.66313(18)	-0.08221(7)	0.0127(3)
S3	4e	1	0.62098(10)	0.17729(19)	-0.00097(7)	0.0136(3)
S4	4e	1	0.57398(10)	0.17026(19)	0.19598(7)	0.0131(3)
S5	4e	1	0.66509(10)	0.63963(19)	0.09443(7)	0.0144(3)
S6	4e	1	0.86909(9)	0.39950(19)	-0.01062(7)	0.0118(3)
S7	4e	1	0.34815(9)	1.13774(18)	0.28096(7)	0.0110(3)
S8	4e	1	0.55809(10)	0.39950(19)	0.37152(7)	0.0145(3)
P1	4e	1	0.48601(10)	0.34206(19)	0.27640(7)	0.0095(3)
P2	4e	1	0.71003(10)	0.46393(19)	-0.00033(7)	0.0100(3)

Table S3.18: Anisotropic Displacement Values (Å^2) for $P_2S_8Te_3$ at 123 K

Atom	U_{11}	U_{22}	U_{33}	U_{12}	U_{13}	U_{23}
Te1	0.01110(16)	0.0304(2)	0.01330(17)	-0.00181(13)	0.00025(12)	0.00049(14)
Te2	0.01366(15)	0.00805(15)	0.01095(15)	-0.00177(11)	0.00115(12)	0.00010(12)
Te3	0.01609(16)	0.00759(15)	0.01124(15)	0.00023(12)	0.00330(12)	0.00029(12)
S1	0.0166(6)	0.0093(6)	0.0102(6)	0.0021(4)	0.0001(4)	0.0001(4)
S2	0.0151(6)	0.0091(6)	0.0139(6)	0.0003(4)	-0.0025(5)	-0.0005(5)
S3	0.0128(6)	0.0075(5)	0.0204(6)	-0.0016(4)	0.0041(5)	-0.0024(5)
S4	0.0131(6)	0.0118(6)	0.0143(6)	0.0021(5)	0.0025(5)	0.0001(5)
S5	0.0205(6)	0.0100(6)	0.0129(6)	-0.0003(5)	0.0059(5)	-0.0030(5)
S6	0.0102(5)	0.0117(6)	0.0135(6)	0.0002(4)	0.0013(4)	0.0001(5)
S7	0.0095(5)	0.0093(5)	0.0143(6)	-0.0006(4)	0.0006(4)	-0.0005(5)
S8	0.0168(6)	0.0148(6)	0.0118(6)	-0.0029(5)	-0.0040(5)	0.0020(5)
P1	0.0096(6)	0.0092(6)	0.0098(6)	-0.0006(4)	-0.0002(4)	0.0009(5)
P2	0.0103(6)	0.0082(6)	0.0114(6)	-0.0007(4)	0.0017(5)	-0.0011(5)

Table S3.19: Selected interatomic distances and angle for $P_2S_8Te_3$ at 123 K

Interatomic distances (Å)		Bond angles (^{o})	
Te2 - Te3	3.183(5)	Te3 - Te2 - S1	97.42(3)
Te2 - S7	2.469(1)	Te3 - Te2 - S7	111.96(3)
Te2 - S1	2.485(1)	S1 - Te2 - S7	85.62(4)
Te2 - S8	3.034(3)	S1 - Te2 - Te3	97.43(1)
Te3 - S2	2.449(1)	S2 - Te3 - S3[6]	87.82(4)
Te3 - S3[2]	2.532(9)	Te2 - Te3 - S2	84.64(3)
Te3 - S6[3]	3.016(1)	Te2 - Te3 - S3[6]	172.43(3)
Te1 - Te1[4]	3.849(5)	S4 - Te1 - S5	96.51(4)
Te1 - S4	2.392(2)	Te2 - S1 - P1	93.11(5)
Te1 - S5	2.386(5)	Te3 - S2 - P2	97.38(6)
P1 - S1	2.058(1)	Te3 - S3 - P2	91.50(6)
P1 - S4	2.092(7)	Te1 - S4 - P1	101.76(6)
P1 - S7[5]	2.090(2)	Te1 - S5 - P2	98.92(6)
P1 - S8	1.969(2)	Te2 - S7 - P1[6]	94.87(5)
P2 - S2	2.069(1)	S1 - P1 - S4	106.09(7)
P2 - S3	2.046(7)	S1 - P1 - S7[7]	108.07(7)
P2 - S5	2.097(8)	S1 - P1 - S8	109.65(7)
P2 - S6	1.991(7)	S4 - P1 - S7[7]	98.58(7)
		S4 - P1 - S8	118.11(8)
		S7 - P1 - S8	115.35(8)
		S2 - P2 - S3	106.70(7)
		S2 - P2 - S5	101.27(7)
		S2 - P2 - S6	114.64(8)
		S3 - P2 - S5	107.09(7)
		S3 - P2 - S6	110.64(7)
		S5 - P2 - S6	115.68(8)

Symmetry code: [1] x-1/2,-y+3/2,z+1/2; [2]x,y+1,z; [3]x,y+1,z; [4]-x+3/2,y-1/2,-z+1/2; [5]x,y-1,z; [6]x,y+1,z; [7]x,y-1,z

Supporting information of Chapter 4

Table S4.1: Atomic coordinates equivalent isotropic displacement parameters and occupation factors a_i in $(P_4S_3)@Zn_7SI_{12}$ at 293 K

Atom	*Wyckoff*	a_i	*x*	*y*	*z*	U_{iso}/Å^2
S-lat	8a	1	0	0	0	0.0207(3)
Zn1	24d	1	1/4	0	0	0.02681(16)
Zn2	32e	0.57(1)	0.43013(11)	*x*	*x*	0.0325(6)
Zn3	32e	0.43	0.06961(11)	*x*	*x*	0.0148(7)
I1	96h	1	0.77269(11)	0.11384(11)	0.00028(5)	0.03016(8)
P1	32e	1/4	0.7007(3)	*x*	*x*	0.120(7)
S1	96h	1/4	0.3023(5)	0.1696(7)	0.7212(8)	0.137(13)
P1	96h	1/4	0.3436(3)	0.2554(7)	0.3436(3)	0.145(9)

Table S4.2: Anisotropic displacement parameters (Å^2) for $(P_4S_3)@Zn_7SI_{12}$ at 293 K

Atom	U_{11}	U_{22}	U_{33}	U_{12}	U_{13}	U_{23}
S-lat	0.0207(5)	U_{11}	U_{11}	0	0	0
Zn1	0.0213(3)	0.0296(2)	U_{22}	0	0	0
Zn2	0.0325(11)	U_{11}	U_{11}	-0.0002(10)	U_{12}	U_{12}
Zn3	0.0148(11)	U_{11}	U_{11}	-0.0004(10)	U_{12}	U_{12}
I1	0.02327(12)	0.02559(12)	0.04162(15)	0.00131(8)	0.0026(5)	0.0020(5)
P1	0.120(13)	U_{11}	U_{11}	-0.058(8)	U_{12}	U_{12}
S1	0.106(13)	0.067(7)	0.24(4)	0.050(10)	0.080(13)	0.008(11)
P1	0.111(10)	0.165(13)	0.16(2)	0.067(16)	-0.093(14)	-0.117(16)

Table S4.3: Selected interatomic distance and angle for $(P_4S_3)@Zn_7SI_{12}$ at 293 K

Metal halide network			
Interatomic distances (Å)		Bond angles (°)	
I1 - Zn1	2.621(4)	Zn2 - S-lat - Zn2^5	109.47(7)
I1 - Zn2^1	2.631(2)	Zn2 - S-lat - Zn3^6	70.53(7)
I1 - Zn3	2.629(2)	Zn2 - S-lat - Zn3^7	180
Zn2^2 - S-lat	2.349(2)	Zn3 - S-lat - Zn3^8	109.47(7)
Zn3^3 - S-lat	2.339(2)	Zn1 - I1 - Zn2^9	98.75(4)
Zn2^4 - Zn3	2.707(3)	Zn1 - I1 - Zn3	98.84(3)
		Zn2 - I1 - Zn3	61.93(4)

Symmetry code: ^{1}y,-x+1/2; -z, ^{2}y,x-1/2,z; ^{3}-x,-y,z; ^{4}y,x-1/2,z; ^{5}y,-x+1/2,-z; ^{6}x,-y,-z; ^{7}-x,y,-z; ^{8}-x,-y,z; ^{9}y,-x+1/2,-z

For cage molecule P_4S_3			
Interatomic distances (Å)		Bond angles (°)	
P1 - S1	2.100(12)	P1 - S1 - P2	102.71(4)
P2 - P2[7]	2.223(14)	P1 - S1 - S1[2]	40.79(2)
P2 - S1	2.099(18)	S1 - S1 - S1[4]	60.00(2)
		P2 - P2 - P2[8]	60.00(3)
		S1 - P2 - P2[6]	107.64(3)
		P2 - S1 - S1	72.30(5)
		P2 - S1 - S1[5]	79.89(3)
		S1 - P1 - S1[1]	98.41(5)

Symmetry code: [1]x+1/2, y,z-1/2; [2]x,y+1/2, z-1/2; [3]x,y+1/2, z-1/2; [4]x+1/2, y,z-1/2; [5]-x+1/2,y+1, [6]-z+1; x,y+1/2, z-1/2; [7]x,y+1/2, z-1/2; [8]x+1,-y+1/2,-z+1

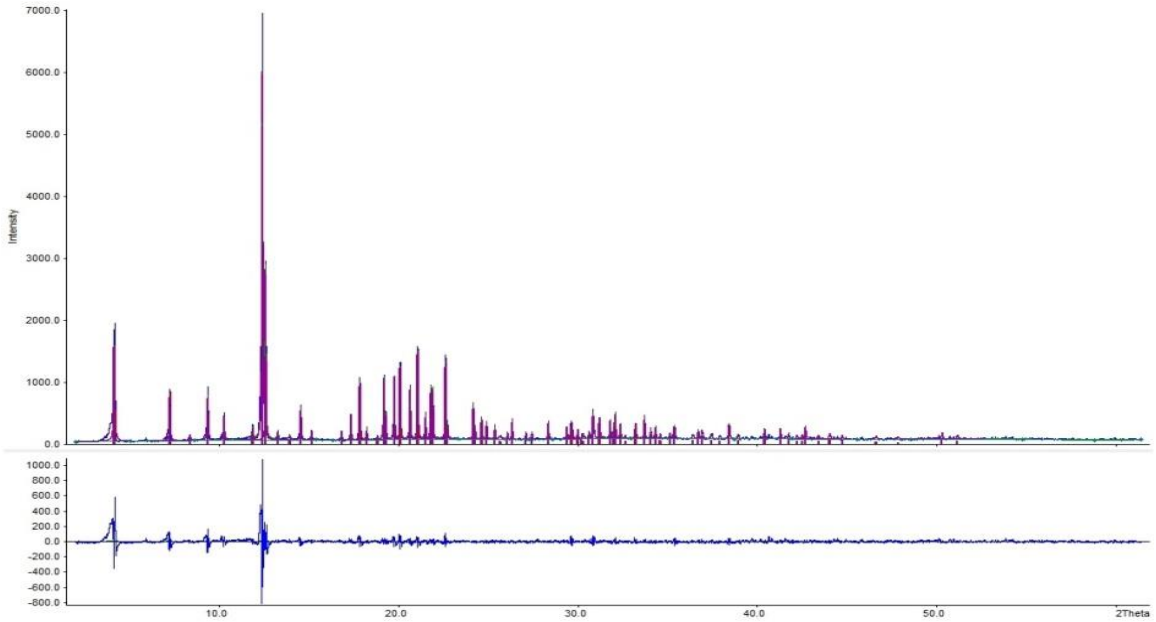

Figure S4.1: Indexed powder diffraction diagram of (P_4S_3)@Zn_7SI_{12}

Table S4.4: Refinement of the powder diffractogram of (P_4S_3)@Zn_7SI_{12}

Wavelength : 0.709300

Number of accepted peaks : 79

2Theta window : 0.040

2Theta zeropoint : 0.0066 (refineable)

Symmetry : Cubic F
Spacegroup : F -4 3 c (No. 219)

Initial cell parameters :
Cell_A : 19.3770

Refined cell parameters :

Cell_A : 19.3770(18)
Cell_Volume: 7275.4(12)

Number of single indexed lines : 75
Number of unindexed lines : 0

2Theta zeropoint : 0.007(3)

Final 2Theta window : 0.0400

N	2Th[obs]	H	K	L	2Th[calc]	obs-calc	Int.	d[obs]	d[calc]
1	4.198	2	0	0	4.196	0.0029	28.3	9.6818	9.6885
2	7.274	2	2	2	7.270	0.0038	12.4	5.5908	5.5936
3	8.400	4	0	0	8.397	0.0030	1.6	4.8425	4.8442
4	9.391	4	2	0	9.390	0.0012	12.6	4.3322	4.3328
5	10.291	4	2	2	10.289	0.0029	6.3	3.9542	3.9553
6	11.888	4	4	0	11.886	0.0026	3.5	3.4246	3.4254
7	12.432	5	3	1	12.432	-0.0005	100.0	3.2754	3.2753
8	12.611	6	0	0	12.609	0.0014	42.8	3.2291	3.2295
9	13.290	6	2	0	13.294	-0.0041	2.1	3.0647	3.0638
10	13.945	6	2	2	13.947	-0.0014	0.9	2.9215	2.9212
11	14.572	4	4	4	14.570	0.0025	8.5	2.7963	2.7968
12	15.175	6	4	0	15.168	0.0066	2.2	2.6859	2.6871
13	16.841	8	0	0	16.839	0.0017	2.4	2.4219	2.4221
14	17.360	8	2	0	17.361	-0.0018	6.3	2.3500	2.3498
15	17.867	6	6	0	17.869	-0.0015	14.4	2.2838	2.2836
16	18.242	7	5	1	18.240	0.0019	2.8	2.2372	2.2375
17	18.839	8	4	0	18.844	-0.0053	0.9	2.1670	2.1664
18	19.198	7	5	3	19.197	0.0005	16.1	2.1268	2.1269
19	19.311	8	4	2	19.314	-0.0026	6.9	2.1145	2.1142
20	19.775	6	6	4	19.773	0.0021	15.9	2.0654	2.0656
21	20.109	9	3	1	20.110	-0.0012	19.1	2.0314	2.0313
22	20.659	8	4	4	20.661	-0.0023	13.3	1.9779	1.9777
23	21.092	10	0	0	21.092	-0.0006	22.0	1.9378	1.9377
24	21.513	10	2	0	21.515	-0.0014	6.5	1.9002	1.9001
25	21.824	9	5	1	21.827	-0.0031	13.3	1.8735	1.8732
26	21.927	10	2	2	21.930	-0.0027	13.1	1.8648	1.8645
27	22.635	9	5	3	22.638	-0.0037	20.1	1.8072	1.8069
28	22.727	10	4	0	22.738	-0.0106	4.6	1.7999	1.7991
29	24.178	11	3	1	24.184	-0.0057	8.8	1.6934	1.6930
30	24.265	8	8	2	24.278	-0.0122	3.4	1.6874	1.6865
31	24.646	10	6	0	24.649	-0.0027	5.4	1.6617	1.6616
32	24.919	9	7	3	24.923	-0.0040	4.6	1.6438	1.6435
33	25.377	12	0	0	25.375	0.0026	3.6	1.6146	1.6147
34	25.679	11	5	1	25.642	0.0370	0.7	1.5959	1.5982
35	26.077	12	2	2	26.082	-0.0050	1.9	1.5720	1.5717
36	26.341	11	5	3	26.343	-0.0015	5.2	1.5565	1.5564
37	27.108	10	8	0	27.111	-0.0035	1.9	1.5133	1.5131
38	27.443	10	8	2	27.446	-0.0029	1.9	1.4951	1.4950
39	28.348	13	3	1	28.349	-0.0005	4.5	1.4483	1.4483
40	29.380	8	8	8	29.382	-0.0028	3.2	1.3985	1.3984
41	29.647	13	5	1	29.616	0.0307	4.4	1.3862	1.3876
42	30.000	14	2	0	30.002	-0.0020	2.4	1.3702	1.3702
43	30.217	11	9	1	30.232	-0.0143	1.1	1.3606	1.3600

44	30.302	14	2	2	30.308	-0.0058	0.9	1.3569	1.3567
45	30.616	12	8	0	30.611	0.0052	1.9	1.3433	1.3436
46	30.848	11	9	3	30.836	0.0116	6.8	1.3335	1.3340
47	31.208	14	4	2	31.209	-0.0003	5.3	1.3184	1.3184
48	31.795	12	8	4	31.796	-0.0013	4.8	1.2947	1.2947
49	32.006	13	7	3	32.014	-0.0087	3.0	1.2864	1.2861
50	32.083	14	4	4	32.087	-0.0040	6.8	1.2834	1.2833
51	32.369	14	6	0	32.375	-0.0057	3.7	1.2724	1.2722
52	32.657	14	6	2	32.660	-0.0031	0.8	1.2614	1.2613
53	33.210	12	10	0	33.225	-0.0144	3.7	1.2410	1.2405
54	33.710	15	5	1	33.712	-0.0025	6.2	1.2232	1.2231
55	34.057	16	0	0	34.056	0.0009	2.5	1.2110	1.2111
56	34.322	16	2	0	34.330	-0.0074	2.8	1.2020	1.2017
57	34.594	16	2	2	34.601	-0.0072	1.0	1.1928	1.1926
58	35.135	16	4	0	35.138	-0.0034	1.4	1.1750	1.1749
59	35.369	15	7	1	35.338	0.0310	3.4	1.1675	1.1685
		16	4	2	35.404	-0.0353			1.1664
60	36.408	13	11	1	36.386	0.0219	1.0	1.1352	1.1359
61	36.706	14	10	0	36.708	-0.0022	2.3	1.1263	1.1263
62	36.921	17	3	1	36.901	0.0208	2.1	1.1200	1.1206
63	37.450	16	6	4	37.472	-0.0221	1.1	1.1047	1.1041
64	37.909	17	5	1	37.912	-0.0029	0.9	1.0918	1.0918
65	38.430	17	5	3	38.409	0.0215	3.9	1.0776	1.0782
66	38.929	15	9	5	38.900	0.0287	1.0	1.0643	1.0651
		18	2	2	38.962	-0.0324			1.0634
67	40.399	16	10	0	40.404	-0.0052	2.6	1.0271	1.0270
68	41.283	19	3	1	41.285	-0.0014	2.7	1.0060	1.0060
69	41.744	17	9	3	41.748	-0.0039	1.3	0.9954	0.9953
70	42.211	19	5	1	42.207	0.0036	0.9	0.9849	0.9850
71	42.484	14	14	0	42.492	-0.0084	0.9	0.9789	0.9787
72	42.673	15	13	1	42.662	0.0108	3.3	0.9747	0.9750
73	43.405	20	2	2	43.394	0.0113	0.9	0.9591	0.9593
74	44.029	19	7	3	44.005	0.0240	1.5	0.9461	0.9466
		20	4	2	44.060	-0.0312			0.9455
75	44.724	20	4	4	44.719	0.0056	1.1	0.9322	0.9323
76	46.615	21	5	1	46.597	0.0180	0.7	0.8963	0.8967
		18	12	0	46.650	-0.0348			0.8957
77	47.847	21	7	1	47.852	-0.0054	0.5	0.8746	0.8745
78	50.290	23	3	1	50.291	-0.0015	1.6	0.8346	0.8346
79	51.134	22	6	6	51.135	-0.0000	0.9	0.8218	0.8218

Average delta(2Theta) = 0.007
Maximum delta(2Theta) = 0.037 (peak 34) = 5.5 * average

Figure of Merit F(30) = 259.0 (0.003, 37)

Durbin-Watson serial correlation = 1.663 (not significant)

Sqrt[sum(w * delta(q)^2) / (Nobs - Nvar)] = 0.00031876

Table S4.5: Atomic co-ordinates, equivalent isotropic displacement parameters and occupation factors a_i in $(P_4S_3)@Cu_7Zn_3I_{13}$ at 123 K

Atom	*Wyckoff*	a_i	*x*	*y*	*z*	U_{iso}/Å^2
I2	8a	1	1/4	1/4	1/4	0.02503(18)
I1	96h	1	0.24936(4)	0.13461(17)	0.06987(16)	0.02099(15)
Zn1	24c	1	1/4	1/4	0	0.0189(3)
Cu1	32e	0.41(2)	0.12554(14)	*x*	*x*	0.0148(7)
Cu2	32e	0.45(3)	0.17416(10)	*x*	*x*	0.0322(6)
Cu3	32e	0.53(3)	0.32717(11)	*x*	*x*	0.0263(4)
Cu4	32e	0.34(1)	0.37561(8)	*x*	*x*	0.0216(6)
P1	32e	1/4	0.05819(20)	*x*	*x*	0.0018(12)
S1	96h	1/4	0.04881(6)	0.07960(10)	-0.04730(3)	0.156(13)
P2	96h	1/4	-0.01005(11)	-0.00356(10)	-0.08324(10)	0.61(4)

Table S4.5: Anisotropic displacement parameters (Å^2) for $(P_4S_3)@Cu_7Zn_3I_{13}$ at 123 K

Atom	U_{11}	U_{22}	U_{33}	U_{12}	U_{13}	U_{23}
I1	0.0297(3)	0.0178(3)	0.0155(2)	-0.0010(3)	0.0005(3)	0.00187(10)
I2	0.0250(3)	U_{11}	U_{11}	0	0	0
Zn1	0.0199(4)	U_{11}	0.0169(5)	0	0	0
Cu1	0.0322(10)	U_{11}	U_{11}	0.0043(14)	U_{12}	U_{12}
Cu2	0.0250(8)	U_{11}	U_{11}	-0.0079(9)	U_{12}	U_{12}
Cu3	0.0263(7)	U_{11}	U_{11}	-0.0097(10)	U_{12}	U_{12}
Cu4	0.0216(10)	U_{11}	U_{11}	-0.0084(11)	U_{12}	U_{12}
P1	0.002(2)	U_{11}	U_{11}	-0.0093(17)	U_{12}	U_{12}
S1	0.079(11)	0.30(3)	0.087(11)	-0.106(19)	-0.065(9)	0.104(18)
P2	0.62(5)	1.14(9)	0.083(11)	-0.84(5)	-0.02(4)	0.01(5)

Table S4.6: Selected interatomic distances and angle for $(P_4S_3)@Cu_7Zn_3I_{13}$ at 123 K

Metal halide network			
Bond distances (Å)		Bond angles (°)	
I1 - Cu1	2.645(2)	Zn1 - I1 - Cu2	98.78(5)
I1 - Cu2	2.614(2)	Zn1 - I1 - Cu1	105.87(5)
I1 - Cu3	2.615(2)	Zn1 - I1 - Cu3	98.67(5)
I1 - Cu4[1]	2.679(2)	Zn1 - I1 - Cu4[4]	105.29(5)
I2 - Cu3	2.5986(19)	Cu2 - I1 - Cu1	36.32(6)
I2 - Cu2	2.5515(19)	Cu2 - I1 - Cu3	69.31(6)
I1 - Zn1	2.6215(4)	Cu2 - I1 - Cu4[5]	103.04(6)
Cu1 - Cu2	1.639(3)	Cu3 - I1 - Cu4[6]	35.75(6)
Cu3 - Cu4[2]	1.627(3)	Cu3 - I1 - Cu1	103.47(6)
Cu1 - P1	2.265(4)	Cu1 - I1 - Cu4[7]	131.77(6)
Cu4 - S1[3]	2.272(11)	Cu2 - I2 - Cu2[8]	109.47(6)
		Cu2 - I2 - Cu3	70.53(6)
		Cu2 - I2 - Cu3[9]	180
		Cu3 - I2 - Cu3[10]	109.47(6)
		I1 - Zn1 - I1[11]	117.59(12)
		I1 - Zn1 - I1[12]	105.57(2)
		I1 - Cu2 - I1	111.68(7)
		I1 - Cu2 - I2	107.16(7)
		I1 - Cu2 - Cu1	72.84(10)
		I1 - Cu3 - I1[13]	112.92(7)
		I1 - Cu3 - I2	105.75(7)
		I1 - Cu3 - Cu4[14]	74.25(10)
		I2 - Cu3 - Zn1	92.98(5)
		I2 - Cu3 - Cu2	53.99(5)
		I1 - Cu1 - P1	109.16(12)
		Cu2 - Cu1 - P1	180
		I1 - Cu4 - I1[15]	108.94(7)
		I1 - Cu4 - Cu3[16]	70.00(10)
		I1 - Cu4 - S1[18]	97.70(4)
		I1 - Cu4 - S1[17]	119.40(4)
		I1 - Cu4 - S1[19]	112.10(2)
		I1 - Cu1 - I1	109.78(7)

Symmetry code: [1]-x+1/2,y,-z+1/2; [2]-x+1/2,y,-z+1/2; [3]x,y,z+1/2; [4]-x+1/2,y,-z+1/2; [5]-x+1/2,y,-z+1/2; [6]-x+1/2,y,-z+1/2; [7]-x+1/2,y,-z+1/2; [8]-x+1/2,-y+1/2,z; [9]-x+1/2,y,-z+1/2; [10]-x+1/2,-y+1/2,z; [11]-x+1/2,-y+1/2,z; [12]-x+1,y,/2,-z; [13]-x+1/2,y,-z+1/2; [14]-x+1/2,y,-z+1/2; [15]-x+1/2,-y+1/2, z; [16]-x+1/2,y,-z+1/2; [17]x,y,z+1/2; [18]-x+1/2,y,-z; [19]x,-y+1/2,-z

For cage molecule P_4S_3			
Bond distances (Å)		Bond angles (°)	
P1 - S1	2.102(8)	P1 - S1 - P2	102.2(9)
P2 - P2	2.22(3)	P1 - S1 - S1	41.8(3)
P2 - S1	2.11(3)	S1 - S1 - S1[3]	61.0(11)
		P2 - P2 - P2[5]	60.0(9)
		S1 - P2 - P2[4]	108.8(13)
		P2 - S1 - S1[1]	71.4(10)

Symmetry code: [1]-x,y,-z; [2]-x,-y,z; [3]-x, y,-z; [4]-x,-y,z; [5]x,-y,-z; [6] -x,-y,z

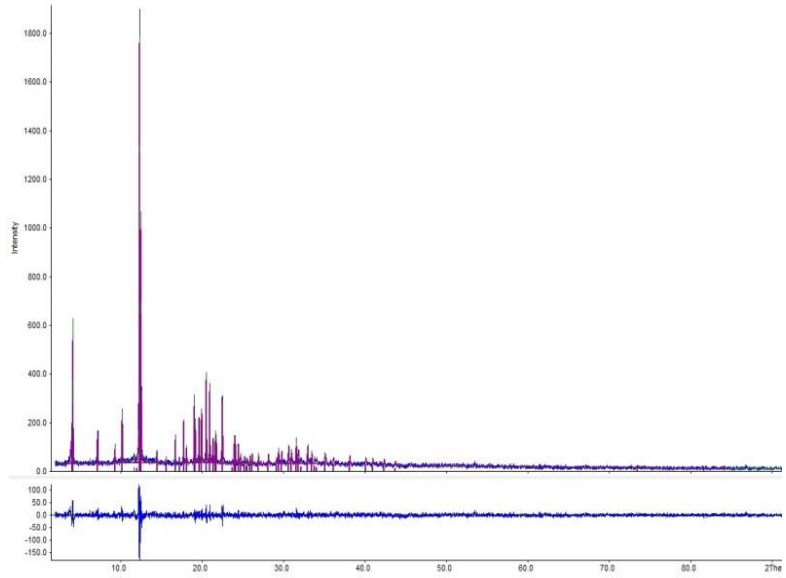

Figure S4.2: Indexed powder diffraction diagram of (P_4S_3)@$Cu_7Zn_3I_{13}$

Table S4.7: Refinement of the powder diffractogram of (P_4S_3)@$Cu_7Zn_3I_{13}$

Wavelength : 0.709300

Number of accepted peaks : 45

2Theta window : 0.040

2Theta zeropoint : 0.0023 (refineable)

Symmetry : Cubic F
Spacegroup : F -4 3 c (No. 219)

Initial cell parameters :
Cell_A : 19.5110

Refined cell parameters :
Cell_A : 19.511(4)
Cell_Volume: 7427.2(25)

Number of single indexed lines : 45
Number of unindexed lines : 0

2Theta zeropoint : 0.002(5)

Final 2Theta window : 0.0300

N	2Th[obs]	H	K	L	2Th[calc]	obs-calc	Int.	d[obs]	d[calc]
1	4.160	2	0	0	4.167	-0.0065	31.6	9.7707	9.7554
2	7.212	2	2	2	7.220	-0.0084	8.8	5.6389	5.6323
3	9.329	4	2	0	9.325	0.0040	5.9	4.3609	4.3627
4	10.216	4	2	2	10.218	-0.0014	13.6	3.9832	3.9826
5	12.346	5	3	1	12.347	-0.0009	100.0	3.2982	3.2979
6	12.529	6	0	0	12.523	0.0067	51.9	3.2501	3.2518

7	14.476	4	4	4	14.469	0.0067	3.9	2.8148	2.8161
8	16.719	8	0	0	16.723	-0.0038	7.4	2.4394	2.4389
9	17.228	8	2	0	17.241	-0.0129	3.0	2.3678	2.3660
10	17.747	6	6	0	17.745	0.0021	10.9	2.2991	2.2994
11	18.106	7	5	1	18.114	-0.0082	5.3	2.2539	2.2529
12	19.069	7	5	3	19.064	0.0045	15.9	2.1411	2.1416
13	19.180	8	4	2	19.180	0.0001	11.4	2.1288	2.1288
14	19.637	6	6	4	19.636	0.0017	11.4	2.0797	2.0799
15	19.971	9	3	1	19.971	-0.0003	13.3	2.0453	2.0453
16	20.518	8	4	4	20.518	-0.0001	20.8	1.9913	1.9913
17	20.946	10	0	0	20.946	0.0005	18.5	1.9510	1.9511
18	21.367	10	2	0	21.366	0.0017	7.1	1.9130	1.9132
19	21.680	9	5	1	21.675	0.0045	8.8	1.8858	1.8862
20	22.489	9	5	3	22.481	0.0076	16.2	1.8188	1.8194
21	24.032	11	3	1	24.016	0.0164	7.3	1.7035	1.7047
22	24.464	10	6	0	24.477	-0.0128	5.8	1.6739	1.6730
23	24.753	9	7	3	24.750	0.0039	3.7	1.6546	1.6549
24	25.209	12	0	0	25.198	0.0108	3.2	1.6252	1.6259
25	25.923	12	2	2	25.900	0.0226	3.1	1.5812	1.5825
26	26.146	11	5	3	26.159	-0.0132	3.8	1.5679	1.5671
27	26.938	10	8	0	26.922	0.0164	3.7	1.5226	1.5235
28	27.505	11	7	1	27.501	0.0037	2.1	1.4918	1.4920
29	28.156	13	3	1	28.150	0.0056	3.5	1.4580	1.4583
30	29.173	8	8	8	29.176	-0.0031	3.0	1.4082	1.4081
31	29.411	13	5	1	29.408	0.0024	4.9	1.3971	1.3972
32	29.793	14	2	0	29.792	0.0014	4.1	1.3796	1.3796
33	30.639	11	9	3	30.620	0.0198	5.6	1.3423	1.3432
34	30.983	14	4	2	30.989	-0.0057	4.6	1.3278	1.3275
35	31.551	12	8	4	31.573	-0.0212	7.3	1.3045	1.3036
36	31.841	14	4	4	31.861	-0.0195	4.9	1.2929	1.2921
37	32.994	12	10	0	32.990	0.0031	5.2	1.2489	1.2491
38	33.475	15	5	1	33.474	0.0006	4.0	1.2315	1.2315
39	33.793	16	0	0	33.816	-0.0226	2.9	1.2202	1.2194
40	35.131	16	4	2	35.153	-0.0222	3.9	1.1751	1.1744
41	36.162	16	6	0	36.192	-0.0297	3.1	1.1427	1.1418
42	38.159	17	5	3	38.135	0.0235	3.2	1.0850	1.0856
43	40.134	16	10	0	40.115	0.0186	2.7	1.0336	1.0341
44	40.975	19	3	1	40.989	-0.0134	2.6	1.0133	1.0130
45	42.373	15	13	1	42.356	0.0171	2.6	0.9813	0.9817

Average delta(2Theta) = 0.009
Maximum delta(2Theta) = 0.030 (peak 41) = 3.2 * average

Figure of Merit F(30) = 85.6 (0.006, 55)

Durbin-Watson serial correlation = 1.776 (not significant)

Sqrt[sum(w * delta(q)^2) / (Nobs - Nvar)] = 0.00043742

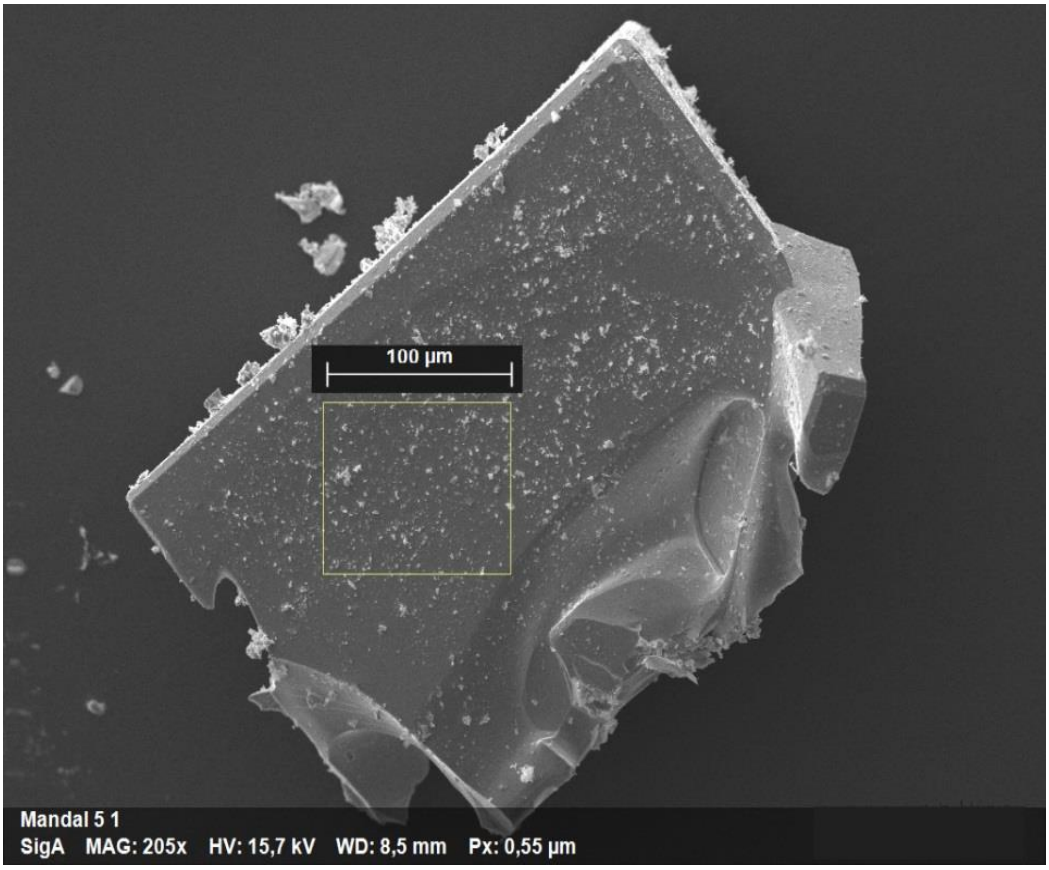

Figure S4.3: SEM image of $(P_4S_3)@Cu_7Zn_3I_{13}$ crystal

Table S4.8: Atomic coordinates, equivalent isotropic displacement parameters and occupation factors a_i in $(P_4S_3)@Cu_7Cd_3I_{13}$ at 123 K

Atom	*Wyckoff*	a_i	*x*	*y*	*z*	U_{iso}/Å^2
I1	96h	1	0.17608(3)	0.11981(3)	-0.00087(8)	0.0341(18)
I2	8a	1	0	0	0	0.0430(3)
Cd1	24c	1	1/4	1/4	0	0.0340(3)
Cu1	32e	0.26(2)	0.1250(14)	*x*	*x*	0.0206(13)
Cu2	32e	0.39(3)	-0.0732(3)	*x*	*x*	0.0194(8)
Cu3	32e	0.61(3)	0.0746(2)	*x*	*x*	0.0528(10)
Cu4	32e	0.48(1)	-0.1270(3)	*x*	*x*	0.0481(13)
P1	32e	1/4	-0.1943(3)	*x*	*x*	0.0112(18)
S1	96h	1/4	0.1700(9)	0.2976(5)	-0.2050(9)	0.3900(4)
P2	96h	1/4	0.2535(9)	0.3359(3)	-0.2591(8)	0.9700(7)

Table S4.9: Anisotropic displacement parameters (Å^2) for $(P_4S_3)@Cu_7Cd_3I_{13}$ at 123 K

Atom	U_{11}	U_{22}	U_{33}	U_{12}	U_{13}	U_{23}
I1	0.0267(3)	0.0299(3)	0.0457(3)	0.00130(16)	-0.0034(9)	-0.0006(9)
I2	0.0430(5)	U_{11}	U_{11}	0	0	0
Cd1	0.0334(6)	0.0343(4)	U_{22}	0	0	0
Cu1	0.021(2)	U_{11}	U_{11}	0.001(3)	U_{12}	U_{12}
Cu2	0.0194(14)	U_{11}	U_{11}	0.006(2)	U_{12}	U_{12}
Cu3	0.0528(18)	U_{11}	U_{11}	-0.003(2)	U_{12}	U_{12}
Cu4	0.048(2)	U_{11}	U_{11}	-0.007(3)	U_{12}	U_{12}
P1	0.011(3)	U_{11}	U_{11}	-0.011(3)	U_{12}	U_{12}
S1	0.18(3)	0.89(11)	0.107(17)	0.40(5)	0.148(19)	0.25(3)
P2	1.35(14)	0.31(6)	1.26(14)	-0.60(9)	-1.27(12)	0.58(9)

Table S4.10: Selected interatomic distances and angle for $(P_4S_3)@Cu_7Cd_3I_{13}$ at 123 K

Metal halide network			
Interatomic distances (Å)		Bond angles (°)	
I1 - Cu1	2.677(8)	Cd1 - I1 - Cu2	96.34(13)
I1 - Cu2	2.642(6)	Cd1 - I1 - Cu1	102.95(17)
I1 - Cu3	2.645(4)	Cd1 - I1 - Cu3	96.13(9)
I1 - Cu4	2.669(6)	Cd1 - I1 - Cu4	103.95(13)
I2 - Cu3	2.545(4)	Cu3 - I1 - Cu1	37.69(19)
I2 - Cu2	2.497(6)	Cu2 - I1 - Cu3	66.83(15)
I1 - Cd1	2.772(6)	Cu3 - I1 - Cu4	105.50(15)
Cu1 - Cu3	1.719(9)	Cu2 - I1 - Cu4	40.43(18)
Cu2 - Cu4	1.835(8)	Cu2 - I1 - Cu1	103.0(2)
Cu4 - P1	2.296(8)	Cu1 - I1 - Cu4	136.4(2)
Cu1 - S1^9	2.365(17)	Cu2 - I2 - Cu2^1	109.47(19)
		Cu2 - I2 - Cu3	70.53(16)
		Cu2 - I2 - Cu3^2	180
		Cu3 - I2 - Cu3	109.47(13)
		I1 - Cd1 - I1^3	116.65(18)
		I1 - Cd1 - I1^4	106.00(4)
		I1 - Cu2 - I1^5	109.5(2)
		I1 - Cu2 - I2	109.4(2)
		I1 - Cu3 - Cu1	72.2(3)
		I1 - Cu3 - I1	111.06(14)
		I1 - Cu3 - I2	107.83(14)
		I1 - Cu2 - Cu4	70.6(3)
		I2 - Cu3 - Cu1	180
		I2 - Cu2 - Cu3	55.50(14)
		I1 - Cu4 - P1	111.0(3)

		Cu2 - Cu4 - P1	180
		I1 - Cu4 - I1[10]	107.9(2)
		I1 - Cu4 - Cu2	69.0(3)
		I1 - Cu1 - S1[6]	97.0(5)
		I1 - Cu1 - S1[7]	118.8(5)
		I1 - Cu1 - S1[8]	112.9(5)
		I1 - Cu1 - I1	109.1(3)

Symmetry code: [1]x,-y,-z; [2]x,-y,-z; [3]x,-y,-z; [4]-x+1/2,-y,z; [5]x,-y,-z; [6]x,-y+1/2; [7]x,-y+1/2,-z, [8]x,-y+1/2,-z; [9]x,-y+1/2,-z; [10]x,-y,-z

For cage molecule P_4S_3			
Interatomic distances (Å)		Bond angles (°)	
P1 - S1	2.101(12)	P1 - S1 - P2	102.7(8)
P2 - P2[6]	2.221(18)	P1 - S1 - S1[1]	40.8(4)
P2 - S1	2.10(2)	S1 - S1 - S1[3]	60.0(2)
		P2 - P2 - P2[7]	60.7(6)
		S1 - P2 - P2[5]	107.6(7)
		P2 - S1 - S1[4]	74.0(6)

Symmetry code: [1]x,-y,-z; [2]x,-y, -z; [3]-x,y,-z; [4]-x+1/2,y,-z-1/2; [5]-x,y,-z; [6]-x,y,-z; [7]x-1/2,-y+1/2,-z

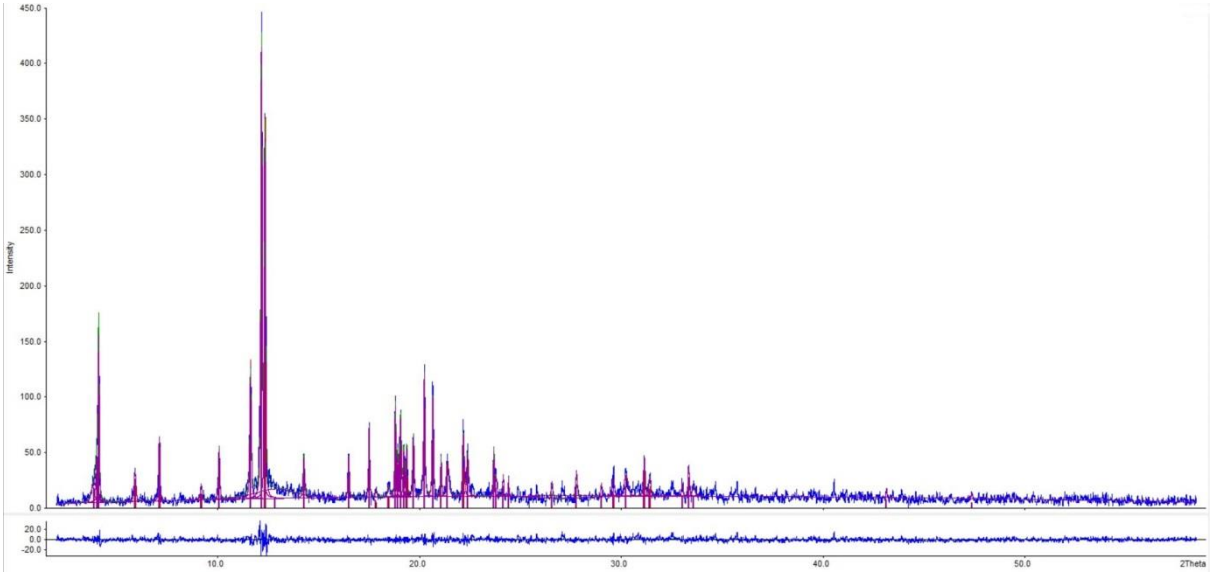

Figure S4.4: Indexed powder diffraction diagram of $(P_4S_3)@Cu_7Cd_3I_{13}$

Table S4.11: Refinement of the powder diffractogram of $(P_4S_3)@Cu_7Cd_3I_{13}$

Wavelength : 0.709300

Number of accepted peaks : 41

2Theta window : 0.030

2Theta zeropoint : 0.0070 (refineable)

Symmetry : Cubic F
Spacegroup : F -4 3 c (No. 219)

Initial cell parameters :
Cell_A : 19.7650

Refined cell parameters :
Cell_A : 19.765(3)
Cell_Volume: 7721.7(23)

Number of single indexed lines : 35
Number of unindexed lines : 6

2Theta zeropoint : 0.007(4)

Final 2Theta window : 0.0300

N	2Th[obs]	H	K	L	2Th[calc]	obs-calc	Int.	d[obs]	d[calc]
1	4.115	2	0	0	4.113	0.0022	39.4	9.8774	9.8826
2	5.928	--- not indexed ---					6.9	6.8583	
3	7.129	2	2	2	7.127	0.0019	11.9	5.7042	5.7058
4	9.195	4	2	0	9.205	-0.0104	2.8	4.4247	4.4197
5	10.086	4	2	2	10.086	0.0002	10.8	4.0345	4.0346
6	11.646	4	4	0	11.651	-0.0053	30.1	3.4956	3.4940
7	12.186	5	3	1	12.187	-0.0009	100.0	3.3412	3.3409
8	12.362	6	0	0	12.361	0.0010	78.8	3.2939	3.2942
9	14.282	4	4	4	14.282	0.0000	9.6	2.8529	2.8529
10	16.502	8	0	0	16.506	-0.0037	8.0	2.4712	2.4707
11	17.515	6	6	0	17.515	0.0005	13.5	2.3293	2.3294
12	17.865	7	5	1	17.879	-0.0143	1.3	2.2841	2.2823
13	18.497	8	4	0	18.470	0.0267	2.3	2.2067	2.2098
14	18.816	7	5	3	18.817	-0.0009	18.3	2.1696	2.1695
15	18.935	8	4	2	18.931	0.0044	9.1	2.1561	2.1566
16	19.074	--- not indexed ---					18.3	2.1406	
17	19.232	--- not indexed ---					9.7	2.1231	
18	19.378	6	6	4	19.380	-0.0022	9.6	2.1072	2.1070
19	19.710	9	3	1	19.711	-0.0010	13.2	2.0721	2.0720
20	20.250	8	4	4	20.251	-0.0008	26.8	2.0174	2.0173
21	20.671	10	0	0	20.673	-0.0018	21.0	1.9767	1.9765
22	21.083	10	2	0	21.087	-0.0040	7.4	1.9385	1.9381
23	21.394	9	5	1	21.393	0.0016	9.5	1.9106	1.9108
24	22.188	9	5	3	22.188	-0.0002	14.1	1.8431	1.8431
25	22.396	--- not indexed ---					10.7	1.8262	
26	23.695	11	3	1	23.702	-0.0072	9.2	1.7274	1.7269

27	23.804	8	8	2	23.794	0.0103	3.8	1.7196	1.7203
28	24.155	10	6	0	24.157	-0.0019	2.8	1.6950	1.6949
29	24.423	9	7	3	24.426	-0.0025	2.0	1.6766	1.6765
30	26.574	10	8	0	26.569	0.0054	1.9	1.5431	1.5434
31	27.789	13	3	1	27.780	0.0086	4.2	1.4769	1.4773
32	29.023	13	5	1	29.021	0.0018	1.8	1.4153	1.4154
33	29.566	--- not indexed ---					2.2	1.3899	
34	29.641	11	9	1	29.624	0.0171	3.0	1.3865	1.3873
35	30.231	11	9	3	30.216	0.0155	6.7	1.3600	1.3607
36	31.152	12	8	4	31.156	-0.0034	8.4	1.3208	1.3206
37	31.422	14	4	4	31.440	-0.0177	4.6	1.3097	1.3090
38	33.028	15	5	1	33.031	-0.0028	2.5	1.2477	1.2476
39	33.353	16	0	0	33.368	-0.0148	6.1	1.2359	1.2353
40	43.149	20	4	2	43.151	-0.0016	1.4	0.9645	0.9644
41	47.378	--- not indexed ---					1.1	0.8827	

Average delta(2Theta) = 0.006
Maximum delta(2Theta) = 0.027 (peak 13) = 4.8 * average

Figure of Merit F(30) = 94.1 (0.005, 62)

Durbin-Watson serial correlation = 1.699 (not significant)

Sqrt[sum(w * delta(q)^2) / (Nobs - Nvar)] = 0.00030581

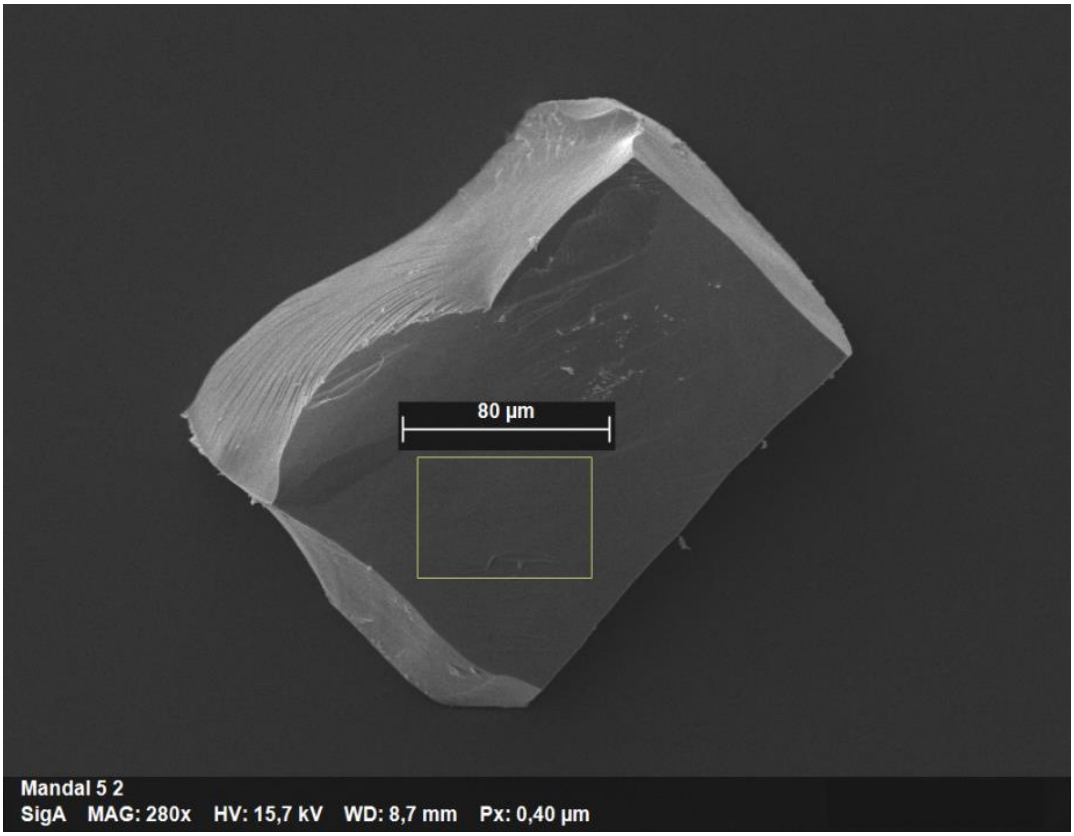

Figure S4.5: SEM image of $(P_4S_3)@Cu_7Cd_3I_{13}$ crystal

Table S4.12: Atomic coordinates equivalent isotropic displacement parameters and occupation factors a_i in $(P_4Se_3)@Cu_7Cd_3I_{13}$ at 123 K

Atom	*Wyckoff*	a_i	*x*	*y*	*z*	U_{iso}/Å^2
I1	8a	1	0	0	0	0.02402(19)
I2	96h	1	0.17687(2)	0.11977(2)	0.00017(7)	0.02639(16)
Cd1	24d	1	1/4	0	0	0.0285(2)
Cu2	32e	0.431(10)	0.07632(19)	*x*	*x*	0.0234(9)
Cu1	32e	0.444(10)	0.1251(2)	*x*	*x*	0.0378(13)
Cu3	32e	0.5311	-0.07612(15)	*x*	*x*	0.0275(6)
Cu4	32e	0.3439	-0.1251(2)	*x*	*x*	0.0190(8)
P1	32e	0.4734	0.19050(18)	*x*	*x*	0.0172(8)
Se1	96h	1/4	0.1569(5)	0.2095(7)	0.2971(4)	0.152(7)
P2	96h	1/4	0.222(3)	0.279(3)	0.3584(11)	0.57(6)

Table S4.13: Anisotropic displacement parameters (Å^2) for $(P_4Se_3)@Cu_7Cd_3I_{13}$ at 123 K

Atom	U_{11}	U_{22}	U_{33}	U_{12}	U_{13}	U_{23}
I1	0.0240(3)	U_{11}	U_{11}	0	0	0
I2	0.0194(3)	0.0230(3)	0.0368(3)	-0.00065(12)	-0.0014(6)	-0.0050(6)
Cd1	0.0293(5)	0.0282(4)	U_{22}	0	0	0
Cu1	0.0234(15)	U_{11}	U_{11}	0.0021(16)	U_{12}	U_{12}
Cu2	0.038(2)	U_{11}	U_{11}	-0.009(2)	U_{12}	U_{12}
Cu3	0.0275(11)	U_{11}	U_{11}	-0.0002(14)	U_{12}	U_{12}
Cu4	0.0190(13)	U_{11}	U_{11}	0.0008(18)	U_{12}	U_{12}
P1	0.0172(14)	U_{11}	U_{11}	-0.0050(13)	U_{12}	U_{12}
Se1	0.129(10)	0.134(11)	0.192(15)	-0.062(8)	0.065(11)	-0.102(9)
P2	0.86(14)	0.77(12)	0.097(16)	-0.80(13)	-0.30(5)	0.27(4)

Table S4.14: Selected interatomic distances and angle for $(P_4Se_3)@Cu_7Cd_3I_{13}$ at 123 K

Metal halide network			
Interatomic distances (Å)		Bond angles (°)	
I2 - Cu1	2.659(4)	Cd1 - I2 - Cu2	96.63(9)
I2 - Cu2	2.622(4)	Cd1 - I2 - Cu1	103.54(9)
I2 - Cu3	2.627(2)	Cd1 - I2 - Cu3^{2}	96.51(5)
I2 - Cu4	2.666(4)	Cd1 - I2 - Cu4^{2}	103.37(9)
I1 - Cu3	2.590(2)	Cu3^{2} - I2 - Cu1	104.54(10)
I1 - Cu2	2.597(4)	Cu2 - I2 - Cu3^{2}	69.57(10)
I2 - Cd1	2.7576(4)	Cu3 - I2 - Cu4^{2}	36.72(10)
Cu1 - Cu2	1.661(6)	Cu2 - I2 - Cu4^{2}	104.60(12)
Cu3 - Cu4	1.668(4)	Cu2 - I2 - Cu1	36.65(12)
Cu1 - P1	2.226(6)	Cu1 - I2 - Cu4^{2}	134.82(12)
Cu4 - Se1^{7}	2.341(12)	Cu2 - I1 - Cu2^{1}	109.47(12)
Cu1 - P2^{5}	2.70(6)	Cu2 - I1 - Cu3	180
		Cu2 - I1 - Cu3^{2}	70.53(10)
		Cu3 - I1 - Cu3^{2}	109.47(6)
		I2 - Cd1 - I2^{3}	117.185(12)
		I2 - Cd1 - I2^{4}	105.76(4)
		I2 - Cu2 - I2	111.74(14)
		I1 - Cu2 - I2	107.09(14)
		I2 - Cu3 - Cu4	72.88(15)
		I2 - Cu3 - I2^{2}	111.72(7)
		I1 - Cu3 - I2^{2}	107.12(7)
		I2 - Cu2 - Cu1	72.91(19)
		I1 - Cu3 - Cu4	180
		I1 - Cu2 - Cu1	180
		I2 - Cu4 - Se1^{7}	91.4(3)
		I2 Cu4 - Se1^{7}	110.1(3)
		I2 - Cu4 - Se1^{7}	125.3(3)
		Cu3 - Cu4 - Se1^{7}	160.1(3)
		I2 - Cu4 - I2^{2}	109.34(14)
		I2 - Cu4 - Cu3	70.40(15)
		I2 - Cu1 - P2^{6}	128.7(11)
		I2 - Cu1 - P2^{6}	112.9(13)
		I2 - Cu1 - P2^{6}	82.6(6)
		I2 - Cu1 - I2	109.38(14)
		P1 - Cu1 - Se1	31.05(19)

Symmetry code: ^{1}-x,y,-z; ^{2}-x,-y,z; ^{3}x,-y,-z; ^{4}-x+1/2,-y,z; ^{5}x,-y+1/2,-z+1/2; ^{6}x,-y+1/2,-z+1/2; ^{7}-x,-y,z-1/2

For cage molecule P_4Se_3			
Interatomic distances (Å)		Bond angles (°)	
P1 - Se1	2.228(9)	P1 - Se1 - P2	116.0(11)
Se1 - Se1	3.409(14)	P1 - Se1 - Se1	40.1(3)
P2 - Se1	2.22(5)	Se1 - Se1 - Se1^{1}	60
P2 - P2	3.29(6)	P2 - P2 - P2	60.0(15)
P1 - -P2	3.77(3)	Se1 - P2 - P2^{1}	61(3)
		Se1 - P1 - Se1	99.8(5)
		P2 - Se1 - Se1	90.4(12)

Symmetry code: ^{1}-x+1/2,-y+1/2,z

Table S4.15: Atomic coordinates, equivalent isotropic displacement parameters and occupation factors a_i in $(As_4S_3)@Cu_7Cd_3I_{13}$ at 223 K

Atom	*Wyckoff*	a_i	*x*	*y*	*z*	U_{iso}/Å^2
I1	8b	1	1/4	1/4	1/4	0.0310(5)
I2	96h	1	0.74685(11)	0.12886(6)	0.07270(6)	0.0368(5)
Cd1	24c	1	3/4	1/4	0	0.0430(8)
Cu2	32e	0.5356	0.3256(3)	*x*	*x*	0.0384(14)
Cu3	32e	0.4586	0.1731(5)	*x*	*x*	0.0407(17)
Cu1	32e	0.4164	0.1235(3)	*x*	*x*	0.0410(19)
Cu4	32e	0.3394	0.3691(7)	*x*	*x*	0.054(3)
As1	32e	1/4	0.4374(4)	*x*	*x*	0.040(3)
S1	96h	1/4	0.5135(11)	0.5134(12)	0.4011(12)	0.037(9)
As2	96h	1/4	0.4772(4)	0.4222(4)	0.4571(6)	0.71(8)

Table S4.16: Anisotropic displacement parameters (Å^2) for $(As_4S_3)@Cu_7Cd_3I_{13}$ at 223 K

Atom	U_{11}	U_{22}	U_{33}	U_{12}	U_{13}	U_{23}
I1	0.0310(9)	U_{11}	U_{11}	0	0	0
I2	0.0518(9)	0.0338(8)	0.0247(7)	0.0109(11)	0.0030(10)	-0.0024(5)
Cd1	0.0479(12)	U_{11}	0.0331(17)	0	0	0
Cu2	0.038(2)	U_{11}	U_{11}	-0.001(3)	U_{12}	U_{12}
Cu3	0.041(3)	U_{11}	U_{11}	0.009(4)	U_{12}	U_{12}
Cu1	0.041(3)	U_{11}	U_{11}	-0.021(3)	U_{12}	U_{12}
Cu4	0.054(5)	U_{11}	U_{11}	0.026(8)	U_{12}	U_{12}
As1	0.040(5)	U_{11}	U_{11}	-0.017(4)	U_{12}	U_{12}
S1	0.04(2)	0.014(14)	0.053(12)	0.011(10)	0.003(14)	0.055(11)
As2	1.9(2)	0.23(5)	0.034(12)	-0.35(8)	-0.19(5)	-0.07(2)

Table S4.17: Selected interatomic distance and angle for $(As_4S_3)@Cu_7Cd_3I_{13}$ at 223 K

Metal halide network			
Interatomic distances (Å)		Bond angles (°)	
I2 - Cu1[1]	2.623(6)	Cd1 - I2 - Cu2[2]	94.83(13)
I2 - Cu2[2]	2.682(6)	Cd1 - I2 - Cu1[3]	104.55(14)
I2 - Cu3[3]	2.598(10)	Cd1 - I2 - Cu3[3]	96.7(2)
I2 - Cu4[2]	2.662(14)	Cd1 - I2 - Cu4[2]	100.8(3)
I1 - Cu3	2.618(10)	Cu3 - I2 - Cu1[3]	37.7(3)
I1 - Cu2	2.573(6)	Cu2 - I2 - Cu3[3]	69.2(3)
I2 - Cd1	2.7773(13)	Cu3 - I2 - Cu4[2]	99.9(4)
Cu1 - Cu3	1.688(11)	Cu2 - I2 - Cu4[2]	32.2(3)
Cu2 - Cu4	1.481(15)	Cu2 - I2 - Cu1[3]	105.26(19)
Cu4 - As1	2.325(16)	Cu1 - I2 - Cu4[2]	132.2(3)
Cu4 - As2	2.931(17)	Cu2 - I1 - Cu2[5]	105.35(5)
		Cu2 - I1 - Cu3	180
		Cu2 - I1 - Cu3[5]	70.5(3)
		Cu3 - I1 - Cu3[7]	109.5(3)
		Cu2 - I1 - Cu2[6]	109.47(19)
		I2 - Cd1 - I2[4]	118.08(4)
		I2 - Cd1 - I2	105.35(5)
		I2 - Cu2 - I2[8]	112.0(2)
		I1 - Cu2 - I2[8]	106.8(2)
		I2 - Cu2 - Cu4	73.2(6)
		I2 - Cu3 - I2[9]	110.9(4)
		I1 - Cu3 - I2[9]	108.1(4)
		I2 - Cu1 - Cu3	70.3(4)
		I2 - Cu1 - I2[9]	109.3(2)
		I1 - Cu3 - Cu1	180
		I1 - Cu2 - Cu4	180
		I2 - Cu4 - As1	105.3(5)
		I2 - Cu4 - As2	119.5(5)
		I2 - Cu4 - As2	102.5(5)
		I2 - Cu4 - As2	93.3(4)
		Cu2 - Cu4 - As1	180
		I2 - Cu4 - I2[8]	113.3(5)
		I2 - Cu4 - Cu2	74.7(6)

Symmetry code: [1]y+1/2,x,z; [2]y+1/2,-x+1/2,-z+1/2; [3]y+1/2,x,z; [4]-x+3/2,-y+1/2,z; [5]y+1/2,-x+1,-z; [6]x,-y+1/2,-z+1/2; [7]-x+1/2,-y+1/2,z; [8]x-1/2,-z+1/2,-y+1/2, [9]y,x-1/2,z

For cage molecule As_4S_3			
Interatomic distances (Å)		Bond angles (°)	
As1 - S1	2.22(2)	As1 - S1 - As2[3]	111.7(10)
S1 - S1	3.11(3)	As1 - S1 - S1	45.5(6)
As2[1] - S1	2.21(2)	S1 - S1 - S1	60.0(7)
As2 - As2[2]	2.459(12)	As2 - As2 - As2[2]	60.0(3)
		S1 - As2 - As2[1]	88.0(6)
		S1 - As1 - S1	89.0(8)
		As2 - S1 - S1	83.4(7)

Symmetry code: [1]x,-y+1,-z+1; [2]-z+1,-x+1,y; [3]-x+1,-y+1,z

Supporting information of Chapter 5

Table S5.1: Atomic co-ordinates, equivalent isotropic displacement parameters and occupation factors a_i in P_4S_9 at 123 K

Atom	*Wyckoff*	a_i	*x*	*y*	*z*	$U_{iso}/Å^2$
P11	*2i*	1	0.66852	0.04475	0.11167	0.0132(3)
P12	*2i*	1	0.81474	-0.23751	-0.0214	0.0135(3)
P13	*2i*	1	0.97406	-0.25604	0.14159	0.0134(4)
P14	*2i*	1	0.58491	-0.32125	0.15811	0.0161(4)
S11	*2i*	1	0.49441	-0.07934	0.16769	0.0169(3)
S12	*2i*	1	0.72497	0.00036	-0.0071	0.0161(3)
S13	*2i*	1	1.02785	-0.30306	0.02359	0.0160(3)
S14	*2i*	1	0.80316	-0.38056	0.20109	0.0171(3)
S15	*2i*	1	0.64216	-0.36179	0.03754	0.0175(3)
S16	*2i*	1	0.88016	-0.01965	0.15737	0.0169(3)
S17	*2i*	1	0.58696	0.26158	0.12567	0.0225(4)
S18	*2i*	1	0.86984	-0.27960	-0.1294	0.0222(4)
S19	*2i*	1	1.17247	-0.30971	0.18054	0.0208(4)
P21	*2i*	1	0.16405	0.22701	0.51965	0.0114(3)
P22	*2i*	1	0.31893	-0.04205	0.37998	0.0113(3)
P23	*2i*	1	0.47169	0.28484	0.36965	0.0121(3)
P24	*2i*	1	0.08402	0.31099	0.33505	0.0132(3)
S21	*2i*	1	-0.0097	0.33366	0.45574	0.0150(3)
S22	*2i*	1	0.30134	0.39775	0.30525	0.0146(3)
S23	*2i*	1	0.37459	0.32012	0.48752	0.0159(3)
S24	*2i*	1	0.14591	0.07014	0.31611	0.0151(4)
S25	*2i*	1	0.22546	-0.01080	0.49887	0.0149(3)
S26	*2i*	1	0.53088	0.04913	0.34846	0.0158(3)
S27	*2i*	1	0.08011	0.25534	0.62812	0.0197(3)
S28	*2i*	1	0.66870	0.36420	0.34183	0.0203(4)
S29	*2i*	1	0.37819	-0.25862	0.36113	0.0185(3)

Table S5.2: Anisotropic Displacement Values ($Å^2$) for P_4S_9 at 123 K

Atom	U_{11}	U_{22}	U_{33}	U_{12}	U_{13}	U_{23}
P11	0.0140(5)	0.0133(5)	0.0102(5)	-0.0014(4)	-0.0008(4)	0.0018(4)
P12	0.0168(6)	0.0150(5)	0.0078(5)	-0.0030(4)	-0.0019(4)	0.0011(4)
P13	0.0133(5)	0.0171(5)	0.0124(5)	-0.0032(4)	-0.0041(4)	0.0019(4)
P14	0.0150(6)	0.0204(6)	0.0154(5)	-0.0069(5)	-0.0027(4)	0.0027(4)
S11	0.0140(5)	0.0208(5)	0.0125(5)	-0.0046(4)	0.0010(4)	-0.0004(4)
S12	0.0193(6)	0.0153(5)	0.0100(5)	-0.0016(4)	-0.0008(4)	0.0026(4)
S13	0.0133(5)	0.0186(5)	0.0135(5)	-0.0011(4)	-0.0024(4)	-0.0003(4)
S14	0.0176(5)	0.0211(5)	0.0140(5)	-0.0070(4)	-0.0044(4)	0.0077(4)
S15	0.0182(6)	0.0207(5)	0.0152(5)	-0.0081(5)	-0.0030(4)	-0.0018(4)
S16	0.0163(5)	0.0194(5)	0.0166(5)	-0.0047(4)	-0.0045(4)	-0.0022(4)
S17	0.0258(6)	0.0137(5)	0.0223(6)	0.0002(5)	0.0013(5)	-0.0010(4)
S18	0.0299(6)	0.0244(6)	0.0093(5)	-0.0046(5)	-0.0029(4)	-0.0009(4)
S19	0.0164(6)	0.0276(6)	0.0218(6)	-0.0057(5)	-0.0087(4)	0.0062(5)
P21	0.0150(5)	0.0109(5)	0.0075(5)	-0.0003(4)	-0.0016(4)	0.0011(4)
P22	0.0136(5)	0.0075(5)	0.0115(5)	-0.0008(4)	-0.0027(4)	0.0005(4)
P23	0.0127(5)	0.0128(5)	0.0134(5)	-0.0037(4)	-0.0027(4)	0.0006(4)
P24	0.0136(5)	0.0126(5)	0.0151(5)	0.0001(4)	-0.0060(4)	0.0008(4)
S21	0.0134(5)	0.0127(5)	0.0152(5)	0.0015(4)	-0.0039(4)	-0.0010(4)
S22	0.0167(5)	0.0117(5)	0.0148(5)	-0.0028(4)	-0.0048(4)	0.0049(4)
S23	0.0157(5)	0.0171(5)	0.0145(5)	-0.0053(4)	-0.0028(4)	-0.0033(4)
S24	0.0167(5)	0.0136(5)	0.0152(5)	-0.0013(4)	-0.0069(4)	-0.0021(4)
S25	0.0198(6)	0.0100(5)	0.0112(5)	-0.0010(4)	-0.0020(4)	0.0024(4)
S26	0.0142(5)	0.0140(5)	0.0162(5)	-0.0019(4)	-0.0019(4)	-0.0026(4)
S27	0.0260(6)	0.0193(5)	0.0081(5)	0.0004(5)	0.0006(4)	0.0007(4)
S28	0.0162(6)	0.0230(6)	0.0259(6)	-0.0097(5)	-0.0052(4)	0.0045(4)
S29	0.0273(6)	0.0072(5)	0.0183(5)	-0.0009(4)	-0.0044(4)	-0.0007(4)

Table S5.3: Selected bond distance and angle for P_4S_9 at 123 K

Interatomic distances (Å)		Bond angles (°)	
P11 - S17	1.9178(12)	S17 - P11 - S16	107.68(6)
P11 - S16	2.0900(14)	S17 - P11 - S12	109.54(6)
P11 - S12	2.1045(14)	S17 - P11 - S11	110.50(5)
P11 - S11	2.0846(13)	S16 - P11 - S12	109.69(5)
P12 - S18	1.9157(15)	S16 - P11 - S11	110.44(6)
P12 - S15	2.0914(13)	S12 - P11 - S11	108.98(6)
P12 - S12	2.1013(12)	S18 - P12 - S15	110.73(7)
P12 - S13	2.0941(14)	S18 - P12 - S12	109.58(6)
P13 - S16	2.0975(12)	S18 - P12 - S13	108.27(5)
P13 - S19	1.9209(14)	S15 - P12 - S12	110.45(5)
P13 - S13	2.0965(15)	S15 - P12 - S13	109.33(6)
P13 - S14	2.0844(13)	S12 - P12 - S13	108.44(6)
P14 - S15	2.1263(15)	S16 - P13 - S19	107.53(6)
P14 - S11	2.1260(12)	S16 - P13 - S13	110.26(6)
P14 - S14	2.1134(14)	S16 - P13 - S14	109.41(5)
P21 - S23	2.1009(13)	S19 - P13 - S13	108.82(5)
P21 - S27	1.9167(13)	S19 - P13 - S14	111.03(6)
P21 - S21	2.0784(13)	S13 - -P13 - S14	109.76(6)
P21 - S25	2.1062(13)	S15 - P14 - S11	105.82(5)
P22 - S29	1.9181(13)	S15 - P14 - S14	108.54(5)
P22 - S24	2.0864(14)	S11 - P14 - S14	108.24(6)
P22 - S25	2.1025(13)	P11 - S11 - P14	111.56(5)
P22 - S26	2.1011(13)	P11 - S12 - P12	109.00(5)
P23 - S23	2.0953(14)	P12 - S13 - P13	109.62(5)
P23 - S26	2.0901(13)	P13 - S14 - P14	110.94(6)
P23 - S28	1.9257(13)	P12 - S15 - P14	111.17(6)
P23 - S22	2.0784(14)	P11 - S16 - P13	108.56(6)
P24 - S24	2.1265(13)	S23 - P21 - S27	108.28(6)
P24 - S21	2.1241(14)	S23 - P21 - S21	110.53(5)
P24 - S22	2.1194(13)	S23 - P21 - S25	109.44(5)
		S27 - P21 - S21	110.72(5)
		S27 - P21 - S25	109.04(5)
		S21 - P21 - S25	108.81(6)
		S29 - P22 - S24	110.76(7)
		S29 - P22 - S25	109.28(6)
		S29 - P22 - S26	108.22(5)
		S24 - P22 - S25	110.17(5)
		S24 - P22 - S26	110.09(6)
		S25 - P22 - S26	108.39(6)
		S23 - P23 - S26	110.24(6)
		S23 - P23 - S28	108.38(7)
		S23 - P23 - S22	109.34(5)
		S26 - P23 - S28	108.39(5)
		S26 - P23 - S22	109.76(6)
		S28 - P23 - S22	110.71(6)
		S24 - P24 - S21	106.05(5)
		S24 - P24 - S22	108.14(5)
		S21 - P24 - S22	108.79(6)
		P21 - S21 - P24	111.32(5)
		P24 - S22 - P23	110.71(6)
		P21 - S23 - P23	108.81(6)

	P22 - S24 - P24	110.78(6)
	P21 - S25 - P22	109.06(5)
	P22 - S26 - P23	109.36(5)

Table S5.4: Atomic co-ordinates, equivalent isotropic displacement parameters and occupation factors a_i in $P_4S_3I_2$ at 123 K

Atom	*Wyckoff*	a_i	*x*	*y*	*z*	$U_{iso}/Å^2$
I11	*4a*	1	0.32884(7)	0.69611(7)	0.19520(19)	0.02231(14)
I22	*4a*	1	0.48436(7)	0.83880(7)	0.09576(19)	0.02149(14)
I12	*4a*	1	1.04607(7)	1.37981(7)	0.24681(19)	0.02119(14)
I21	*4a*	1	-0.20700(8)	1.54713(8)	0.15040(19)	0.02616(16)
S11	*4a*	1	0.5737(3)	1.2734(3)	0.2627(2)	0.0197(5)
S12	*4a*	1	0.7276(3)	1.0492(3)	0.1947(2)	0.0221(5)
S21	*4a*	1	0.3692(3)	1.3115(3)	0.0803(2)	0.0207(5)
S13	*4a*	1	0.6555(3)	0.7786(3)	0.2615(2)	0.0250(6)
S23	*4a*	1	-0.1268(3)	1.2208(3)	0.0828(2)	0.0258(6)
S22	*4a*	1	0.1528(3)	1.1471(3)	0.1482(2)	0.0222(5)
P24	*4a*	1	0.2636(3)	1.0481(3)	0.0675(2)	0.0190(5)
P13	*4a*	1	0.3992(3)	0.8870(3)	0.2460(2)	0.0201(5)
P14	*4a*	1	0.8343(3)	1.1617(3)	0.2751(2)	0.0190(5)
P12	*4a*	1	0.4829(3)	1.1368(3)	0.2174(2)	0.0196(6)
P22	*4a*	1	0.2316(3)	1.3963(3)	0.1258(2)	0.0208(6)
P11	*4a*	1	0.8640(3)	0.9387(3)	0.2372(2)	0.0218(6)
P23	*4a*	1	-0.0223(3)	1.4775(3)	0.0985(2)	0.0215(6)
P21	*4a*	1	0.0418(3)	1.0130(3)	0.1056(2)	0.0216(6)

Table S5.5: Anisotropic Displacement Values ($Å^2$) for $P_4S_3I_2$ at 123 K

Atom	U_{11}	U_{22}	U_{33}	U_{12}	U_{13}	U_{23}
I11	0.0248(3)	0.0222(2)	0.0200(2)	-0.00760(19)	0.00137(19)	-0.00395(19)
I22	0.0221(2)	0.0193(2)	0.0231(3)	0.00544(18)	0.00133(19)	0.00229(19)
I12	0.0190(2)	0.0222(2)	0.0223(2)	-0.00508(18)	0.00178(19)	-0.00101(19)
I21	0.0271(3)	0.0262(3)	0.0252(3)	0.0103(2)	0.0040(2)	0.0001(2)
S11	0.0188(9)	0.0177(9)	0.0227(9)	0.0015(7)	-0.0007(7)	-0.0049(7)
S12	0.0240(9)	0.0244(10)	0.0179(9)	-0.0029(8)	0.0034(7)	-0.0010(7)
S21	0.0204(9)	0.0177(9)	0.0242(10)	0.0002(7)	0.0016(7)	0.0002(7)
S13	0.0257(10)	0.0187(9)	0.0306(11)	-0.0027(8)	-0.0073(8)	0.0079(8)
S23	0.0189(10)	0.0272(10)	0.0312(11)	0.0034(8)	-0.0063(8)	-0.0067(8)
S22	0.0263(10)	0.0241(10)	0.0162(9)	0.0035(8)	-0.0015(7)	0.0021(7)
P24	0.0188(9)	0.0205(10)	0.0176(10)	0.0020(7)	-0.0006(7)	-0.0036(7)
P13	0.0207(10)	0.0228(10)	0.0169(9)	-0.0037(8)	0.0016(7)	-0.0023(8)
P14	0.0198(9)	0.0191(9)	0.0181(9)	-0.0023(7)	-0.0031(7)	0.0020(7)
P12	0.0193(9)	0.0185(9)	0.0211(10)	0.0012(7)	-0.0035(7)	-0.0001(7)
P22	0.0202(10)	0.0200(10)	0.0222(10)	-0.0004(7)	-0.0016(7)	-0.0059(7)
P11	0.0175(10)	0.0194(10)	0.0285(11)	0.0031(7)	-0.0001(8)	-0.0015(8)
P23	0.0244(10)	0.0205(10)	0.0195(10)	0.0033(8)	0.0005(8)	0.0001(8)
P21	0.0201(10)	0.0193(10)	0.0254(11)	-0.0037(7)	0.0015(7)	-0.0020(8)

Table S5.6: Selected bond distance and angle for $P_4S_3I_2$ at 123 K

Interatomic distances (Å)		Bond angles (°)	
I11 - P13	2.475(9)	S12 - P11 - S13	102.9(2)
I22 - P24	2.476(5)	S12 - P11 - P14	101.6(2)
I12 - P14	2.475(5)	S13 - P11 - P14	92.0(3)
I21 - P23	2.484(9)	S11 - P12 - S12	103.2(2)
P11 - S12	2.094(9)	S11 - P12 - P13	92.9(4)
P11 - S13	2.137(6)	S12 - P12 - P13	101.37(17)
P11 - P14	2.208(8)	I11 - P13 - S11	138.6(3)
P12 - S11	2.134(9)	I11 - P13 - S13	101.7(2)
P12 - S12	2.090(5)	I11 - P13 - P12	96.6(4)
P12 - P13	2.220(6)	S13 - P13 - P12	101.97(17)
P13 - I11	2.475(9)	I12 - P14 - S11	102.1(2)
P13 - S13	2.115(4)	I12 - P14 - S13	139.2(3)
P13 - P12	2.220(6)	I12 - P14 - P11	96.4(3)
P14 - I12	2.475(5)	S11 - P14 - S13	86.03(12)
P14 - S11	2.121(4)	S11 - P14 - P11	102.5(3)
P14 - P11	2.208(8)	P14 - S11 - P12	106.7(3)
P21 - S23	2.143(5)	P12 - S12 - P11	100.7(4)
P21 - S22	2.091(9)	P13 - S13 - P14	94.77(11)
P21 - P24	2.211(8)	P13 - S13 - P11	107.3(3)
P22 - S21	2.131(9)	S23 - P21 - S22	102.8(2)
P22 - S22	2.095(5)	S23 - P21 - P24	93.3(3)
P22 - P23	2.215(6)	S22 - P21 - P24	101.4(2)
P23 - S23	2.110(4)	S21 - P22 - S22	103.0(2)
P23 - P22	2.215(6)	S21 - P22 - P23	94.0(4)
P24 - S21	2.127(4)	S22 - P22 - P23	101.73(16)
P24 - P21	2.211(8)	I21 - P23 - S21	138.2(3)
		I21 - P23 - S23	102.8(2)
		I21 - P23 - P22	96.6(3)
		S23 - P23 - P22	101.79(16)
		I22 - P24 - S21	102.5(2)
		I22 - P24 - S23	138.1(3)
		I22 - P24 - P21	95.9(3)
		S21 - P24 - S23	85.53(13)
		S21 - P24 - P21	102.2(3)
		P24 - S21 - P22	106.7(3)
		P24 - S21 - P23	94.08(11)
		P22 - S21 - P23	44.05(19)
		P22 - S22 - P21	100.3(4)
		P23 - S23 - P21	107.4(3)

Curriculum Vitae

Personal Data

Name	Ria Mandal
D.O.B	07.01.1989
Place of birth	Chinsurah, India
Parents	Dr. Jaharlal Mandal and Mrs. Dipika Mandal

Education

Doctoral studies	June 2016- Research guide: Prof. Dr. Arno Pfitzner University of Regensburg, Germany
Master of Technology	2012 – 2014 Materials Science and Engineering Indian Institute of Technology Kharagpur, India
Master of Science	2010 – 2012 Chemistry University of Burdwan, India
Bachelor of Science	2007 – 2010 Chemistry University of Burdwan, India
School studies	1995-2007 Krishna Bhabini Nari Siksha Mandir West Bengal, India